Transmission and Detection Techniques for MIMO Systems

Raymundo Ramirez Gutierrez

Submitted in accordance with the requirements for the degree of Doctor of Philosophy

The University of Leeds
School of Electronic and Electrical Engineering

October 2014

Declaration

The candidate confirms that the work submitted is his own, except where work which has formed part of jointly authored publications has been included. The contribution of the candidate and the other authors to this work has been explicitly indicated below. The candidate confirms that appropriate credit has been given within the thesis where reference has been made to the work of others.

The material contained in the chapters of this thesis has been previously published in research articles written entirely by the author of this work (Raymundo Ramirez Gutierrez) who appears as lead (first) author in all of them. The research has been supervised and guided by Dr. Li Zhang and Prof. Jaafar Elmirghani, and so they appear as co-authors of the articles. All the material included in this document is of the author's entire intellectual ownership.

The work in chapter 3 of the thesis has appeared in publication as follows:

- *Generalized Phase Spatial Shift Keying Modulation for MIMO Channels,* by R. Ramirez Gutierrez, L. Zhang, J. M. H. Elmirghani and R. Fa. VTC Spring 2011: 1-5.

  R. Fui provided support for simulations and technical issues.

The work in chapter 4 of the thesis has appeared in publication as follows:

- *Antenna Beam Pattern Modulation with Lattice Reduction Aided Detection,* by R. Ramirez Gutierrez, L. Zhang and J. M. H. Elmirghani. IEEE Transaction on Vehicular Technology. Accepted subject to revision.

- *Antenna Beam Pattern Modulation for MIMO Channels,* by R. Ramirez Gutierrez, L. Zhang, J. M. H. Elmirghani and A. F. Almutairi. IWCMC 2012: 591-595.

  A. F. Almutairi provided guidance for the system model design.

The work in chapter 5 of the thesis has appeared in publication as follows:

- *Antenna Pattern Shift Keying Modulation for MIMO Channels,* by R. Ramirez Gutierrez, L. Zhang and J. M. H. Elmirghani. EW 2013.

The work in chapter 6 of the thesis has appeared in publication as follows:

- *Lattice Reduction based on Pre-Coding Aided Spatial Modulation with Sub-optimal Detection,* by R. Ramirez Gutierrez, L. Zhang and J. M. H. Elmirghani. IEEE Wireless Communications Letters. Under revision.

This work is dedicated entirely to...

God and my "dones"

Acknowledgements

It is difficult to remember everybody who has crossed my path during this important period of my life when I have been studying at University of Leeds. However, all the effort, ups and downs are priceless and they would be impossible to describe. Even with a thanks or whatever word used, it would not be enough to describe the impact of this amazing period in my life. This dream came true thanks to all of you.

Firstly, I would like to mention that without the funding and support of the CONACyT Mexico, I would never have gotten any academic achievement. CONACyT sponsored my academic career for almost 5 years and they were always there in the best position to help and solve any difficulty.

Secondly, my gratitude is for my supervisor Dr. Li Zhang. Li is an extraordinary person, extremely kind and supportive not only as a supervisor, Li was always concerned regarding my personal life and always tried to make me feel better on any difficult circumstance. Also, Li encouraged me to do an internship in Alcatel-Lucent which has remarked my professional expectations and made me grew up as person.

Thirdly, all my friends around this time in England, all the staff, etc. The list is so long and I do not want to miss anyone but all of them helped me to build up this achievement.

Finally, three persons have been crucial during this stage. My parents, they are out of this planet because regardless the distance they always had the exact words and advices to keep my chin up

to every problem. Sofia Runebrand, thank you so much for everything, you changed my stay in Leeds and my life in general. We walked together during this resounding adventure. Te amo

Abstract

It is well-known that Multiple-Input Multiple-Output (MIMO) wireless systems are disposed by two conclusive goals: high data rate and high performance. This thesis is concerned with transmission and detection techniques of MIMO systems, particularly on Spatial Modulation (SM). SM is a lately developed transmission technique for multiple antenna systems. The idea behind SM is to map a block of information bits into two parts, carried separately by the index of the active transmitter and the symbol chosen from constellation points. All four transmission techniques presented in this thesis are based on the SM principle. The first system, called spatial phase shift keying (SPSK) modulation, follows the idea of SM but uses multiple active transmitters and it shows a gain of 2 dB over a transmission technique based on SM. Antenna beam pattern modulation (ABPM) is the second proposed technique. In this technique, the antenna beam patterns are utilised to transmit information. The contribution of this scheme is to improve the data rate utilizing different beam patterns in order to generate another dimension to the constellation diagram. Optimization of the beam pattern design results in improved system performance. In addition to all the benefits of ABPM at the transmission design, a sub-optimal detection method based on lattice reduction (LR) is used to reduce the computational complexity in comparison to the optimal maximum likelihood (ML) method. The aim of this proposed sub-optimal detection method (LR) is to achieve performance similar to that of the ML scheme at affordable complexity. ABPM shows a gain of more than 2 dB over transmission techniques based on SM. The third scheme is called antenna pattern

shift keying (APSK) modulation. This scheme combines the idea of SPSK and ABPM because the antenna beam patterns and the indices of the active transmitters carry the symbol chosen from a constellation diagram. APSK improves the data rate and the overall system performance. APSK has similar performance as a spatial multiplexing scheme but APSK reduces the number of RF chains and it has a gain of 3.5 dB in comparison to that of a technique based on SM. The last scheme included in this thesis, is a pre-coder technique based on LR. This novel LR pre-coder is applied to the generalised pre-coding aided spatial modulation (GPSM) scheme to improve the system's performance and it shows a gain of more than 1 dB over the traditional GPSM. Additionally, a sub-optimal detector scheme is proposed to achieve performance similar to that of the ML detector but with lower complexity. Using that in combination with the LR pre-coding technique means that the performance of the GPSM scheme is preserved with a much lower detection complexity.

Contents

List of Figures

List of Tables

Abbreviations

3GPP	Third Generation Partnership Project
4G	Fourth Generation
5G	Fifth Generation
ABPM	Antenna Beam Pattern Modulation
ADC	Analog-to-Digital Converter
AoD	Angle of Departure
APM	Amplitude/Phase Modulation
APSK	Antenna Pattern Shift Keying
AWGN	Additive White Gaussian Noise
BER	Bit Error Rate
CN	Cooperative Network
CR	Cognitive Radio
CSI	Channel State Information
FDD	Frequency-Division Duplexing
GPSSK	Generalized Phase Spatial Shift Keying
GSSK	Generalized Space Shift Keying
HSPA	High Speed Packet Access
IEEE	Institute of Electrical and Electronics Engineers
ISI	Inter-Symbol Interference
LLL	Lenstra, Lenstra and Lovász algorithm
LR	Lattice Reduction
LTE-A	Long-Term Evolution Advanced
MF	Matched Filter
MIMO	Multiple-Input–Multiple-Output
MISO	Multiple-Input–Single-Output
MMSE	Minimum Mean Square Error
ML	Maximum Likelihood

OFDM	Orthogonal Frequency Division Multiplexing
OFDMA	Orthogonal Frequency Division Multiple Access
OSTBC	Orthogonal Space-Time Block Coding
PAM	Pulse-Amplitude Modulation
PSK	Phase-Shift Keying
QAM	Quadrature Amplitude Modulation
QoS	Quality of Service
RF	Radio Frequency
SC-FDMA	Single Carrier Frequency Division Multiple Access
SIMO	Single-Input–Multiple-Output
SISO	Soft-Input–Soft-Output
SM	Spatial Modulation
SNR	Signal-to-Noise Ratio
SPSK	Spatial Phase Shift Keying
STC	Space-Time Coding
TD-SCDMA	Time Division Synchronous Code Division Multiple Access
TDD	Time-Division Duplexing
TDMA	Time-Division Multiple Access
V-BLAST	Vertical Bell Laboratories Layered Space-Time
WCDMA	Wideband Code-Division Multiple Access
ZF	Zero Forcing

Chapter 1

Introduction

Since 1864, with James C. Maxwell predicting electromagnetic radiation, wireless communications have grown from something unknown to a technology that gives services to billions of people. There are two fundamental aspects for both analogue and digital wireless communications: fading and interference. Dealing with these aspects is essential in the design of wireless communication systems. The system design is usually focused on either increasing the reliability of the transmission or improving the spectral efficiency. Since the frequency spectrum is limited, it has to be utilised in a very efficient manner.

From old cellular systems to current and future systems, the requirement for high data rates varies depending on their applications. Recently, the increasing demand for wireless communication services has resulted in numerous proposals and deployments of new systems, which consequently require high spectrum efficiency with the available resources. The concept of spectrum efficiency proposes to mitigate the spectrum scarcity by improving the efficiency of the spectrum usage.

In cellular mobile radio systems, the management of the electromagnetic spectrum has to be effective and efficient, this is one of the main regulatory challenges across the world. Traditionally, the spectrum management has been structured by the governments which have control over the spectrum, issue spectrum licenses and control the usage of particular services or technologies.

Over the past years, spectrum management has increased with emphasis on technology and service neutrality, which is driving towards increased demand for spectrum and convergence. The result of this is that services which were once handed over in specific bands, they are now on a range of different platforms which are spreading into many different spectrum bands.

Future generation networks is a concept that includes both the core and the access networks and these may be delivered by a number of technologies including fibre, cable, terrestrial fixed, copper, satellite or mobile wireless. The development of modern wireless communications has been based on numerous technological innovations and implementations, such as multiple-input multiple-output (MIMO), orthogonal frequency division multiplexing (OFDM), cooperative network (CN), cognitive radio (CR), etc. Among all these innovations, MIMO has been a watershed having many advantages which never could have been achieved in the past.

Traditional MIMO systems have been established providing solutions to some of the issues previously mentioned. Among the main attributes of MIMO are: higher spectrum efficiency, robustness against multi-path dispersive channels and capability of dynamic resource management. These characteristics have made MIMO a promising technology which benefits the spectrum sharing system. Thus, intensive research has been carried out on MIMO based on spectrum sharing systems. Consequently, the promising performance shown in the recent research has demonstrated the MIMO systems' increase in the spectrum efficiency and this may reinvigorate the future of wireless communications [2]. In Chapter 2, MIMO systems will be discussed in detail.

The mobile network operators are dealing to swiftly increase the cellular network capacity through the addition of radio spectrum. Then, spectral efficient radio access technologies such as fourth generation (4G) networks which are based on long term evolution (LTE) are essential to use the radio spectrum in the most efficient manner. Many options exist to increase the system capacity. Many of those include the increment of the number of frequency carriers deployed and improvement of the spectral efficiency through the scalability to

more advanced technologies such as high speed packet access (HSPA), LTE or MIMO systems.

Moreover, the goal of the 4G wireless communication systems is to allow peak data rates in the range of 100 Mbps for vehicular mobility networks and 1 Gbps for nomadic networks. 4G services have to fully exploit the benefits of advanced techniques such as MIMO, cooperative communications, macro diversity, interference cancellation, multi-hop relay techniques, adaptive modulation, multi-resolution techniques, multi-user environments, block transmission techniques, carrier aggregation, etc. The aforementioned improvement methods allow for improvements in coverage of high data rate transmission, in system performance and in the features required for 4G.

The main challenge that the mobile telecommunications industry has to face is how to continuously improve the user experience, service interaction and attractiveness. The technology has to achieve better performance, higher throughputs, improved capacities and higher spectral efficiencies.

The increased use of mobile terminals has created a significant environmental footprint. To supply the operation of mobile terminals and the network infrastructure, a huge quantity of electrical power is required. This currently represents up to 50% of the operational costs [3, 4]. Thus, energy efficiency in wireless communications contributes to the implementation of the green cellular networks concept due to the fact that they help to reduce the carbon emission footprint. The green network concept is approached through three main dimensions:

- Energy provisioning: new strategies to generate power based on the use of renewable energy sources.

- Architecture and protocols: novel transmission techniques, network protocols and architectures which improve the overall system performance.

- Hardware implementation: more efficient components in terms of energy dissipation and dependency.

The dimensioning and adjustments that are necessary to reduce the energy consumption are achieved at the network level. It is possible to carry out these modifications without radically compromising the network performance and the spectral efficiency. Thus, a reduction in the transmit power between the base station and the mobile terminals can be achieved [5].

Another alternative to reduce the carbon emission footprint is to study a new energy supplying strategy based on the use of renewable energy sources. This study has to include the implementation of wind generators and photovoltaic cells at the base station. At the receiver side, the implementation of photovoltaic cells can be used by the mobile terminals [6].

1.1 Motivation

The wireless system data traffic is exponentially increasing across the globe. As the number of devices increases, the radio spectrum becomes a scarce resource due to the high amount of data consumed. MIMO systems have demonstrated their advantages and benefits through improving the spectral efficiency and becoming an important solution to the spectrum scarcity resource.

However, MIMO systems have some drawbacks such as high inter-channel interference (ICI), large decoding complexity due to the ICI, high number of radio frequency (RF) chains, high power consumption and an increased hardware cost due to multiple parallel transmitters and receivers as it is shown in Figure 1.1. There is also a tradeoff between improvement of robustness and spectrum efficiency.

The improvement of spectral efficiency and throughput are not the only major concerns for researchers in wireless communication systems. As the energy consumption and complexity issues have had little or no attention, it is now clear that the information and communication technology sector have a substantial contribution to the global carbon emissions. Then, “Green Radio” has been developed as a research discipline that intends to identify the fundamental tradeoffs between system-wide performance and energy efficiency.

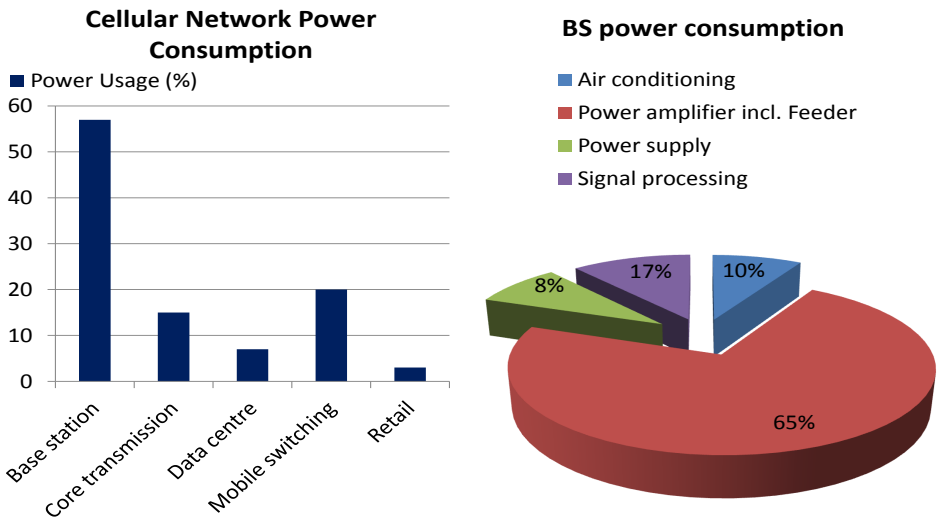

Figure 1.1: *Cellular network and base station power consumption [1].*

Transmission techniques based on spatial modulation (SM) have been proposed as a solution to deal with these issues because only a single transmitter is used at any time. SM offers a simple design which achieves high data rate. In these forms, combinations of antenna index in addition to conventional amplitude/phase modulation (APM) symbols are used to convey the transmitted messages. Therefore, a single RF chain will be utilised in the design of the system. SM systems use maximum likelihood (ML) as a decoding method, which is not feasible for implementation with larger number of antennas and/or higher-order forms of modulation.

Inspired by the SM techniques, further investigation is carried out to propose higher spectrum and energy efficiency transmission techniques [7, 8]. In particular considering potential application in future wireless communication systems such as large-scale MIMO, where the ML detector is not feasible due to its high complexity [2, 9]. Novel decoding techniques are also proposed, which would not compromise the system performance but have reduced its complexity.

1.2 Overview of the Thesis

The focus of this thesis is on the design transmission techniques based on the SM principle but with low complexity, high spectrum efficiency and high system performance. The systems proposed have to improve the system capabilities to accommodate for the user demands.

In **Chapter 2**, a general overview of key systems such as MIMO systems, SM and large-scale MIMO are described. This overview includes the main features and disadvantages of each one. The lattice basis reduction is also reviewed in this chapter as a key technique used in this thesis for the purpose of complexity reduction. As massive MIMO involves hundreds of antennas at both sides, the detector complexity plays an important role for these systems. As lattice reduction (LR) in combination with linear equalisers has shown performance similar to that of ML [10, 11], it can be a suitable solution for detection complexity reduction.

In **Chapter 3**, a scheme based on SM named Spatial Phase Shift Keying (SPSK) modulation is introduced. SPSK improves the spectral efficiency by not only sending energy on the active antenna indices, instead, SPSK sends different APM symbols on its active antennas. A criteria to select these APM symbols is deployed to maximise the distance between the SPSK vectors and to achieve a better performance. The results show improvements in terms of BER and a theoretical analysis validates the results.

Chapter 4 describes a transmission technique which uses all the transmitters available. This scheme is called Antenna Beam Pattern Modulation (ABPM) and the idea behind this transmission technique is to transmit different beam patterns which convey APM symbols. Based on this idea, an optimal criterion for selecting the beam pattern is proposed. The criterion takes into consideration the correlation of the main beam patterns based on their degrees of difference. LR is proposed as a sub-optimal detection method and the system achieves performance similar to that of ML detector in terms of BER and with lower computational complexity. Theoretical derivation is also presented to validate the simulation results.

Chapter 5 introduces a transmission technique named Antenna Pattern Shift Keying (APSK) modulation. APSK combines both the SPSK and ABPM techniques explained in Chapter 3 and Chapter 4, respectively. APSK exploits the advantages of these two techniques by dividing the transmit symbol into three blocks. The first block selects the active transmitters to convey the extra information. The second block chooses the beam pattern radiated by the active transmitters. Finally, the third block carries the APM symbol information. Therefore, APSK increases the spectral efficiency and outperforms techniques based on SM and spatial multiplexing.

In **Chapter 6**, a pre-coding method based on LR is proposed to improve performance in wireless communication systems where the channel state information at the transmitter (CSIT) is available. This pre-coding scheme is applied in Generalised Pre-coding Aided Spatial Modulation (GPSM) system. The idea of GPSM is to use the indices of the active receivers as additional information to improve the spectral efficiency. GPSM utilises the ML algorithm as the detection method, which for practical implementation may not be suitable due to its high computational complexity. Thus, when LR is implemented as a pre-coder, it facilitates the use of a low complexity detection method and a linear equaliser instead of ML. This contributes to the reduction of the computational complexity but maintains performance at a level similar to that of the ML detector.

Finally, the thesis is concluded in **Chapter 7**. In this chapter, some potential applications of the transmission schemes in future wireless communication protocols are suggested and some possible future work related to the LR as a pre-coding and detection method are proposed.

1.3 Major Contribution

The work presented in this thesis provides a number of original contributions about the transmission and detection techniques for multiple antenna wireless systems. These contributions are:

1. Three transmission methods are proposed to improve the spectral efficiency. They are based on the SM principle and use antenna indices of the active transmitters (SPSK), beam patterns (ABPM) and a combination of antenna indices and beam patterns (APSK) to convey extra information. In SPSK and APSK, not all the transmitters are used, it reduces the power consumption which results in a reduction of the system complexity.

2. The ML detector is not feasible when the number of antennas increase or with high modulation orders. Then, a sub-optimal detection based on LR is proposed to reduce the computational complexity of the system but preserving performance similar to that of the ML detector.

3. Finally, a novel pre-coding scheme based on LR in combination with a sub-optimal detection scheme is proposed to reduce the system complexity. These schemes are applied to GPSM.

1.4 Publication List

The research featured in this thesis has also been presented in the following publications:

- R. Ramirez-Gutierrez, L. Zhang, and J. Elmirghani, "Antenna pattern shift keying modulation for MIMO channels," *in Proc. Eur. Wireless Conf.*, Apr. 2013, pp. 1-5.

- R. Ramirez-Gutierrez, L. Zhang, J. Elmirghani, and A. F. Almutairi, "Antenna beam pattern modulation for MIMO channels," *in Proc. IEEE Int. Wireless Commun. Mob. Comput. Conf.*, Aug. 2012, pp. 591-595.

- R. Ramirez-Gutierrez, L. Zhang, J. Elmirghani, and R. Fa, "Generalized phase spatial shift keying modulation for MIMO channels," *in Proc. IEEE Veh. Technol. Conf. Spring*, May 2011.

- R. Ramirez-Gutierrez, L. Zhang, and J. Elmirghani, "Antenna beam pattern modulation with lattice reduction aided detection," *IEEE Trans. Veh. Technol.*, accepted subject to revision.

- R. Ramirez-Gutierrez, L. Zhang, and J. Elmirghani, "Lattice Reduction Pre-Coding Aided Spatial Modulation," *IEEE Wireless Commun. Lett.*, under revision.

1.5 Notations

The following notation is used throughout this thesis. Italicized letters/symbols denote scalar values while boldface lower and upper case letters/symbols denote vectors and matrices respectively.

$(\cdot)^T$	Transpose
$(\cdot)^H$	Conjugate-transpose
$(\cdot)^*$	Conjugate
$\|\cdot\|$	2-norm
$\lceil \cdot \rfloor$	Rounding function
$\det(\cdot)$	Matrix determinant
$\mathcal{CN}(n, \sigma^2)$	Complex Gaussian distribution of a random variable
$\mathcal{N}\left(n, \frac{\sigma^2}{2}\right)$	Independent Gaussian distributed real and imaginary parts with mean n and variance $\frac{\sigma^2}{2}$
I_N	$N \times N$ identity matrix
$\mathbb{C}$	Complex number set
$\mathcal{O}(\cdot)$	Computational complexity in terms of number of arithmetic operations
$Tr(\cdot)$	Matrix trace
P_e	Error probability
η	Spectral efficiency
$\mathbf{H}$	Complex valued, channel matrix

Chapter 2

Literature Review

2.1 Evolution of MIMO

2.1.1 MIMO

NOWADAYS, wireless communications have become the most important growing technological industry of the modern world. Mobile communications have been serving billions of people around the world for a little more than a decade. The demand for services is still growing, which is the reason that future generation systems face a big challenges in supplying these. One way in which the spectrum efficiency has been significantly increased, is by the use of array antenna, also called MIMO systems. The antenna spacing must be larger than the coherence distance to ensure independent fading across different antenna elements [12].

Fig. 2.1 shows the different antenna configurations such as single input single output (SISO), single input multiple output (SIMO), multiple input single output (MISO) and the already mentioned MIMO. The MISO and SIMO architectures are forms of transmit and receive diversity schemes, respectively. MIMO combined these two forms of diversity to transmit parallel data or spatial multiplexing.

There are many system models within the MIMO field but all these system models may be adequately illustrated by a general multidimensional linear model shown in Fig. 2.2. MIMO has shown extensive improvements over

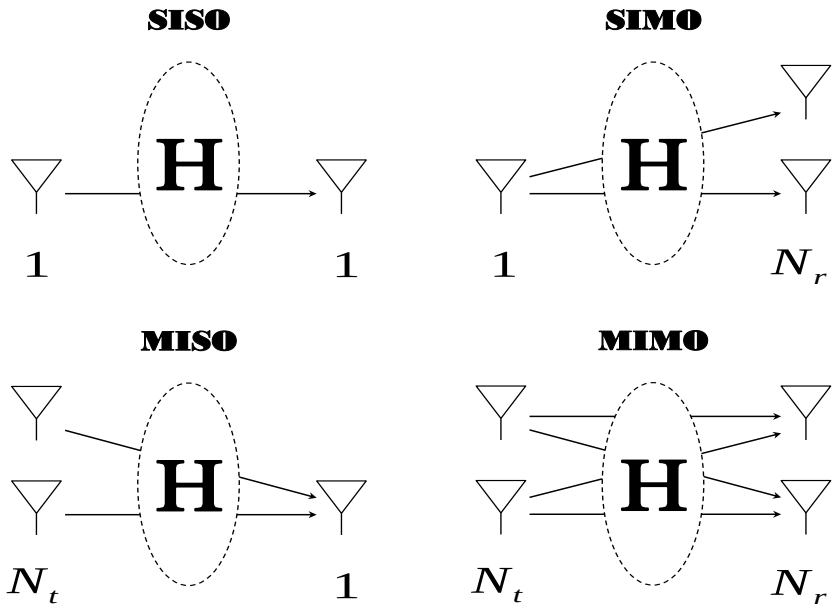

Figure 2.1: *Antenna architectures.*

typical single antenna systems. The most known MIMO techniques are space-time coding (STC) [13] and spatial multiplexing [14] in cases where channel state information (CSI) is not available at the transmitter.

MIMO schemes are utilised to improve the performance or capacity as much as possible with the same spectrum bandwidth. However, MIMO provides these improvements at the cost of an obvious increase in complexity.

2.1.2 Transmission techniques for MIMO

MIMO systems use several antennas to simultaneously transmit multiple data streams over a wireless channel. MIMO improves the data rate, increases reliability, increases energy efficiency and reduces interference. Transmit diversity was implemented in the early 2000s and it is particularly used in the downlink system because the use of multiple transmitters improves reliability. The two most commonly used transmission techniques systems are transmit diversity (for example STC) and spatial multiplexing [2].

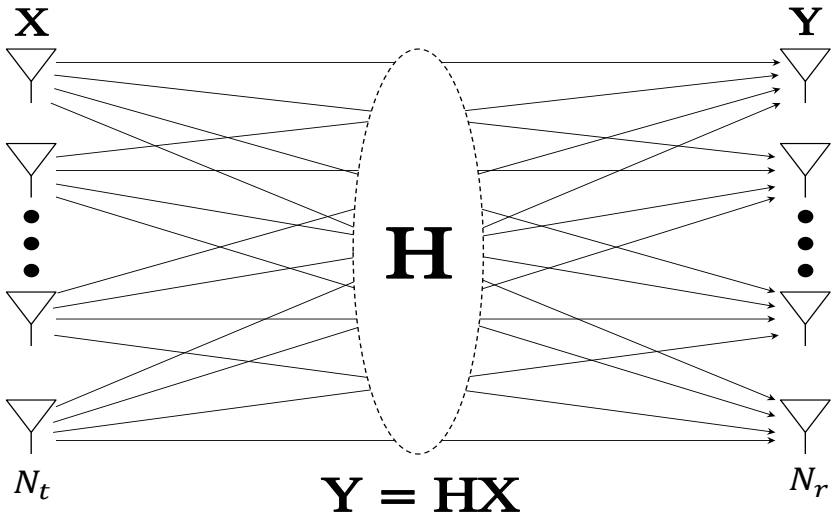

Figure 2.2: *Traditional MIMO system model.*

Beamforming

The beamforming idea is to use multiple antennas to control the direction of the beam pattern by appropriately weighting the phase and magnitude of each antenna signal (transmit beamforming), which provides better coverage to specific users [15]. This is achieved because every single antenna in the array makes a contribution to the steered signal, achieving an array gain called beamforming gain. Using beamforming at the receiver side makes it possible to determine the direction from which the signal will arrive, also called direction of arrival (DoA). It can be used to suppress selected interfering signals by choosing a beam pattern null in the direction of the undesirable signal.

The beamforming technique tries to provide the best signal possible to an user at a specific location. Two basic methods for finding the weight vector can be used which also affect the arrangement of the antenna array: determining the weights utilising either DoA or channel estimation.

- Determining the weights using DoA: if the location of the user is known, the beamforming weights can be adapted to optimise the transmission. A

Table 2.1: *Transmission Table of Alamouti Code.*

	$Antenna1$	$Antenna2$
$Time1$	s_1	s_2
$Time2$	$-s_2^*$	s_1^*

uniform linear array (ULA) is usually used, where the distance between each antenna is the same and has to be equal to or greater than $\lambda/2$ in order to determine the DoA.

- Determining the weights using channel estimation: this method uses training sequences to estimate the channel conditions and then generate the optimum beamforming weights. In a TDD system, downlink and uplink are on the same frequency and therefore the channel characteristics are similar. That makes feedback unnecessary when a suitable uplink signal is present and thus the base station can be used to estimate the channel.

Transmit Diversity

The most popular transmit diversity scheme is STC, in which the receiver has to know the channel to decode the signal. STC aims to improve the reliability of the link which can be achieved though the simultaneous transmission of multiple replicas of the same information through independent fading paths [13, 14], reducing the probability that the signal fades completely, at it is unlikely for several signals to fade at the same time. There are many types of space-time codes but space time block codes (STBCs) are the most studied due to their simple implementation. The simplest STBC is called the Alamouti code. It uses two transmit antennas and two symbols (s_1 and s_2) which are transmitted over two symbol times.

The Alamouti scheme provides a coding gain over the repetition code. This is the transmit diversity scheme that has been proposed in several 3G

standards. Table 2.1 shows the design of the Alamouti scheme for two transmit antennas. This scheme works for any constellation for the symbols s_1 and s_2. The two symbols are transmitted over two symbol times instead of one symbol, but with half the power in each symbol.

This Alamouti scheme can only be used in a system with two transmitters. However, it belongs to a generic class of codes called orthogonal STBCs. The distinctive feature of STBCs is that all rows of the transmitted sequences are orthogonal to each other [13].

Spatial Multiplexing

The main idea of the spatial multiplexing process is to convert the sequence of information bits into streams that will be treated differently. Thus, spatial multiplexing improves the spectral efficiency by transmitting multiple independent streams across multiple antennas. The encoding process of these techniques are divided into three different encoding cases:

- Horizontal: in this encoding case, the bits are demultiplexed into sub-streams equal to the total number of transmitters that are encoded, interleaved and modulated independently.

- Vertical: first, the data stream is encoded, interleaved and modulated. Then, the resulting symbols are demultiplexed into sub-streams equal to the total number of transmit antennas.

- Diagonal: this encoding case is similar to the horizontal case and the only difference is that the sub-streams of symbols undergo a stream interleaver, i.e. it has a diagonally-layered coding structure in which the sub-streams are dispersed across diagonals in space-time.

An example of a spatial multiplexing scheme is the vertical Bell Laboratories layered space-time (V-BLAST) architecture [16], which requires complex detection and equal or higher number of antennas at the receiver side compared to the transmitter side. In V-BLAST, the information data is treated

according to the vertical encoding case. The transmitted symbols are independent of each other and each set of symbols is dispersed in space-time through the transmit antenna array.

The V-BLAST scheme has the characteristics of an interference avoidance technique since each received signal is treated as an interferer to the rest and the best received signal in terms of SNR is selected for detection. Then, this selected signal is removed from the remaining signals, which have one interferer less.

2.1.3 Precoding

MIMO requests to separate data streams which is one of the main difficulties in the detection process. The pre-coding or pre-equaliser method of generating the transmitted signals for MIMO systems needs to have the CSI at the transmitter. The CSI is obtained for a fixed channel (non-mobile) or an approximately constant channel over a reasonably large time period.

When CSI is available at the transmitter side, the transmitted symbols can be partially separated by means of pre-equalisation at the transmitter. There are two types of systems, in which the pre-coding may separate the data streams [7]:

- MIMO Single-user systems: as only one user is served over multiple streams, is assumed that out-of-cell interference is treated as additional Gaussian noise by the base station and users. Then, the channel model is reduced to a point-to-point MIMO channel. Therefore, the equalisation is divided between the transmitter and the receiver. A popular strategy is based on the singular value decomposition of the channel matrix. In this scheme, neither transmit power is increased, nor channel noise is enhanced.

- MIMO Multi-user systems: since there is no collaboration between receivers, a joint procedure is not possible. Therefore, the schemes for single-user systems cannot be applied and schemes such as *QR factorization* are applied to the channel matrix.

2.1.4 MIMO Drawbacks

As was explained, on one hand diversity techniques increase the robustness of the signal path but not the data rates. On the other hand, spatial multiplexing increases the channel capacity with the addition of transmit and receive antennas. Therefore, some hybrid encoding schemes have been suggested which increase diversity [17] and capacity [18] at the cost of increased computational complexity. Also, diverse constrains have been identified in the implementation of MIMO transmission schemes that have not been fully investigated [2, 19, 20], for instance:

- There is high inter-channel interference (ICI) at the receiver in BLAST transmission systems due to simultaneous transmissions from multiple antennas.

- The algorithm complexity of the receiver increases due to the presence of high ICI.

- Performance of BLAST schemes degrades significantly under non-ideal channel conditions [20].

- The above limitations are overcome with full diversity STCs [14, 18]. However, full-diversity STC systems can achieve maximum spectral efficiency of one symbol per symbol duration for any number of transmitters. Therefore, full-diversity STCs need to use higher modulation schemes to achieve similar spectrum efficiency to that of BLAST techniques at the cost of reduced reliability.

- To obtain efficient operation, the number of transmitters in BLAST schemes must be smaller than or equal to the number of receivers [21]. On the other hand, STCs can be designed for different number of transmitters and receivers. However, the design of STCs for more than two transmitters decreases the data rate to achieve full diversity.

2.2 Spatial Modulation

As previously mentioned, there is a wide range of MIMO transmission techniques available, notably STCs, spatial multiplexing and the hybrid transmission technique multi-layered STCs [18] in cases where CSIT is not available. STCs exploit the additional diversity of multiple antennas to combat channel fading. It aims to improve the reliability of the link by transmitting multiple replicas of the same information through independent fading paths [22] which also reduces the probability of signal fades. Spatial multiplexing exploits multiple antennas to increase transmission rate. The V-BLAST architecture requires complex detection and an equal or greater number of antennas at receiver. Some hybrid encoding schemes have been suggested to achieve a tradeoff between diversity and capacity in [17] and [18]. Despite the attractive benefits offered by the above schemes, they have drawbacks in common described in the previous section. The mentioned disadvantages stimulate the continuous research in multiple antenna transmission.

Recently, one technique named spatial modulation (SM) [4, 8] has been proposed to deal with the previously mentioned MIMO issues. In SM, only one transmit antenna is active at any instant. The index of the active transmitter can carry information, this increases the spectral efficiency. This feature makes SM different from other MIMO schemes such as space-time bit-interleaved coded modulation [23], in which the antenna pattern is part of the spatial constellation but in SM does have an impact, improving the spectral efficiency.

SM increases the spectral efficiency since it extends the constellation into three dimensions: a spatial dimension in addition to the two at the complex plane usually used. For that reason, SM is a spatial multiplexing MIMO technique that increases the spectral efficiency to overcome the ICI. The spectral efficiency is improved because the transmit antenna index carries additional information.

The SM research shows that performance can be improved by reducing computational complexity in comparison to other MIMO schemes [8, 24, 25]. SM enables just one transmitter to radiate power at any time. Thus, the inter-antenna-interference (IAI) and multiple radio frequency (RF) chains can

easily be avoided at the transmitter side. The technique assumes that the information can be delivered by the station whether the transmit antennas are switched on or off.

The general concept of SM is to map the symbol information bits into two blocks: the first block is a unique transmit antenna index, which is selected from the set of transmitters in the antenna array (the three-dimensional spatial-constellation diagram Fig. 2.3, proposed in [25]) and the second block is an APM symbol, which is chosen from a complex signal-constellation diagram [4].

Fig. 2.3 demonstrates two unique characteristics of SM:

1. The three-dimensional diagram is generated with the APM signal-constellation diagram (PSK or QAM modulation schemes) and a third dimension is provided by the antenna array (spatial dimension).

2. The active transmitter may change at every channel realisation according to the bits of the first block symbol. Then, the antenna switch performs effectively as a mapper of the first block, increasing the transmission rate. This principal is proposed in [26].

The transmission process begins with the bit stream being mapped into symbols, which are divided into two blocks. The first block contains $\log_2(N_t)$ bits and the second block $\log_2(M)$, where M is the total number of APM symbols. Then, the length of the SM symbol is $\log_2(N_t) + \log_2(M)$. Thus, the receiver solves the $N_t \times M$ hypothesis detection problem to estimate both blocks jointly to properly decode the SM transmitted symbol. SM obtains high capacity through the joint ML decoding technique for the data streams at the receiver. The ML-optimum decoder calculates the Euclidean distance between the received signal and the set of the total SM symbols. However, the complexity of this decoder increases exponentially with higher number of transmitters or high APM constellations [8, 9, 24, 27, 28, 29].

Therefore, SM is a spatial multiplexing MIMO scheme which offers multiplexing gain with a single antenna system without requiring extra bandwidth

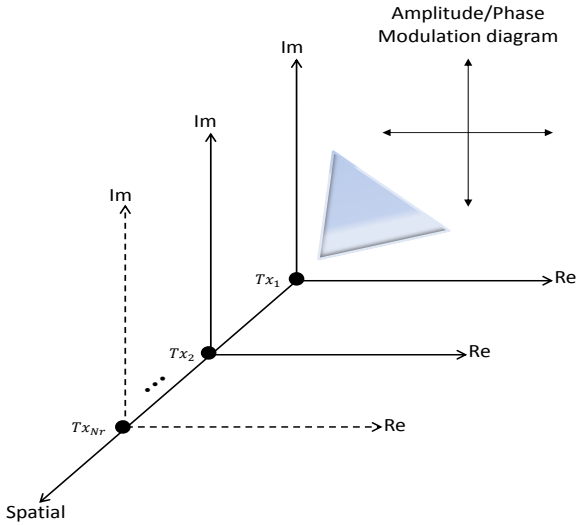

Figure 2.3: *SM constellation diagram.*

or extra transmission power. At the receiver, SM is designed for ML-optimum decoding [4, 30].

Potentially, SM has many promising application areas due to its wide range of features and characteristics previously mentioned. Among these potential applications are:

- Recently, SM has been considered in green wireless communications due to its energy efficient design. In traditional MIMO schemes, it is possible to reduce the power consumption through the diversity and multiplexing gains [31]. However, these schemes do not take the static power consumption of the circuits into account. The work presented in [32, 33, 34] has shown that systems using single-antenna transmission are more energy efficient than traditional MIMO schemes if the total dissipated power (circuit and RF chains) is taken into consideration. Thus, SM increases the spectral efficiency when passive transmitter elements are used with only a single RF chain. It also avoids the static power consumption of the power amplifiers. SM also decreases the RF power consumption

through the diversity and multiplexing gains achieved by the transmitter hop encoding with the aim of reducing the use of only a few active RF chains. All these considerations show the potential energy saving in terms of green wireless networks, which are expected to be considered more as a compulsory feature than an additional benefit in future wireless communication systems [3].

- Other potential techniques for future wireless applications are relaying and user cooperation [35]. Cooperative communications improve the transmission resources, which brings some benefits such as decreasing the extra bandwidth required and minimising the resources of the network nodes (relays). The combination of SM with relaying may bring some benefits such as:
  - Reduced transmit power and increased diversity: consider a relay equipped with multiple antennas in the downlink cellular network. Under this condition, SM transmission can be used instead of traditional MIMO to improve the performance and to achieve power gains due to the SM characteristics previously mentioned [36].
  - Energy and spectral efficiency in the uplink transmission: as only a single RF chain is used for transmission, the SM scheme may be exploited during uplink where the terminals can construct a large scale virtual MIMO system. Thus, the indices of the terminals are encoded into the information bits, which are spread across the spatial domain, similar to SM during downlink [37].
  - Energy and spectral efficiency relay-aided transmission: the spatial-constellation diagram shown in Fig. 2.3 illustrates SM's ability to improve the bandwidth efficiency of half-duplex relaying due to the addition of the spatial dimension. The APM-constellation diagram conveys the data from the source and the spatial-constellation diagram conveys the data from the relay. Then, both data symbols may be transmitted at the same channel, which enhances the energy and spectral efficiency [3, 38, 39].

- SM may also be considered for visible light communications (VLC). The VLC concept was introduced in 1880 and then not used for many years until 1979 in [40]. Recently, VLC has sparked interest due to the congestion with the RF spectrum, which has been used for wireless communication systems. Optical SM was introduced in [41], which follows the same principle as for RF application. The information data is mapped into the index of a single light-emitting diode (LED) and into the light intensity level. The results show that having some idle LEDs at transmission reduces the channel's correlation, which enhances the spatial multiplexing and SM performances. These characteristics make VLC a promising scheme for MIMO techniques.

- The single-RF and large-scale MIMO systems are two techniques with promising fields of research in future wireless communication systems. The combination of these techniques may lead to the development of a new air interface, which can offer flexibility in energy and spectrum efficiency, complexity, error probability, reliability, etc. SM may avoid two major problems in large-scale MIMO schemes: power consumption/dissipation and high-cost hardware design [4].

Although SM has many benefits, the scheme also has some disadvantages [4] such as:

- Suboptimal spectrum efficiency: as not all the transmitters are active, SM offers a lower throughput than spatial multiplexing. SM needs a larger number of transmitters to achieve the same spectral efficiency as spatial multiplexing.

- Training overhead: the throughput of SM increases logarithmically with the number of transmitters. Even though conventional SM schemes are open loop and do not need CSIT, the receiver still needs to estimate the channel impulse responses of all the transmitters for ML demodulation. Then, large-scale SM implementation may incur in a non-negligible training overhead for channel estimation. However, if close-loop SM schemes

are considered, the feedback overhead for CSIT reporting needs to be taken into consideration.

- Fast antenna switching: as a single antenna is used in every channel use, the RF implementation needs a sufficiently fast switch operating at the symbol rate that introduces low insertion/switching losses. Then, high-speed RF switches represent an important challenge for the transmitter design.

- Propagation conditions: the efficient of SM schemes depend on the radio environment, which implies that the channel impulse responses of the transmit-to-receive links are different enough from each other. In fact, the channel impulse responses represent the unique points of the spatial-constellation diagram, which implies the demodulation process is easier when there is a larger difference between them. As a consequence, the lack of scattering in the propagation environment degrades the error probability and the energy efficiency.

2.3 Massive MIMO

Multiple-antenna technology for wireless communications is becoming prominent and incorporated into emerging wireless broadband standards such as LTE and 5G. As mobile data traffic exponentially increases, further capacity enhancement is needed. The more antennas the transmitter/receiver is equipped with, the more the possible signal paths, the better the performance in terms of data rate and link reliability. However, there are disadvantages associated with this, such as increased complexity of the hardware (number of RF amplifier front-ends) and the complexity and energy consumption of the signal processing at both ends [42].

It has been suggested that massive MIMO (also known as large-scale MIMO, hyper MIMO, full-dimension MIMO and Argos[1]) is becoming very different

[1] Argos is a giant with 100 eyes in the Greek mythology. Then, Argos' vision is analogous to the increased capacity of tens-antennas at the base station.

from current practice through the use of a large excess of service-antennas over active terminals and time division duplex (TDD) mode. The use of extra antennas helps to steer energy into precise regions of space to improve the overall throughput and radiated energy efficiency. This technique includes other benefits such as: reduced latency, simplified media access control (MAC) layer and increased robustness to intentional jamming [43].

This technology benefits from all the advantages of traditional MIMO systems but is used on a greater scale. The channel acquisition in massive MIMO is essential, which is rather difficult particularly for the downlink. Therefore, TDD mode with channel reciprocity is adopted in most of the research [44, 45] because for massive MIMO systems, a good channel knowledge is required on both sides [42]. On the uplink, the process is simple as the base station estimates the channel responses of the pilots sent by the terminals. The downlink on the other hand, involves a more complicated procedure as the terminals have to estimate big amount of channel responses which are proportional to the number of antennas at the base station. Thus, the downlink pilots and CSI feedback consume a big amount of the system capacity. The base station sends pilots for which the terminals have to estimate their channel response. This is not feasible in massive MIMO systems because the amount of time/frequency resources utilised for downlink pilots is proportional to the number of antennas therefore it would require hundreds of times more resources than conventional systems. Generally, operating in TDD mode with reciprocal channel is the solution [45].

The anticipated throughput depends on the propagation environment providing asymptotically orthogonal channels to the terminals. However, massive MIMO faces other challenges [43] such as:

- Making low cost and low precision components that work efficiently together.
- Reducing the complexity in design, acquisition and synchronisation for terminals.
- Reducing power consumption which results in energy reductions.

- Exploiting of excess degrees of freedom.
- Improving TDD calibration.
- Developing techniques to avoid pilot contamination and easier channel estimation measurements.

2.4 Lattice Basis Reduction

Transmission techniques based on SM seems to be a good candidates for being used in large-scale MIMO systems due to its capabilities previously mentioned. However, SM techniques utilise the ML detector [4], which can be infeasible in the large-scale MIMO implementation. It is well-known that using the ML algorithm to implement as a sequence estimator is the optimal way to remove the effect of ISI for digital transmission communication systems. However, the implementation of this algorithm may be infeasible for practical implementation when the number of antennas and/or the constellation size is large because the decoding complexity exponentially increases. For high-rate transmission systems, the performance of symbol-to-symbol estimation becomes inaccurate since the ISI cannot be solved by simply raising the transmitted power. Linear equalisers do not perform as well as the ML detector.

Linear equalisers are possible solutions [46] for lower complexity detection schemes. However, for ill-conditioned channels these techniques show an inferior performance compared to the ML detector. The concept of basis reduction was proposed more than a century ago [47] to find simultaneous rational approximations to real numbers and to solve the integer linear programming problem in fixed dimensions. The main purpose of lattice basis reduction is to find a good basis for a given lattice. A basis is considered to be good when the basis' vectors are close to orthogonal. The concept of LR is to find a reduced set of basis vectors for a given lattice to obtain certain properties such as short and nearly orthogonal vectors [47].

A lattice can be represented by many different bases. A lattice is a set of discrete points representing integer linear combinations of linearly independent vectors, which are called basis. Given n linearly independent vectors

$c_1, c_2, ..., c_n \in \mathbb{R}^n$, the lattice generated by them is defined as $\mathcal{L}(c_1, c_2, ..., c_n) = \{\Sigma_{i=1}^{n} s_i c_i | s_i \in \mathbb{Z}\}$. The $c_1, c_2, ..., c_n$ are referred to as the basis of the lattice [48].

The representation of MIMO systems as a lattice and decoding them with a lattice scheme, was first introduced in [49]. In this approach, the authors separate the imaginary and real part of the channel matrix to get the lattice representation of the channel model. The LR technique is exploited to improve BER performance in wireless MIMO systems [46, 50, 51, 52], in which detectors are used for MIMO systems to achieve performance with full diversity and low complexity. In [50, 51, 53, 54], the results show the LR improvements over linear detectors with only a small increase in complexity. LR can be applied to MIMO systems to achieve a better conditioned channel matrix by improving its orthogonality conditions. Arjen Lenstra, Hendrik Lenstra and Laszlo Lovász introduced the LLL algorithm, as a polynomial-time lattice reduction. It was proposed in 1982 and used in fields such as computer algebra, cryptology and algorithmic number theory [55]. The original applications of the LLL algorithm were to give polynomial time algorithms for factorizing polynomials, to find simultaneous rational approximations to real numbers and to solve the integer linear programming problem in fixed dimensions. For all its features, the LLL algorithm is adopted by LR for being used in combination with linear detectors in MIMO systems [56].

Taking the received signal in a MIMO system as:

$$\mathbf{y} = \mathbf{Hx} \ + \ \mathbf{v}, \tag{2.1}$$

where $\mathbf{H}, \mathbf{x}$ and $\mathbf{v}$ are the channel matrix, the transmit signal and the noise vector respectively. $\mathbf{x} \in \mathbb{Z}$, $\mathbf{Hx}$ forms a lattice spanned by the columns of $\mathbf{H}$ [10].

Therefore, the detector estimates $\mathbf{x}$ as the lattice point closest to $\mathbf{y}$. To guarantee a correct estimation, the lattice basis must be orthogonal or close to that. This does not affect the performance of the ML detector, since it performs the same without taking the channel conditions into account. However, the channel conditions are important when other detectors are used and the performance degrades when the orthogonal conditions are not satisfied.

To quantify the orthogonality of a matrix, the orthogonality deficiency (*od*) [57] for a matrix $\mathbf{H}$ is defined as:

$$\mathrm{od}(\mathbf{H}) = \mathbf{1} - \frac{\det(\mathbf{H}^H\mathbf{H})}{\prod_{\mathbf{n=1}}^{\mathbf{N_t}} \|\mathbf{h}_n\|}, \tag{2.2}$$

where $\mathbf{h}_n$ is the nth column of the channel matrix $\mathbf{H}$. It is important to note that $0 \leq \mathrm{od}(\mathbf{H}) \leq 1$. If $\mathrm{od}(\mathbf{H}) = 1$, $\mathbf{H}$ is singular and when $\mathrm{od}(\mathbf{H}) = 0$ all the columns of $\mathbf{H}$ are orthogonal. Generally, it is not possible to get $\mathrm{od}(\mathbf{H}) = 0$. If $\mathrm{od}(\mathbf{H})$ is close to "0", it is said that $\mathbf{H}$ is close to being orthogonal.

Figure 2.4, the LLL algorithm procedure is illustrated. δ is the parameter which controls the performance and complexity of the LLL algorithm, it is randomly selected from $(\frac{1}{2}, 1)$, to guarantee a firm basis reduction. However, the computational complexity increases with larger values of δ [11, 54]. The output of the LLL algorithm is an unimodular matrix $\mathbf{T} \in \mathbb{Z}$ with the following properties: it is formed only by integers and its determinant is ± 1. Then, the channel matrix with better orthogonal conditions is calculated as: $\tilde{\mathbf{H}} = \mathbf{HT}$.

The fundamental principle, as previously stated, is to combine a lattice reduction approach with low complexity linear detectors to establish an effective channel matrix $\tilde{\mathbf{H}}$. Therefore, if the matrix $\tilde{\mathbf{H}}$ represents a new basis from the same lattice which is more orthogonal than $\mathbf{H}$, it is anticipated that the performance using linear equalisers should be closer to that of the ML detector. The new channel matrix $\tilde{\mathbf{H}}$ is obtained through the LR technique. The LLL is the most popular algorithm used in LR aided detectors because in spite of not guaranteeing that the optimal basis will be found, it guarantees finding a basis with a better value of *od*. In attempting to find a new basis using the LLL algorithm, the highest complexity in terms of number of arithmetic operations is $\mathcal{O}(R^4)$, where R is the size of the basis [52].

2.5 Summary

MIMO systems have been studied to overcome fading and to create wireless communication systems with high reliability and high data rate. The main idea behind MIMO is to spread the signals in the spatial domain at both the

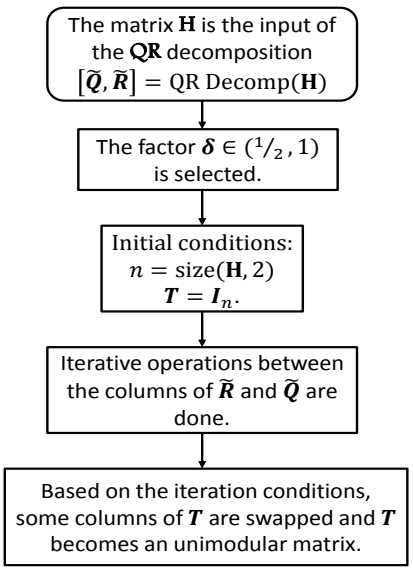

Figure 2.4: *The LLL algorithm block diagram.*

transmitter and receiver side. Then, they are combined to generate effective parallel spatial data sub-streams (spatial multiplexing) and/or improve the BER performance through the diversity.

Higher data rates are required to satisfy the user demands and services. Recently, large-scale MIMO or massive MIMO has been introduced as a good alternative to accomplish these aims. Massive MIMO is a traditional MIMO but with a larger number of antennas at both ends. Increasing only the antennas may supply the need for increased data rate but this solution is not optimal due to the high cost of RF-chains and the power consumption. Additionally, future standards are focusing not only on the improvement of the spectral efficiency, but also the systems' energy efficiency. Thus, the SM scheme which is a 13-year old technology, seems to be a good solution to solve these issues. The research community recommends the SM's features to be exploited by massive MIMO since SM increases the spectral efficiency by making use of the index of the active transmitter and reduces the amount of RF-chains used, as only a single transmitter is active at any time.

In this chapter the concept of LR was also introduced, where the main idea is to treat the channel matrix $\mathbf{H}$ as a lattice. Then, through the LLL algorithm, it is possible to find a channel matrix with better conditions in terms of orthogonality. This procedure of transforming a basis into a reduced one is called a basis reduction algorithm, which in combination with a linear equaliser can improve the system performance keeping lower complexity than the optimal ML.

Chapter 3

Spatial Phase Shift Keying Modulation

3.1 Introduction

MIMO has attracted intensive research due to its improved transmission rate and/or robustness compared to single antenna systems [24] as discussed in Chapter 2. Also, in Chapter 2, SM was introduced which is designed to reduce the number of RF chains while preserving comparable performance with full MIMO schemes. SM offers a considerable reduction of the receiver complexity as compared to V-BLAST since only a single antenna is used for transmission.

Generalized space shift keying (GSSK) was introduced in [58] and it is considered as an SM variation that uses multiple transmitters. However, GSSK transmits only energy on the active antennas. This motivated the design of a scheme which transmits phase shift keying (PSK) signals on the selected antennas, which provides higher spectrum efficiency with similar receiver complexity.

Spatial phase shift keying (SPSK) modulation conveys information by exploiting both the antenna index and conventional APM symbols. At each symbol period, part of the information is carried by the antenna indices as in GSSK. The remaining part of the information is conveyed by the M-ary PSK symbols transmitted by the selected antennas. In this way, the proposed scheme greatly improves the spectrum efficiency compared to GSSK and SM.

At the receiver, both the index and the transmitted symbol are estimated based on the ML principle. SPSK utilises the same ML decoding scheme, so the complexity of decoding does not change. However, the proposed SPSK scheme offers better BER performance than GSSK. The average BER performance is analysed by deriving a tight upper bound, which is used to determine the optimum criterion to choose the appropriate modulated symbols to be transmitted on the selected antennas.

3.2 System Model

The SPSK system model is shown in Figure 3.1. The general system model consists of a MIMO wireless link with N_t transmit and N_r receive antennas. During the transmission of SPSK, not all antennas are active. The number of selected antennas is denoted as n_t. In this modulation scheme, the indices of the active antennas are determined by the transmitted information bits. For each symbol period, a block of information bits is divided into two parts: the first part is used to select n_t active antennas from N_t and the second part is used to determine the transmitted signals on the active antennas, which have the same amplitude but different phases. In this way, the group of bits are mapped to a size $N_t \times 1$ transmission vector, referred to as the transmission vector in this chapter and denoted as $\mathbf{x} = [x_1, \quad x_2, \quad \cdots, \quad x_{N_t}]^T$. The transmission vector is conveyed over a $N_r \times N_t$ wireless channel $\mathbf{H}$. The received signal is given by $\mathbf{y} = \sqrt{\rho}\mathbf{H}\mathbf{x} + \mathbf{v}$, where $\mathbf{v} = [v_1, \quad v_2, \quad \cdots, \quad v_{N_r}]^T$ represents the additive white Gaussian noise (AWGN) and ρ is the average signal-to-noise ratio (SNR) at each receive antenna. Both $\mathbf{H}$ and $\mathbf{v}$ have independent and identically distributed (i.i.d.) entries with $\mathcal{CN}(0, 1)$. At the receiver, the indices of the active antennas and the phases of the signals are estimated by the SPSK detector, and de-mapped into the transmitted bits.

3.3 Transmission

Figure 3.1 shows that for each symbol period, a block of independent information bits, denoted as $\mathbf{b} = [b_1 \quad b_2 \quad \cdots \quad b_m]$, is sent to the SPSK mapper. The

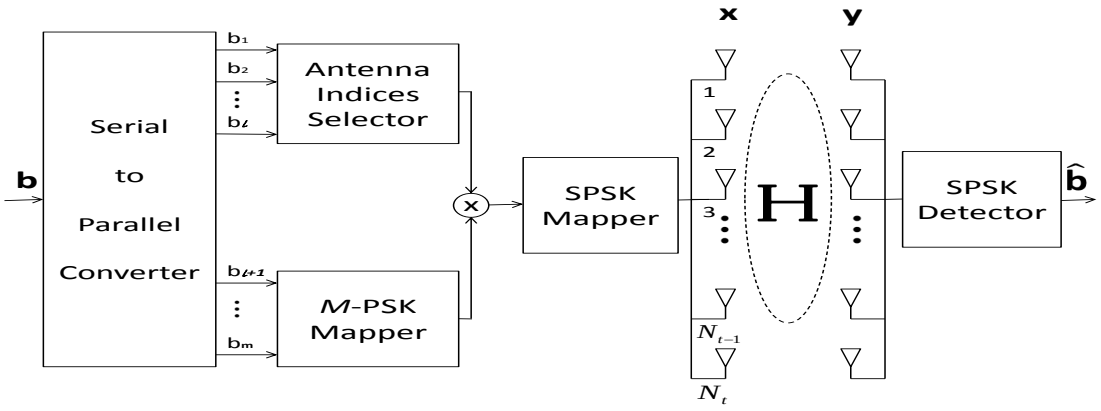

Figure 3.1: *SPSK system model*

SPSK symbol has a length of m bits. The SPSK symbol vector $\mathbf{b}$ is divided into two blocks:

- The first l bits are used to determine the indices of the n_t active antennas, where

$$l \leqslant \lfloor \log_2 M' \rfloor, \tag{3.1}$$

$$M' = \binom{N_t}{n_t}. \tag{3.2}$$

  Clearly, 2^l must be smaller than or equal to M'. Hence the maximum number of bits which can be conveyed by n_t antenna indices is $\lfloor \log_2(M') \rfloor$. Assuming the CSI is only available at the receiver, $\mathbf{c} = 2^l$ antenna combinations are randomly selected from the overall M' possibilities.

- The remaining $m - l$ bits indicate the M different phases. $M = 2^{m-l}$ and each phase is represented as $e^{i\phi}$. All signals have the same amplitude of $\frac{1}{\sqrt{n_t}}$ to ensure unity power transmission, they are distinguished by their phases and the positions of the transmit antennas.

The SPSK symbol vector $\mathbf{b}$ is mapped into a transmission vector denoted as $\mathbf{x} = [x_1, \quad x_2, \quad \cdots, \quad x_{N_t}]^T$. A spatial vector $\mathbf{s}$ collects the indices of the active antennas, $\mathbf{s} = [s_1, \ s_2, \ \cdots, \ s_{n_t}] \in [1, \cdots, N_t]$. The value of $\mathbf{s}$ is chosen

by the first l bits. Then, the phase vector is $\mathbf{p} = [\frac{1}{\sqrt{n_t}}e^{i\phi_1}, \frac{1}{\sqrt{n_t}}e^{i\phi_2}, ..., \frac{1}{\sqrt{n_t}}e^{i\phi_{n_t}}]$, selected by the second block. Therefore, the transmission vector is expressed as

$$x_n = \begin{cases} 0, & n \notin \mathbf{s} \\ \mathbf{p}(k), & n \in \mathbf{s}, n = \mathbf{s}(k), \end{cases} \tag{3.3}$$

for $n = 1, ..., N_t$ and $k = 1, ..., n_t$. Figure 3.2 illustrates an example of SPSK transmission process using the following setup: $N_t = 5$, $n_t = 2$ and $M = 2$. Then, $l = \left\lfloor \log_2 \binom{5}{2} \right\rfloor = 3$, $m = \log_2(M) + l = 4$. So, the SPSK symbol transmits 4 bits.

As defined earlier, the transmission vector contains the phase values transmitted by the n_t active antennas. All the signals have the same amplitude but different phases, i.e. the phases are selected based on Figure 3.3, where the circumference of a circle with radius of $\frac{1}{\sqrt{n_t}}$ to ensure unity power transmission.

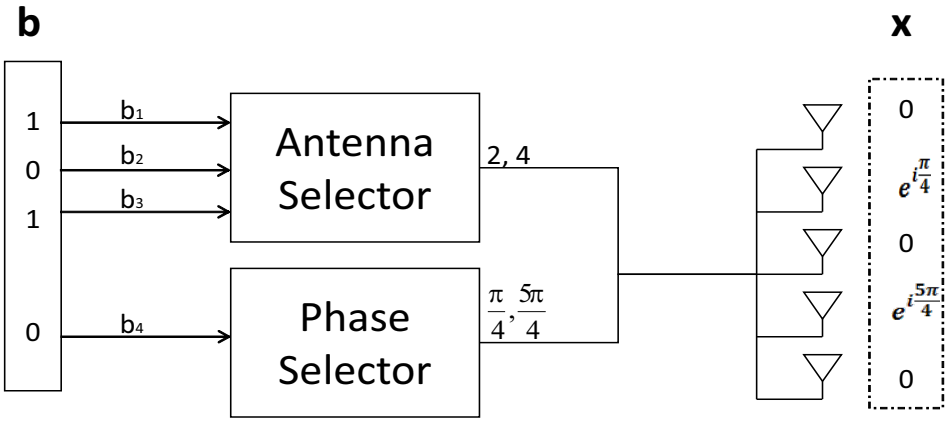

Figure 3.2: 2-*SPSK transmission system model with a specific example which selects* 2^{nd} *and* 4^{rd} *antenna to transmit* $\frac{\pi}{4}$ *and* $\frac{5\pi}{4}$.

3.3.1 Proposed Mapping Design

In Section 3.3, the transmission design of the proposed SPSK was discussed, where the phases were randomly selected. However, in order to guarantee a better performance, the selection principle's aim is to maximise the distance

between the transmission vectors in the 2^l dimension space. Figure 3.3 shows the potential transmit phases, which can be selected. The selection criteria is to maximise the distance between the M transmit vectors, which contain n_t phases selected on the circle shown in Figure 3.3. This can be explained more clearly with the following example: 2-SPSK (Section 3.3.2), 4-SPSK (Section 3.3.3) and 8-SPSK (Section 3.3.4). When $M > 8$, it has been found that the transmission performance of the system significantly degrades as in the conventional modulation systems. This is due to the fact that the difference between the used phases decreases in the signal vectors, the Euclidean distance between transmission vectors also decreases and this increases the probability of erroneous detection. For this reason, this chapter only investigates M-SPSK with M=2, 4 and 8. Figure 3.3 illustrates all the possible points transmitted in the proposed modulation schemes. The M different phases must be selected from these points in such a way that the distance between the transmission vectors is maximized to achieve the best performance. Figure 3.4 illustrates the geometric model, which represents the transmission vector in the 2^l dimensional space.

The mapping tables (Tables 3.1, 3.2 and 3.3) are described for $M = 2$, 4 and 8 respectively. To transmit the m information bits, the number of possible transmission vectors is 2^m for each table. For convenience, an index vector is defined as $\mathbf{j} = [\mathbf{s},\ q]$, $q \in [0,\ \ldots, M-1]$, to identify the transmission vector in the mapping table, where $\mathbf{s}$ is the index vector and q is the index of the APM symbol. Since $\mathbf{j}$ is unique for each transmission vector, correctly decoding $\mathbf{j}$ will de-map the bit information successfully.

In order to compare the SPSK performance system with the work proposed in [58], the SPSK scheme is examined for $M = 2$, 4 and 8 under the same system configuration: $N_t = 5$, $n_t = 2$ and $N_r = 4$.

3.3.2 2-SPSK modulation scheme

In this section, SPSK is analysed with $M = 2$, where 2 different phases are selected as shown in Figure 3.2. The 2-SPSK parameters are $N_t = 5$, $n_t = 2$ and $M = 2$. Then, $l = \left\lfloor \log_2 \binom{N_t}{n_t} \right\rfloor = 3$, $m = \log_2(2) + l = 4$ and the total

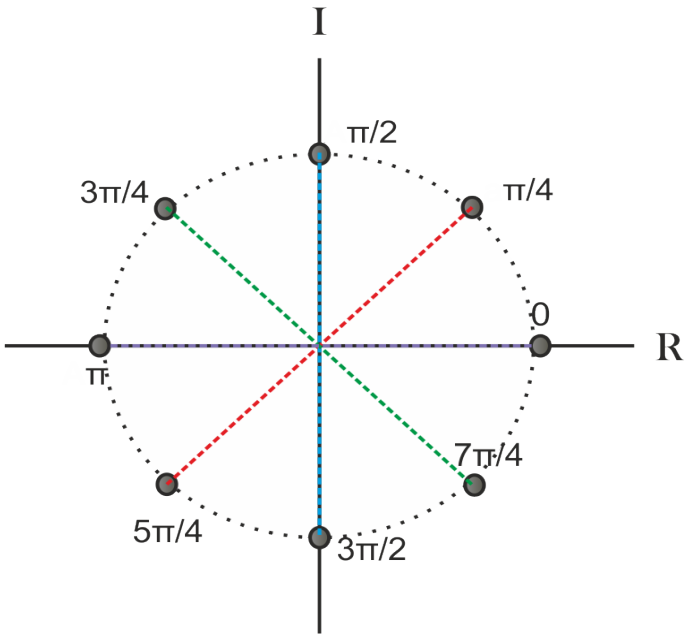

Figure 3.3: *Phase constellation circumference diagram*

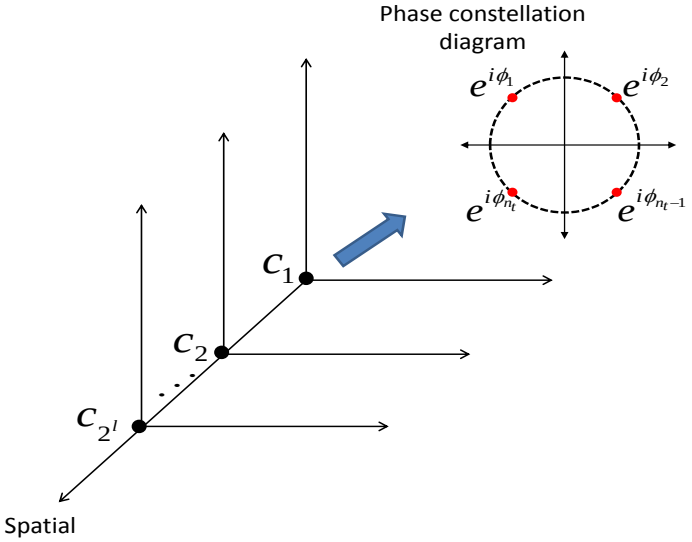

Figure 3.4: *SPSK geometric model.*

number of transmission vectors $2^4 = 16$. The first three bits $[b_1, b_2, b_3]$ are used to choose one set of n_t antennas. Note that the 2^l selection from the overall M' combinations is random in this chapter assuming no CSI available at the transmitter. 2-SPSK is designed to transmit one more bit per symbol (b_4) compared to the GSSK system proposed in [58]. This additional bit identifies two sets of phases from Figure 3.3 to be transmitted by the n_t active antennas.

The value of the signal vector $[\frac{1}{\sqrt{n_t}}e^{i\phi_1}, \frac{1}{\sqrt{n_t}}e^{i\phi_2}]$ is selected by the fourth bit b_4 as follows: for $b_4 = 0$, the phases selected are $\phi_1 = \frac{\pi}{4}$ and $\phi_2 = \frac{5\pi}{4}$, corresponding to the two points at the ends of the red diameter shown in Figure 3.3. For $b_4 = 1$, the phases selected are $\phi_1 = \frac{5\pi}{4}$ and $\phi_2 = \frac{\pi}{4}$, corresponding to the same two points at the ends of the red diameter in Figure 3.3, but with a phase shift of π. Clearly, the distance between these two vectors, with different b_4 only, is the maximum possible. Note that the selection of the diameter is random (a phase rotation has no material effect). The mapping table for this scheme is illustrated in Table 3.1, in which the first column shows the four transmission bits. The second column shows the vector $\mathbf{j}$, containing the indices of active antennas, which are enclosed in a pair of parentheses, and the index of the corresponding index of the APM symbol, q. Finally, the third column is the corresponding transmission vector. For example, the four bits: [1 0 1 1] are mapped to a transmission vector $\left[0, \ \frac{e^{i\frac{5\pi}{4}}}{\sqrt{2}}, \ 0, \ \frac{e^{i\frac{\pi}{4}}}{\sqrt{2}}, \ 0\right]$ (i.e. to transmit $\frac{e^{i\frac{5\pi}{4}}}{\sqrt{2}}$ and $\frac{e^{i\frac{\pi}{4}}}{\sqrt{2}}$ on the second and fourth antenna), with $\mathbf{j} = [(2, 4), \ 1]$.

3.3.3 4-SPSK modulation scheme

The 4-SPSK parameters are $N_t = 5$, $n_t = 2$ and $M = 4$. The number of different sets of phases is $M = 4$, which can convey two bits. Therefore, the total number of bits transmitted per symbol is $m = \log_2(4) + l = 5$ ($l = 3$ as in 2-SPSK) and this makes the total number of transmission vectors $2^5 = 32$. As in 2-SPSK, the first three bits $[b_1, b_2, b_3]$ select the active antenna indices, using the same mapping rule as in 2-SPSK (shown in Table 3.1). The last two bits $[b_4, b_5]$ determine the transmitted signals on the two active antennas. Then, this pair of bits generates four possible phase combinations, which will

Table 3.1: *Mapping table of a 2-SPSK scheme with the proposed selection of phase constellation points*

$\mathbf{b} = [b_1\ b_2\ b_3\ b_4]$	$\mathbf{j}$	$\mathbf{x_j} = [x_1 \quad x_2 \quad \cdots \quad x_5]^T$
[0 0 0 0]	[(1,2), 0]	$\left[\frac{e^{i\frac{\pi}{4}}}{\sqrt{2}} \quad \frac{e^{i\frac{5\pi}{4}}}{\sqrt{2}} \quad 0 \quad 0 \quad 0\right]^T$
[0 0 0 1]	[(1,2), 1]	$\left[\frac{e^{i\frac{5\pi}{4}}}{\sqrt{2}} \quad \frac{e^{i\frac{\pi}{4}}}{\sqrt{2}} \quad 0 \quad 0 \quad 0\right]^T$
[0 0 1 0]	[(1,3), 0]	$\left[\frac{e^{i\frac{\pi}{4}}}{\sqrt{2}} \quad 0 \quad \frac{e^{i\frac{5\pi}{4}}}{\sqrt{2}} \quad 0 \quad 0\right]^T$
[0 0 1 1]	[(1,3), 1]	$\left[\frac{e^{i\frac{5\pi}{4}}}{\sqrt{2}} \quad 0 \quad \frac{e^{i\frac{\pi}{4}}}{\sqrt{2}} \quad 0 \quad 0\right]^T$
[0 1 0 0]	[(1,4), 0]	$\left[\frac{e^{i\frac{\pi}{4}}}{\sqrt{2}} \quad 0 \quad 0 \quad \frac{e^{i\frac{5\pi}{4}}}{\sqrt{2}} \quad 0\right]^T$
[0 1 0 1]	[(1,4), 1]	$\left[\frac{e^{i\frac{5\pi}{4}}}{\sqrt{2}} \quad 0 \quad 0 \quad \frac{e^{i\frac{\pi}{4}}}{\sqrt{2}} \quad 0\right]^T$
[0 1 1 0]	[(1,5), 0]	$\left[\frac{e^{i\frac{\pi}{4}}}{\sqrt{2}} \quad 0 \quad 0 \quad 0 \quad \frac{e^{i\frac{5\pi}{4}}}{\sqrt{2}}\right]^T$
[0 1 1 1]	[(1,5), 1]	$\left[\frac{e^{i\frac{5\pi}{4}}}{\sqrt{2}} \quad 0 \quad 0 \quad 0 \quad \frac{e^{i\frac{\pi}{4}}}{\sqrt{2}}\right]^T$
[1 0 0 0]	[(2,3), 0]	$\left[0 \quad \frac{e^{i\frac{\pi}{4}}}{\sqrt{2}} \quad \frac{e^{i\frac{5\pi}{4}}}{\sqrt{2}} \quad 0 \quad 0\right]^T$
[1 0 0 1]	[(2,3), 1]	$\left[0 \quad \frac{e^{i\frac{5\pi}{4}}}{\sqrt{2}} \quad \frac{e^{i\frac{\pi}{4}}}{\sqrt{2}} \quad 0 \quad 0\right]^T$
[1 0 1 0]	[(2,4), 0]	$\left[0 \quad \frac{e^{i\frac{\pi}{4}}}{\sqrt{2}} \quad 0 \quad \frac{e^{i\frac{5\pi}{4}}}{\sqrt{2}} \quad 0\right]^T$
[1 0 1 1]	[(2,4), 1]	$\left[0 \quad \frac{e^{i\frac{5\pi}{4}}}{\sqrt{2}} \quad 0 \quad \frac{e^{i\frac{\pi}{4}}}{\sqrt{2}} \quad 0\right]^T$

[1 1 0 0]	[(2,5), 0]	$\left[0 \quad \frac{e^{i\frac{\pi}{4}}}{\sqrt{2}} \quad 0 \quad 0 \quad \frac{e^{i\frac{5\pi}{4}}}{\sqrt{2}}\right]^T$
[1 1 0 1]	[(2,5), 1]	$\left[0 \quad \frac{e^{i\frac{5\pi}{4}}}{\sqrt{2}} \quad 0 \quad 0 \quad \frac{e^{i\frac{\pi}{4}}}{\sqrt{2}}\right]^T$
[1 1 1 0]	[(3,4), 0]	$\left[0 \quad 0 \quad \frac{e^{i\frac{\pi}{4}}}{\sqrt{2}} \quad \frac{e^{i\frac{5\pi}{4}}}{\sqrt{2}} \quad 0\right]^T$
[1 1 1 1]	[(3,4), 1]	$\left[0 \quad 0 \quad \frac{e^{i\frac{5\pi}{4}}}{\sqrt{2}} \quad \frac{e^{i\frac{\pi}{4}}}{\sqrt{2}} \quad 0\right]^T$

be transmitted by the selected antennas. As in the previous section, the first vector is selected at the two ends of the red diameter as illustrated in Figure 3.3, i.e. $\phi_1 = \frac{\pi}{4}$ and $\phi_2 = \frac{5\pi}{4}$ and the second vector with π offset to the first one, i.e. $\phi_1 = \frac{5\pi}{4}$ and $\phi_2 = \frac{\pi}{4}$. Then, the third vector is selected with $\pi/2$ offset to the second one, the two ends of the green diameter, i.e. $\phi_1 = \frac{3\pi}{4}$ and $\phi_2 = \frac{7\pi}{4}$. Finally, the fourth vector has π offset with respect to the third vector, i.e. $\phi_1 = \frac{7\pi}{4}$ and $\phi_2 = \frac{3\pi}{4}$. Table 3.2 shows the mapping table which contains the phase constellation points selected for the two bits $[b_4, b_5]$. The mapping of the first part of the SPSK symbol ($[b_1, b_2, b_3]$) remains the same as in the case of 2-SPSK. The complete constellation of transmission vectors for all 5 bits can easily be found from Table 3.1 and Table 3.2. For example, the five bits: [1 0 1 1 0], will transmit $e^{i\frac{5\pi}{4}}$ and $e^{i\frac{\pi}{4}}$ at the second and the fourth antennas respectively, resulting in a transmission vector of $\left[0, \quad \frac{e^{i\frac{5\pi}{4}}}{\sqrt{2}}, \quad 0, \quad \frac{e^{i\frac{\pi}{4}}}{\sqrt{2}}, \quad 0\right]$, with $\mathbf{j} = [(2,4),\ 2]$.

3.3.4 8-SPSK modulation scheme

The 8-SPSK parameters are $N_t = 5$, $n_t = 2$ and $M = 8$ (which can convey three bits). In the 8-SPSK modulation scheme, the total number of bits transmitted per symbol is $m = \log_2(8) + l = 6$ ($l = 3$ as in 2-SPSK) and this makes the total number of transmission vectors $2^6 = 64$. The three bits $[b_1, b_2, b_3]$ correspond to the antenna indices using the mapping rule defined in Table 3.1. In 8-SPSK, the last three bits determine the signals transmitted on the two antennas. The mapping of the last three bits $[b_4, b_5, b_6]$ to eight possible phase vectors

Table 3.2: *Transmission Table of a 4-SPSK System with proposed selection of phase constellation points*

$\mathbf{b} = [b_4 \quad b_5]$	q	n_{t1}	n_{t2}
0 0	0	$\frac{1}{\sqrt{2}}e^{i\frac{\pi}{4}}$	$\frac{1}{\sqrt{2}}e^{i\frac{5\pi}{4}}$
0 1	1	$\frac{1}{\sqrt{2}}e^{i\frac{3\pi}{4}}$	$\frac{1}{\sqrt{2}}e^{i\frac{7\pi}{4}}$
1 0	2	$\frac{1}{\sqrt{2}}e^{i\frac{5\pi}{4}}$	$\frac{1}{\sqrt{2}}e^{i\frac{\pi}{4}}$
1 1	3	$\frac{1}{\sqrt{2}}e^{i\frac{7\pi}{4}}$	$\frac{1}{\sqrt{2}}e^{i\frac{3\pi}{4}}$

is shown in Table 3.3. The first four vectors are assigned as in 4-SPSK, and the other four vectors can be selected with $\pi/4$ offset as Figure 3.3 illustrates with the blue and purple diameter respectively. The complete constellation of transmission vectors, with the phase constellation points selection can be found using Table 3.1 and Table 3.3. For example, the six bits: [1 0 1 1 0 1], will transmit $e^{i\frac{7\pi}{4}}$ on the second antenna and $e^{i\frac{3\pi}{4}}$ on the fourth antenna, resulting in a transmission vector of $\left[0, \quad \frac{e^{i\frac{7\pi}{4}}}{\sqrt{2}}, \quad 0, \quad \frac{e^{i\frac{3\pi}{4}}}{\sqrt{2}}, \quad 0\right]$, with $\mathbf{j} = [(2,4),\ 5]$.

3.4 Detection

As described in the Section 3.2, the received SPSK signal is

$$\mathbf{y} = \sqrt{\rho}\mathbf{H}\mathbf{x} \ + \ \mathbf{v}. \tag{3.4}$$

The objective of the detector is to estimate $\mathbf{j}$, which contains the antenna indices and the index of the transmitted phases (q), and to de-map $\mathbf{j}$ to its corresponding information bits. As the transmission of all the transmission vectors is equally likely, the optimum detection technique is the ML method

$$\widehat{\mathbf{j}} = \arg\min_{\tilde{\mathbf{j}}} \|\mathbf{y} - \sqrt{\rho}\mathbf{H}\mathbf{x}_{\tilde{\mathbf{j}}}\|^2, \tag{3.5}$$

for $\tilde{\mathbf{j}} = 1, \ldots, 2^m$.

Because of the presence of multiple 0's in the transmission vector $\mathbf{x_j}$, the matrix-vector multiplication $\mathbf{Hx_j}$ becomes the linear combination of n_t

Table 3.3: *Transmission table of* 8*-SPSK system*

$\mathbf{b} = [b_4 \quad b_5 \quad b_6]$	q	n_{t1}	n_{t2}
0 0 0	0	$\frac{1}{\sqrt{2}}e^{i\frac{\pi}{4}}$	$\frac{1}{\sqrt{2}}e^{i\frac{5\pi}{4}}$
0 0 1	1	$\frac{1}{\sqrt{2}}e^{i\frac{3\pi}{4}}$	$\frac{1}{\sqrt{2}}e^{i\frac{7\pi}{4}}$
0 1 0	2	$\frac{1}{\sqrt{2}}e^{i0}$	$\frac{1}{\sqrt{2}}e^{i\pi}$
0 1 1	3	$\frac{1}{\sqrt{2}}e^{i\frac{\pi}{2}}$	$\frac{1}{\sqrt{2}}e^{i\frac{3\pi}{2}}$
1 0 0	4	$\frac{1}{\sqrt{2}}e^{i\frac{5\pi}{4}}$	$\frac{1}{\sqrt{2}}e^{i\frac{\pi}{4}}$
1 0 1	5	$\frac{1}{\sqrt{2}}e^{i\frac{7\pi}{4}}$	$\frac{1}{\sqrt{2}}e^{i\frac{3\pi}{4}}$
1 1 0	6	$\frac{1}{\sqrt{2}}e^{i\pi}$	$\frac{1}{\sqrt{2}}e^{i0}$
1 1 1	7	$\frac{1}{\sqrt{2}}e^{i\frac{3\pi}{2}}$	$\frac{1}{\sqrt{2}}e^{i\frac{\pi}{2}}$

columns in the channel matrix $\mathbf{H} = [\mathbf{h}_1, \mathbf{h}_2, \dots \mathbf{h}_{N_t}]$. Taking as an example the second vector in column $\mathbf{j}$ in Table 3.1 ($\mathbf{j} = [(1,2),\ 1]$), $\mathbf{H}\mathbf{x}_j$ is expressed as:

$$\mathbf{H}\mathbf{x}_\mathbf{j} = z_\mathbf{j} = \mathbf{h}_1 x_1 + \mathbf{h}_2 x_2,$$

where $x_1 = \frac{1}{\sqrt{2}}e^{i\frac{5\pi}{4}}$ and $x_2 = \frac{1}{\sqrt{2}}e^{i\frac{\pi}{4}}$. h_1 and h_2 are the respective columns in the channel matrix $\mathbf{H}$ corresponding to the position of the non-zero values in the transmission vector. As the channel is known at the receiver, the ML detection of $\widehat{\mathbf{j}}$ can be performed by an exhaustive search over all possible $z_\mathbf{j}$ values for the minimum Euclidean distance:

$$\widehat{\mathbf{j}} = \arg\min_{\tilde{\mathbf{j}}} \|\mathbf{y} - \sqrt{\rho} z_{\tilde{\mathbf{j}}}\|^2. \tag{3.6}$$

Once the index vector $\widehat{\mathbf{j}}$ is detected, the bit information $\mathbf{b}$ can be demapped. For the case of the 2-SPSK modulation system, there are 16 candidates for $z_\mathbf{j}$ corresponding to 16 distinct index vectors $\mathbf{j}$. Similarly, there are 32 and 64 candidates for $z_\mathbf{j}$ in 4-SPSK and 8-SPSK, respectively. Due to the presence of zero elements in transmission vectors, the computational complexity is significantly reduced. Then, even for the 8-SPSK scheme, the complexity load at the receiver is not significantly increased comparing to the GSSK modulation scheme.

3.5 Random Selection vs. Proposed Selection

Figure 3.5 shows the performance comparison when the selection of the phase constellation points are randomly selected or with the proposed method. In the case of 2-SPSK scheme, the two pairs of phase constellation points randomly selected can be any values. In the simulation, the phase selected are e^{i0} and $e^{i\frac{\pi}{4}}$ for transmitter one and two respectively, when $b_4 = 0$. On the other hand, when $b_4 = 1$, the first transmitter conveys $(e^{i\frac{\pi}{4}})$ and the second transmitter (e^{i0}). Then, a performance improvement is achieved using the maximum distance between the phase constellation points (based on Figure 3.3). The performance decreases, as Figure 3.5 shows, when this distance is shorter.

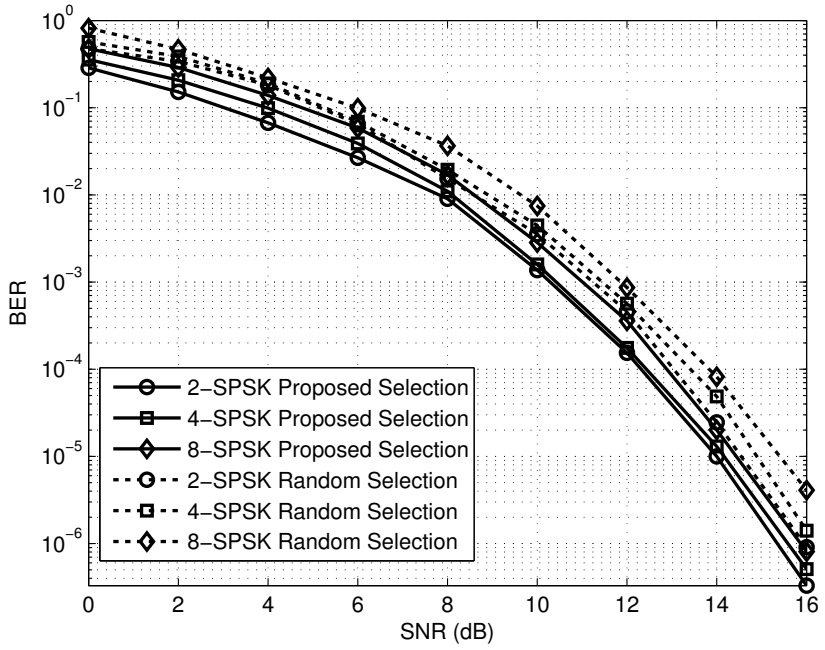

Figure 3.5: *BER versus SNR for SPSK in the cases of two, four and eight vectors with different selection of phase constellation points, MIMO system with* $N_t = 5$*,* $n_t = 2$ *and* $N_r = 4$

In Table 3.4, 3.5 and 3.6, a random selection of phase constellation points is given for 2-SPSK, 4-SPSK and 8-SPSK respectively. In Figure 3.5, the resulting performances for both proposed and random selection are shown.

Table 3.4: *Transmission table of a 2-SPSK system with a random selection of phase constellation points*

$\mathbf{b} = [b_4]$	q	n_{t1}	n_{t2}
0	0	$\frac{1}{\sqrt{2}}e^{i0}$	$\frac{1}{\sqrt{2}}e^{i\frac{\pi}{4}}$
1	1	$\frac{1}{\sqrt{2}}e^{i\frac{\pi}{4}}$	$\frac{1}{\sqrt{2}}e^{i0}$

Table 3.5: *Transmission table of a 4-SPSK system with a random selection of phase constellation points*

$\mathbf{b} = [b_4 \quad b_5]$	q	n_{t1}	n_{t2}
0 0	0	$\frac{1}{\sqrt{2}}e^{i0}$	$\frac{1}{\sqrt{2}}e^{i\frac{\pi}{4}}$
0 1	1	$\frac{1}{\sqrt{2}}e^{i\frac{\pi}{2}}$	$\frac{1}{\sqrt{2}}e^{i\frac{3\pi}{4}}$
1 0	2	$\frac{1}{\sqrt{2}}e^{i\frac{\pi}{4}}$	$\frac{1}{\sqrt{2}}e^{i0}$
1 1	3	$\frac{1}{\sqrt{2}}e^{i\frac{3\pi}{4}}$	$\frac{1}{\sqrt{2}}e^{i\frac{\pi}{2}}$

Table 3.6: *Transmission table of a 8-SPSK system with a random selection of phase constellation points*

$\mathbf{b} = [b_4 \quad b_5]$	q	n_{t1}	n_{t2}
0 0 0	0	$\frac{1}{\sqrt{2}}e^{i\frac{\pi}{4}}$	$\frac{1}{\sqrt{2}}e^{i\frac{5\pi}{4}}$
0 0 1	1	$\frac{1}{\sqrt{2}}e^{i\frac{3\pi}{4}}$	$\frac{1}{\sqrt{2}}e^{i\frac{7\pi}{4}}$
0 1 0	2	$\frac{1}{\sqrt{2}}e^{i0}$	$\frac{1}{\sqrt{2}}e^{i\pi}$
0 1 1	3	$\frac{1}{\sqrt{2}}e^{i\frac{\pi}{2}}$	$\frac{1}{\sqrt{2}}e^{i\frac{3\pi}{2}}$
1 0 0	4	$\frac{1}{\sqrt{2}}e^{i0}$	$\frac{1}{\sqrt{2}}e^{i\frac{\pi}{2}}$
1 0 1	5	$\frac{1}{\sqrt{2}}e^{i\frac{5\pi}{4}}$	$\frac{1}{\sqrt{2}}e^{i\frac{3\pi}{4}}$
1 1 0	6	$\frac{1}{\sqrt{2}}e^{i\pi}$	$\frac{1}{\sqrt{2}}e^{i\frac{7\pi}{4}}$
1 1 1	7	$\frac{1}{\sqrt{2}}e^{i\frac{3\pi}{2}}$	$\frac{1}{\sqrt{2}}e^{i\frac{\pi}{4}}$

Table 3.7: *Minimum Euclidean distance with random and proposed phase selection.*

M	*Random Selection*	*Proposed Selection*
2	0.5412	1.4142
4	0.5412	1.4142
8	0.5412	1.4142

All system models show improvement in terms of BER performance when the phase selection is maximised as opposed to random. Therefore, to achieve a better performance of the system, the distance between signal vectors and the points within each signal vector has to be maximised.

Table 3.7 shows the minimum Euclidean distance between the transmission vector phases, when the phases are selected randomly and with the proposed method for $M = 2,\ 4$ and 8. As in SM (Section 2.2), each antenna combination is considered a different space dimension.

3.6 Performance Analysis

In the following section, the performance of SPSK is analysed and a tight upper bound on the BER is derived. As an ML detector is used at the receiver side, the pairwise error probability (PEP) is given by

$$P(\mathbf{x}_j \rightarrow \mathbf{x}_{\hat{j}}) = \mathbf{Prob}\left[\parallel \mathbf{y} - \mathbf{H}\mathbf{x}_j \parallel^2 > \parallel \mathbf{y} - \mathbf{H}\mathbf{x}_{\hat{j}} \parallel^2 \right]. \tag{3.7}$$

Using the union bounding technique analysed in [59], the BER of SPSK is union bounded as follows:

$$\begin{aligned} P_{e,bit} &\leq \mathbf{E}_{\mathbf{x}_j}\left[\sum_{\hat{j}} N(j,\hat{j}) P(\mathbf{x}_j \rightarrow \mathbf{x}_{\hat{j}}) \right] \\ &\leq \sum_{j} \sum_{\hat{j},\hat{j}\neq j} \frac{N(j,\hat{j})}{2^l\ m} P(\mathbf{x}_j \rightarrow \mathbf{x}_{\hat{j}}), \end{aligned} \tag{3.8}$$

where j and $\hat{j}$ denote the indices of the transmitted and estimated transmission vectors, $\mathbf{x}_j$ and $\mathbf{x}_{\hat{j}}$ respectively; $N(j,\hat{j})$ is the number of different information

between the transmission vector $\mathbf{x}_j$ and $\mathbf{x}_{\hat{j}}$ and $P(\mathbf{x}_j \rightarrow \mathbf{x}_{\hat{j}})$ is the PEP of detecting $\mathbf{x}_{\hat{j}}$ for transmitted $\mathbf{x}_j$, which is calculated as [60]

$$P(\mathbf{x}_j \rightarrow \mathbf{x}_{\hat{j}}) = \left(\frac{1-\frac{1}{u}}{2}\right)^{\Lambda} \sum_{k=0}^{\Lambda-1} 2^{-k} \binom{\Lambda-1+k}{k} \left(1+\frac{1}{u}\right)^{k}, \tag{3.9}$$

where $u = \sqrt{1+\frac{1}{(\frac{d(j,\hat{j})\rho}{4n_t N_r})}}$, $\Lambda = N_t N_r$ and $d(j,\hat{j})$ is the Euclidean distance between $\mathbf{x}_j$ and $\mathbf{x}_{\hat{j}}$, which is determined by both the antenna indices (positions of the non-zero values in the vector) and the phases (actual values on the columns). Therefore, the phase and the active indices can be detected simultaneously by the ML detector. As in traditional modulation techniques, a better performance is achieved with a larger minimum $d(j,\hat{j})$. To calculate the upper bound of the BER for SPSK, (3.9) is substituted into (3.8) and it is expressed as

$$\begin{aligned} P_{e,bit} \leq & \sum_{j} \sum_{\hat{j},\hat{j}\neq j} \frac{N(j,\hat{j})}{2^l\ m} \left(\frac{1-\frac{1}{u}}{2}\right)^{\Lambda} \\ & \sum_{k=0}^{\Lambda-1} 2^{-k} \binom{\Lambda-1+k}{k} \left(1+\frac{1}{u}\right)^{k}. \end{aligned} \tag{3.10}$$

3.7 Simulation Results

In this section, the performance of both the GSSK [58] and SPSK schemes with $M = 2$, 4 and 8 are evaluated through simulation. For the purpose of comparison, all the schemes are evaluated using the same configuration with $N_t = 5$, $n_t = 2$ and $N_r = 4$, over a flat Rayleigh fading channel. Monte Carlo simulations are performed and are run for 10^7 channel realisations. It is assumed that the receiver has channel state information.

In Figure 3.6, the average BER is shown against the average SNR per receive antenna of 2-SPSK in comparison to that of GSSK and the upper bound of SPSK. At $P_e = 10^{-5}$, 2-SPSK presents a gain of approximately 8.5 dB over GSSK and the bit rate transmitted per symbol is improved from 3 bits to 4 bits. As discussed in Section 3.4, the correct detection of $z_{\mathbf{j}}$ (3.6) plays an important

role in this scheme because it contains the antenna indices and phases. The performance improvement of SPSK over GSSK is because the transmission vector is encoded by the signal vector and thereby the distance between the transmission vectors is significantly increased. Besides, the simulated BER performance of 2-SPSK is efficiently validated by the upper bound, which is a very tight bound at high SNRs values.

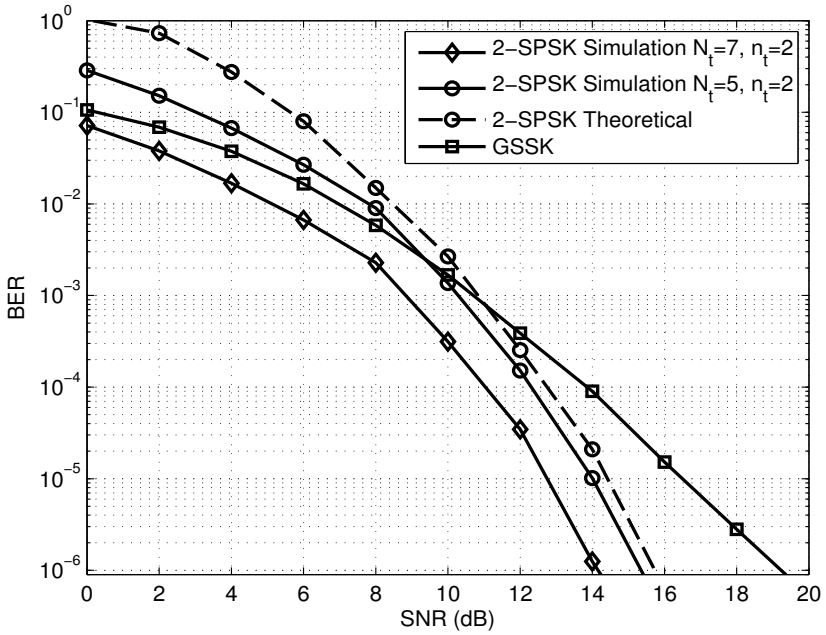

Figure 3.6: *BER performance of GSSK vs 2-SPSK with* $M = 2$

The spectrum efficiency can be further improved by transmitting additional $\log_2(M)$ bits/symbol using bigger M. Therefore, the cost of achieving higher spectrum efficiency is a slight performance degradation and an increased complexity of the receiver with higher values of M. Figure 3.7 shows the BER performance for 4-SPSK and 8-SPSK, with data rates $\eta = 5$ and 6 bits/s/Hz per period respectively. The increased number of bits only slightly degrades the BER performance since the performance of the SPSK scheme is determined by the minimum Euclidean distance between the transmission vectors. Then, the minimum distance between two transmission vectors is obtained when both vectors have the same combination of active transmitters n_t, i.e.

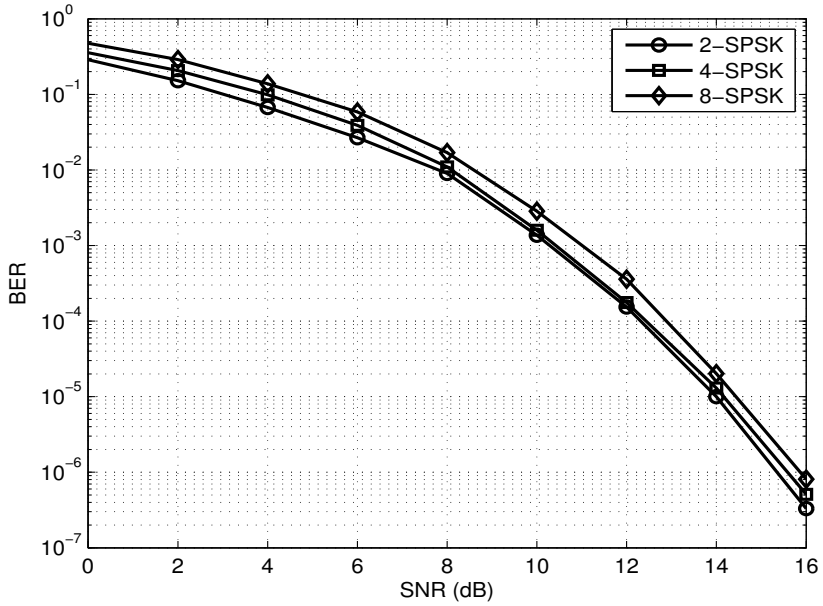

Figure 3.7: *BER versus SNR for SPSK in the cases of* $M = 2, 4$ *and* 8

in these examples when b_1, b_2 and b_3 are the same. As the three schemes have the same configuration system ($N_t = 5$, $n_t = 2$ and $N_r = 4$), and thereby the same minimum distance between phases selected, then it is not surprising that their BER performances are very similar.

Figure 3.8 demonstrates 2-SPSK's performance compared to Alamouti and V-BLAST. Alamouti uses 16-QAM transmission with $N_t = 2$ and $N_r = 4$. V-BLAST uses $N_t = 2$ and $N_r = 4$ with QPSK modulation and three different decoding techniques: zero forcing (ZF), minimum-mean square error (MMSE) and sphere decoding. The transmission rate for all systems is the same, $\eta = 4$ bits/s/Hz.

The results shown in Figure 3.8 demonstrate the significant improvement in terms of BER in comparison to both V-BLAST and Alamouti schemes [21]. The simulation shows that SPSK achieves a SNR gain of about 7 dB over Alamouti at $P_e = 10^{-4}$ and 8 dB over V-BLAST (SD), at $P_e = 10^{-3}$. Finally, SPSK shows a gain of 7.5 dB and 9 dB over V-BLAST (MMSE) and V-BLAST (ZF) respectively.

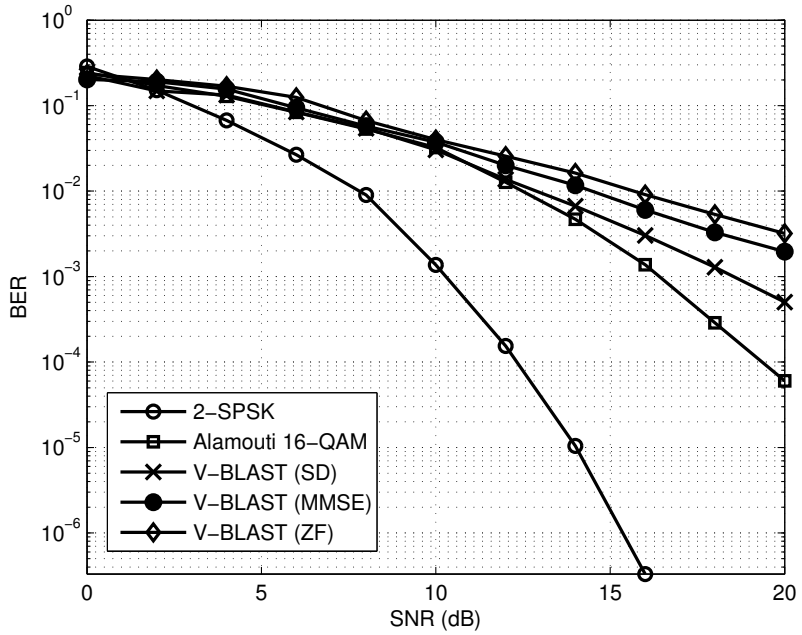

Figure 3.8: *BER performance of SPSK versus Alamouti and Spatial Multiplexing Systems, for $\eta = 4$ bits/s/Hz; two transmit and receive antennas*

All these systems can be designed with various modulation sizes to achieve the desired data rate and number of antennas. However, in this simulation, the identical transmission rates and identical numbers of active transmitters and receivers are used to allow fair comparison between different systems.

3.8 Summary

This chapter introduces a novel technique within the SM transmission family, called spatial phase shift keying (SPSK) modulation. The GSSK modulation is a type of SM scheme, which reduces the number of RF chains and improves performance over traditional MIMO techniques. SPSK exploits all the advantages of GSSK proposed in [58] including the inherent indices of the active transmitters.

In addition to this, SPSK symbols transmit different phases to convey more information. SPSK shows improvements over other well-known transmission techniques in terms of BER. An upper bound has been derived to validate the

results. Thus, SPSK enhances the spectral efficiency while its design flexibility makes SPSK a rising candidate for future generations of wireless systems.

Chapter 4

Antenna Beam Pattern Modulation

4.1 Introduction

MIMO utilises multiple element antennas to improve spectral efficiency almost linearly with respect to the number of transmitters and receivers. This is discussed in Chapter 2. These kind of architectures have been included in communication standards such as 3GPP and IEEE 802.11n. Directional antennas provide enhancement in system performance and maximise the signal-to-interference noise ratio (SINR) by estimating direction of arrival (DOA) and direction of interference (DOI). Such antennas direct the main beam radiation at the intended user and steer radiation nulls towards the interference users. A beamspace-MIMO which maps PSK modulated symbols onto orthogonal basis functions on the wavevector domain of the multi-element antenna is proposed in [61, 62]. Its performance is comparable to traditional MIMO systems although only a single active element is used for different beam patterns.

The first part of the chapter introduces the scheme called antenna beam pattern modulation (ABPM). The proposed modulation technique further exploits the spatial channel in order to achieve more robust and efficient information transmission. The ABPM scheme, unlike the previously mentioned schemes, conveys information using both antenna beam pattern (which can be determined by the antenna weights) and the conventional modulated symbols,

to improve the spectrum efficiency. The beams are generated in a simple way, using the angle of departures (AoD) from the transmitter antenna array. At the receiver, the antenna pattern and the transmitted symbol are estimated based on the ML principle to de-map the transmitted information bits. The implied cost of using ML is high computation complexity, especially when the number of antennas and/or the constellation size are very large, such as in massive MIMO systems. Linear detection schemes based on the ZF or the MMSE criteria are possible solutions [46, 63] for lower complexity detection schemes. However, for ill-conditioned channels these techniques show an inferior performance compared to ML detection. For this reason, the LR technique [50, 51, 52, 64, 65] is exploited to achieve performance close to that of the ML detector but with lower complexity. LR can be applied to MIMO systems to achieve a better conditioned channel matrix by improving its orthogonality conditions.

In the second part of the chapter, the ABPM scheme is evaluated by numerical simulation over a Rayleigh fading channel. The result proves the feasibility and potential improvement in both reliability and efficiency that could be offered by the ABPM technique. The ABPM performance is compared to other SM schemes and other transmission techniques such as STC and spatial multiplexing. In addition, to validate the results, an upper bound expression for BER is provided for ABPM with ML detection.

This chapter is structured as follows: Section 4.2 reviews the concept of ABPM and introduces the transmission design and the selection of antenna beam pattern. The sub-optimal detection based on the LR scheme is explained in Section 4.3. Analytic calculation of BER is shown in Section 4.4. Simulation results and comparisons with other transmission techniques follow in Section 4.5. The chapter's summary is in Section 4.6.

4.2 ABPM Description

The general ABPM system model consists of a MIMO wireless link between N_t transmit and N_r receive antennas. Figure 4.1 illustrates the block diagram

of ABPM. As shown in the figure, a random sequence of independent bits $\mathbf{b} = [b_1 \quad b_2 \quad \cdots \quad b_k]^T$ enters the serial to parallel converter. The first m bits select an antenna pattern and the remaining $k-m$ bits choose the conventional APM symbols. The output is mapped to a vector $\mathbf{x} = [x_1, \quad x_2, \quad \cdots, \quad x_{N_t}]^T$. The modulated signal is then transmitted over a $N_r \times N_t$ wireless channel $\mathbf{H}$. The received signal is given by $\mathbf{y} = \mathbf{Hx} + \mathbf{v}$, where $\mathbf{v} = [v_1 \quad v_2 \quad \cdots \quad v_{N_r}]^T$ represents the AWGN vector observed at the receive antennas with zero mean and covariance matrix $E[\mathbf{vv}^H] = \sigma_v^2 \boldsymbol{I}_{Nr}$. The matrix channel $\mathbf{H}$ has i.i.d. entries with $\mathcal{CN}(0, 1)$. The channel is assumed to be flat-fading, time invariant and independently changing from symbol to symbol. Therefore, in this system it is assumed that CSI is available at the transmitter, as in massive MIMO, which is feasible in reciprocal propagation channels as in time-division duplex (TDD) systems [42]. At the receiver, the antenna patterns and the APM symbol of the signals are estimated by the ABPM detector, and de-mapped to the transmitted bits.

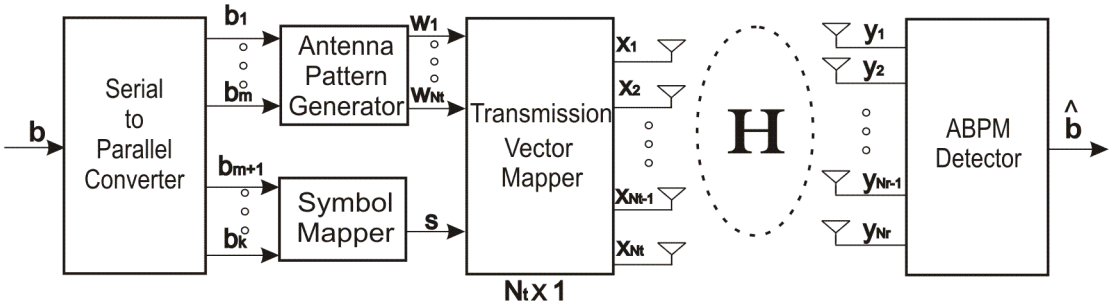

Figure 4.1: *ABPM system model.*

4.2.1 ABPM Transmission

For each symbol period, a stream of independent bits $\mathbf{b}$ is sent to the serial to parallel converter and the output of the converter is divided into two blocks. The first m bits are used to indicate the antenna pattern which is realised by antenna weight vector denoted as $\mathbf{w} = [w_1, \quad w_2, \quad \cdots, \quad w_{N_t}]^T$. The second part of the symbol will determine the transmitted signal s on each

antenna. The ABPM transmitted signal vector is a linear combination of s and $\mathbf{w}$, denoted as $\mathbf{x} = [w_1 \cdot s, \quad w_2 \cdot s, \quad \cdots, \quad w_{Nt} \cdot s]^T$.

The proposed ABPM is capable of transmitting symbols towards different AoD at the transmitter side. Antenna patterns are realised by antenna weights, which can be selected to make the best channel utilisation by exploiting the CSIT. In order to facilitate the detection process, it is desirable for the selected patterns to have minimum correlation between them. The array response vector can be expressed as $\mathbf{a}(\theta) = [1 \quad e^{-i2\pi \frac{q \cdot \sin\theta}{\lambda}} \quad \ldots \quad e^{-i2\pi(N_t-1)\frac{q \cdot \sin\theta}{\lambda}}]^T$, where q is the space between antenna elements, θ indicates the AoD and λ is the wavelength [66]. The distance between antenna elements has to be $q \geq \frac{\lambda}{2}$ to avoid correlation.

The weight vectors $\mathbf{w}$ should be obtained to satisfy $\mathbf{w}^H[\mathbf{a}(\theta_1) \quad \mathbf{a}(\theta_2) \quad \ldots \quad \mathbf{a}(\theta_{Nt})] = \mathbf{w}^H\mathbf{A} = [1, \quad \cdots 0, \quad \cdots 1, \quad \cdots 0, \quad \cdots 0]^T$. Note that the "1" and "0" in this vector represents the main beam or nulls in the radiation pattern, respectively. In the case of where the steering of the main beam is wanted, "1" is selected. On the other hand, "0" is chosen when the pattern's nulls are desirable for design purposes. In this way, the beam patterns can be specified based on CSIT by the angles for the main beam and nulls. Clearly, as long as the number of independent columns in $\mathbf{A}$ is larger than N_t, $\mathbf{w}$ can be solved. Therefore, it is only possible to include N_t columns in $\mathbf{A}$.

The main contribution of this scheme is to use the antenna pattern to transmit symbol information, in addition to the conventional modulation symbols. ABPM transmits conventional APM symbols by the selected beam patterns. The transmitted vector is defined as $[w_1 \cdot s, \quad w_2 \cdot s, \quad \cdots, \quad w_{Nt} \cdot s]^T$ (i.e. ABPM symbol constellation points). Similar to traditional pulse-amplitude modulation (PAM), larger distance between two possible transmitted vectors will result in better performance. For ABPM, it is possible to maximise the distance between transmit vectors by choosing vectors with minimum correlation between them. The correlation between antenna beam patterns is denoted as γ with a range between 1 and 0, indicating completely correlated to no correlation, which is not always possible to achieve. Table 4.1 illustrates the correlation (γ) between two patterns (determined by AoD). Angles are sepa-

Table 4.1: *Correlation Table.*

angle difference between main beam patterns	γ
10°	0.9281
20°	0.4885
30°	0.3536
40°	0.2953
50°	0.2679
60°	0.2556
70°	0.2511
80°	0.2503
90°	0.2493

Table 4.2: *Transmission Table of* 2*-ABPM System.*

$[b_1 \quad b_2 \quad b_3]$	*Beam*	*s*
0 0 0	1	1 + i
0 0 1	1	1 - i
0 1 0	1	-1 - i
0 1 1	1	-1 + i
1 0 0	2	1 + i
1 0 1	2	1 - i
1 1 0	2	-1 - i
1 1 1	2	-1 + i

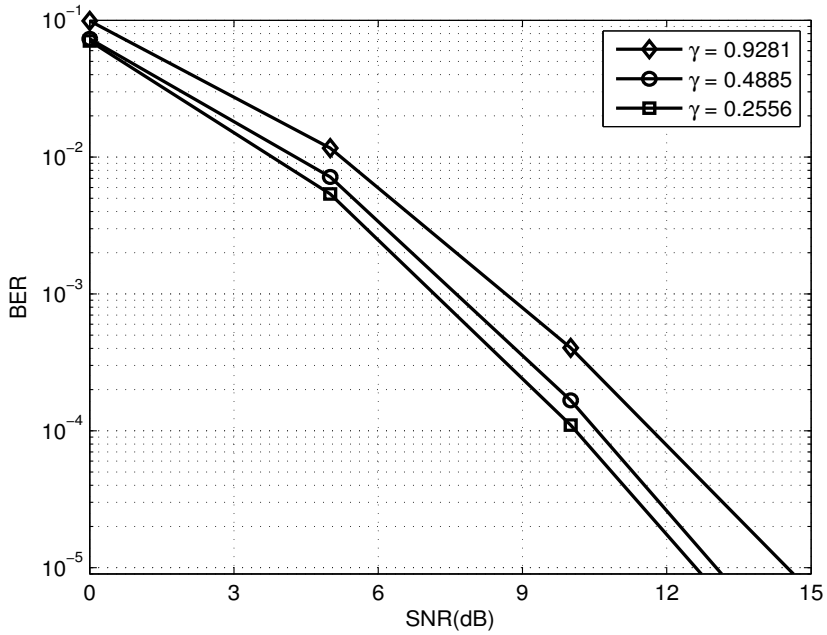

Figure 4.2: *BER versus SNR for cases of using different values of correlation (γ) between antenna beam patterns.*

rated by 10°. One of the angles is selected to 0° as starting angle for simplicity and demonstrative purposes without loss of generality.

The 2^m antenna weight vectors $\mathbf{w}$ are combined with the APM symbol (selected by the second block), to generate the transmit vector $\mathbf{x}$ which is transmitted over the channel. Thus, the information is carried by both the beam pattern and the APM symbol through the channel $\mathbf{H}$. To clarify the transmission process an example is given below.

4.2.2 2-ABPM scheme

Using two different beam patterns and QPSK modulation, each ABPM symbol carries 3 bits. The first block only has one bit and the second block contains two bits. The mapping table for 3 bits transmission using QPSK signal modulation and 2x4 MIMO antenna configuration is shown in Table 4.2. The column 'beam' in Table 4.2 indicates which weight vector is selected at transmission, in other words, which antenna beam pattern is used to transmit s.

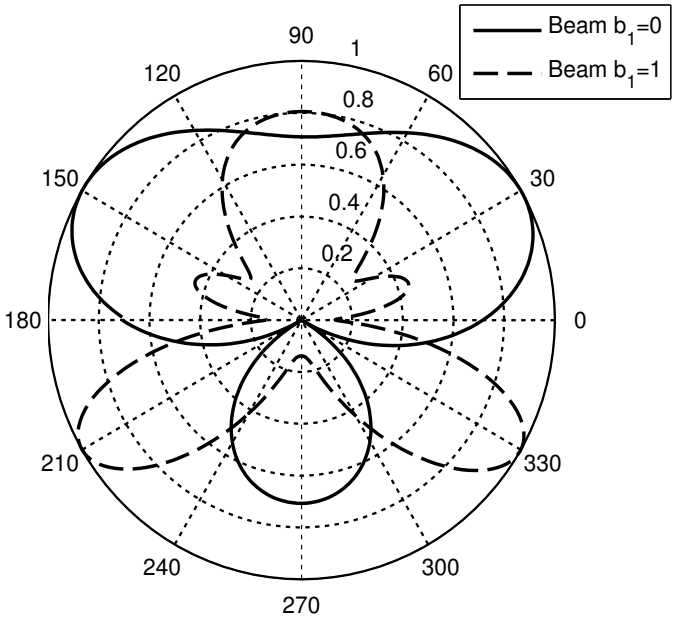

Figure 4.3: *The two possible beam patterns used in ABPM* $2X4$ *with* 3 *bits/s/Hz.*

Fig. 4.3 shows both antenna beam patterns corresponding to $\mathbf{w}_1$ and $\mathbf{w}_2$ in the example above. The solid line shows the pattern corresponding to weight vector $\mathbf{w}_1$ in which the main beam is observed at 30° and the angle of the null at −30°. The dashed line represents the second pattern which has the main beam at −30° and the angle of the null at 0° to increase the directivity of the main lobe, corresponding to weight vector $\mathbf{w}_2$.

Thus, the weight vectors can be calculated by

$$\mathbf{w}_1^H[\mathbf{a}(30°) \;\; \mathbf{a}(-30°)] = \begin{bmatrix}1\\0\end{bmatrix} \qquad \mathbf{w}_2^H[\mathbf{a}(-30°) \;\; \mathbf{a}(0°)] = \begin{bmatrix}1\\0\end{bmatrix}.$$

Solving the equations the weight vectors are: $\mathbf{w}_1 = [0.5000{+}0.0000i \;\; 0.0000{-}0.5000i]^T$ and $\mathbf{w}_2 = [0.5000 - 0.5000i \quad -0.5000 + 0.5000i]^T$ and b_2 and b_3 are mapped to QPSK symbols according to Table 4.2.

From Table 4.1, it is concluded that the ABPM design for each of the 2^m patterns should have at least 20° separation in their main lobe to ensure a low correlation. One of the beams was fixed to 0° and the second beam was selected based on Table 4.1, to show the impact of different correlation values

on the ABPM BER performance. Figure 4.2 depicts the BER performance of ABPM based on different values of γ. The three curves are obtained under the same conditions: $N_t = 2$, $N_r = 4$, two beam patterns, QPSK symbols and the spectral efficiency (η) of 3 bits/s/Hz. The detection used for this figure is based on ML to demonstrate the impact of correlation between beam patterns on the performance. The different angles selected are 60°, 20° and 10°. Each of these angles have a corresponding correlation value: $\gamma = 0.2556$, 0.4885 and 0.9281 respectively. It is shown that roughly 2 dB gain is obtained by low correlation patterns ($\gamma = 0.2556$), compared to the highly correlated $\gamma = 0.9281$. When $\gamma = 0.4885$, the gain is less than 1 dB. However, in realistic application there are many other factors to take into account, such as channel conditions, pattern correlation and ICI mitigation. These factors are not being considered in this chapter but are discussed in future work.

4.2.3 Detection

As previously stated, ML is used as the detection scheme. The output of the channel is

$$\mathbf{y} = \mathbf{H}\mathbf{x} \ + \ \mathbf{v}. \tag{4.1}$$

The objective of the detector is to estimate the antenna pattern and then de-map them to the information bits. Assuming all the weight vectors transmitted are equally likely, the optimal detection is given by the ML method

$$\widehat{j} = \arg\min_{j} \|\mathbf{y} - \mathbf{H}\mathbf{x}_j\|^2. \tag{4.2}$$

The ML detection of $\widehat{j}$ is performed by an exhaustive search across all possible $\mathbf{x}_j$ for the minimum Euclidean distance $\|\mathbf{y} - \mathbf{H}\mathbf{x}_j\|^2$. Then, the information block can be de-mapped.

The computational complexity of ML is $\mathcal{O}((N_t N_r)^2 L)$, where L denotes the size of the constellation points [67]. The complexity increases when L is large, which causes problems when ML based on ABPM is applied. Linear detectors such as ZF and MMSE equalisers are good solutions with low complexity. However, their BER performance is far worse than ML.

The ZF equaliser removes all inter-symbol interference (ISI), and is ideal when the channel is noiseless. However, when the channel is noisy, the ZF equaliser will amplify the noise greatly in the attempt to invert the channel completely. The MMSE equaliser, on the other hand, does not usually eliminate ISI completely but instead minimises the total power of the noise and ISI components in the output.

4.3 Lattice Reduction Aided Linear Equilisation

LR aided detectors have been used for MIMO systems to achieve performance with full diversity and low complexity. In [50, 51, 53, 54] is shown that some improvements over linear detectors can be achieved by using LR, with only a small increase in complexity in comparison to traditional linear detectors such as ZF or MMSE as discussed in Section 2.4. A basis is considered to be good when the basis vectors are close to orthogonal. Recently, these LR aided linear equalisers have been utilised for detection in MIMO systems. Taking the model in (4.1), $\mathbf{x} \in \mathbb{Z}$, $\mathbf{Hx}$ forms a lattice spanned by the columns of $\mathbf{H}$ [10]. Therefore, the estimate of $\mathbf{x}$ (based on the received signal $\mathbf{y}$) is the point on the lattice that is the closest to $\mathbf{y}$. High estimation accuracy is achieved when the lattice basis is orthogonal or close to that. This does not affect the performance of the ML detector, since it performs the same without taking the channel conditions into account. However, when the ML detector is not used, the channel conditions are important and in consequence when this condition (orthogonality between lattice vectors) is not satisfied, the performance tends to degrade.

The fundamental principle, as previously stated, is to combine a lattice reduction approach with low complexity linear detectors to establish an effective channel matrix $\tilde{\mathbf{H}}$ via the unimodular matrix $\mathbf{T} \in \mathbb{Z}$. The matrix $\mathbf{T}$ is obtained based on the LLL algorithm [56] which is explained in Section 2.4. This $\mathbf{T}$ has two properties: it is formed only by integers and its determinant is ± 1. Figure 4.4 illustrates the system model of LR. The model in (4.1) is

rewritten as:

$$\mathbf{y} = \mathbf{HTT^{-1}x} \ + \ \mathbf{v} = \tilde{\mathbf{H}}\mathbf{z} \ + \ \mathbf{v}, \tag{4.3}$$

where $\tilde{\mathbf{H}} = \mathbf{HT}$ and $\mathbf{z} = \mathbf{T^{-1}x}$. With the basis changed, the traditional detector is used to compensate for the new channel $\tilde{\mathbf{H}} = \mathbf{HT}$. Then, it produces the estimation of $\hat{\mathbf{z}}$, and $\hat{\mathbf{x}}$ can be estimated through $\hat{\mathbf{x}} = \mathbf{T}\hat{\mathbf{z}}$. In this way, the LR algorithm is integrated into the linear detection equaliser.

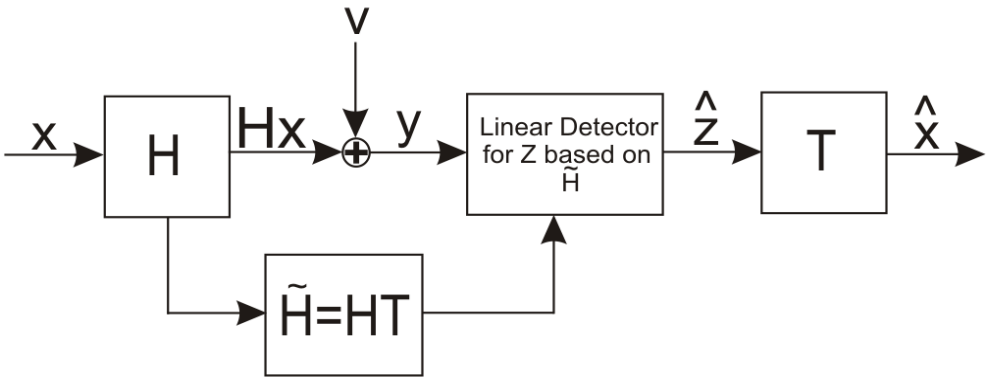

Figure 4.4: *Block diagram of the LR method in combination with linear detection equaliser for MIMO system.*

With this new system model, linear equalisers are applied to the channel matrix $\tilde{\mathbf{H}}$ to estimate $\mathbf{z}$. When ZF and MMSE are applied to the received signal $\mathbf{y}$, the estimation of $\mathbf{z}$ is expressed as:

$$\hat{\mathbf{z}}_{ZF} = \mathcal{Q}((\tilde{\mathbf{H}}^H\tilde{\mathbf{H}})^{-1}\tilde{\mathbf{H}}^H\mathbf{y}), \tag{4.4a}$$

$$\hat{\mathbf{z}}_{MMSE} = \mathcal{Q}((\tilde{\mathbf{H}}^H\tilde{\mathbf{H}} \ + \ \sigma_v^2\mathbf{T}^H\mathbf{T})^{-1}\tilde{\mathbf{H}}^H\mathbf{y}). \tag{4.4b}$$

The output of the equalisers LR-ZF and LR-MMSE are shown in (4.4a) and (4.4b) respectively. Thus, the estimate $\hat{\mathbf{x}}$ can be calculated as:

$$\hat{\mathbf{x}} = \mathbf{T}\hat{\mathbf{z}}. \tag{4.5}$$

It is known that $\hat{\mathbf{x}}$ contains both the weight vector and the symbol information. Thus, $\hat{\mathbf{w}}$ is estimated as the weight vector which has the highest correlation with the transmitted vector $\hat{\mathbf{x}}$

$$\hat{\mathbf{w}} = \arg\max_{\ell} \|\mathbf{w}_\ell\hat{\mathbf{x}}\|^2, \tag{4.6}$$

where $\ell \quad \{1, ..., 2^m\}$. The second block of data is estimated based on the estimation of the first block and the channel matrix. The detection of $\hat{s}$ is calculated as follows:

$$\hat{s} = (\mathbf{H}\hat{\mathbf{w}})^{-1}\mathbf{y}. \tag{4.7}$$

As was explained, the estimation of the antenna weight vector is critical since it directly affects the symbol estimation. Therefore, as the ABPM symbol detection is obtained in two steps, an error on the antenna weight vector will be propagated to the APM symbol detection.

4.4 Performance Analysis

The ABPM scheme has been described as hybrid modulation due to its combination of antenna pattern with conventional APM schemes [68]. The ABPM transmission design changes depending on the N_t transmitters and beam patterns, i.e. different designs for different scenarios. Thus, it is not possible to derive an exact BER probability equation. For this reason, a tight upper bound on the BER is derived to validate and analyse the performance of ABPM. The PEP of an ML detector is given by:

$$\begin{aligned} P\left(\mathbf{x}_j \to \mathbf{x}_{\hat{j}}\right) & \\ &= \mathbf{P}\Big(\left[\| \mathbf{y} - \mathbf{H}\mathbf{x}_{\hat{j}} \|^2 - \| \mathbf{y} - \mathbf{H}\mathbf{x}_j \|^2 \right] \leq 0 \Big) \\ &= \mathbf{P}\Big(\left[\| \mathbf{H}\left(\mathbf{x}_j - \mathbf{x}_{\hat{j}}\right) + \mathbf{v} \|^2 - \| \mathbf{v} \|^2 \right] \leq 0 \Big) \\ &= \mathbf{E}\left[Q\left(\sqrt{\frac{1}{2N_0} \sum_j \sum_{\hat{j}} \| \mathbf{H}\left(\mathbf{x}_j - \mathbf{x}_{\hat{j}}\right) \|^2} \right) \right]. \end{aligned} \tag{4.8}$$

Using the union bounding technique presented in [59], the BER of ABPM is union bounded as:

$$\begin{aligned} P_{e,bit} &\leq \mathbf{E}_{\mathbf{x}_j}\left[\sum_{\hat{j}} N(j,\hat{j}) P(\mathbf{x}_j \to \mathbf{x}_{\hat{j}}) \right] \\ &\leq \sum_{j}^{L} \sum_{\hat{j},\hat{j}\neq j}^{L} \frac{N(j,\hat{j})}{kL} P(\mathbf{x}_j \to \mathbf{x}_{\hat{j}}), \end{aligned} \tag{4.9}$$

where k is the number of information bits carried by one ABPM symbol, j and $\hat{j}$ denote the indices of the transmitted and estimated symbols, $\mathbf{x}_j$ and $\mathbf{x}_{\hat{j}}$ respectively; $\mathbf{E}_{\mathbf{x}_j}$ is the mean value of $P(\mathbf{x}_j \to \mathbf{x}_{\hat{j}})$, $N(j,\hat{j})$ is the number of different bits between symbols $\mathbf{x}_j$ and $\mathbf{x}_{\hat{j}}$ and $P(\mathbf{x}_j \to \mathbf{x}_{\hat{j}})$ is the PEP of detecting $\mathbf{x}_{\hat{j}}$ for transmitted $\mathbf{x}_j$ [60], which is calculated as:

$$P(\mathbf{x}_j \to \mathbf{x}_{\hat{j}}) = \left(\frac{1-\frac{1}{u}}{2}\right)^{\Lambda} \sum_{n=0}^{\Lambda-1} 2^{-n} \binom{\Lambda-1+n}{n} \left(1+\frac{1}{u}\right)^{n}, \tag{4.10}$$

where $u = \sqrt{1+\frac{1}{(\frac{d(j,\hat{j})\rho}{2+b})}}$, $\Lambda = N_t N_r$, b is the number of beams and $d(j,\hat{j})$ is the Euclidean distance between $\mathbf{x}_j$ and $\mathbf{x}_{\hat{j}}$.

As expected, a larger minimum $d(j,\hat{j})$ results in better performance, similar to other conventional modulation techniques. Substituting (4.10) into (4.9), the upper bound of the bit error probability for ABPM can be expressed as:

$$\begin{aligned} P_{e,bit} \leq & \sum_{j}^{L} \sum_{\hat{j},\hat{j}\neq j}^{L} \frac{N(j,\hat{j})}{kL} \left(\frac{1-\frac{1}{u}}{2}\right)^{\Lambda} \\ & \sum_{n=0}^{\Lambda-1} 2^{-n} \binom{\Lambda-1+n}{n} \left(1+\frac{1}{u}\right)^{n}. \end{aligned} \tag{4.11}$$

Note that $PEP = 0$ implies no error in the detection of $\mathbf{x}_j$, this is only possible if u has the value "1" in (4.10). Therefore, the accuracy of the tight upper bound depends on if u is close to "1". The parameter u depends on the minimum Euclidean distance $d(j,\hat{j})$. With larger d, u is closer to "1". As d and b are inversely related, if b increases, d decreases and therefore the system performance degrades.

This means that the larger distance between transmit vectors leads to better performance. Therefore, it is desirable that the selected antenna beam patterns have low correlation.

4.5 Simulation results

In this section, examples are presented in order to show the benefits achieved by ABPM. Monte Carlo simulations are performed, and are run for at least

10^6 channel realisations. A flat Rayleigh fading channel with AWGN is used and CSIT and CSIR are assumed for simulation purposes.

Figure 4.5 shows the BER performance of ABPM under different detection schemes. It compares the optimal detector ML with high computational complexity, to an LR aided detector combined with MMSE as a linear detector with low computational complexity, for data rates of $\eta = 3$ and 4 bits/s/Hz. When $\eta = 3$ bits/s/Hz, two different beam patterns are used to carry QPSK, the angle difference selected is 60° to guarantee low correlation as explained in Section 4.2. When $\eta = 4$ bits/s/Hz, four different beam patterns are used, carrying QPSK, the minimum angle separation is 30° between each beam with $\gamma = 0.3536$ (Table 4.1). This implies that the four AoDs used are 50°, 20°, −20° and −50°. All schemes are presented with the same number of transmitters $N_t = 2$ and receivers $N_r = 6$.

It should be noted that in the case of $\eta = 3$ bits/s/Hz, the LR-MMSE has a performance very close to that of the optimal ML detector. This is possible due to low correlation between the patterns used. However, in the case of $\eta = 4$ bits/s/Hz, it can be noticed a bigger difference between the two methods (2 dB at $P_{e,bit} = 10^{-5}$). The reason for this is that the distance between transmit vectors when $M = 4$, is smaller than when the system is using only 2 patterns. Another factor that impacts the BER performance, is that the detection is made in two stages. If the estimation of the first stage (antenna beam pattern represented by weights) is wrong, this error is carried through to the second stage which degrades the system performance.

Figure 4.6 depicts ABPM's performance using both optimal and sub-optimal detections in comparison with SM [27], GSSK [58] and V-BLAST with LR aided MMSE equalisation [52] with targeted $\eta = 3$ bits/s/Hz and $N_r = 5$. Four different transmission techniques are investigated to compare with the proposed ABPM which has QPSK modulation and two different antenna beam patterns resulting in 8 constellation points. The first one is SM with $N_t = 4$ antennas and BPSK modulation. The second is SM with $N_t = 2$ antennas and QPSK modulation (both result in $N_t \times M = 8$ constellation points). The third transmission scenario is GSSK with $N_t = 5$ and two active transmitters

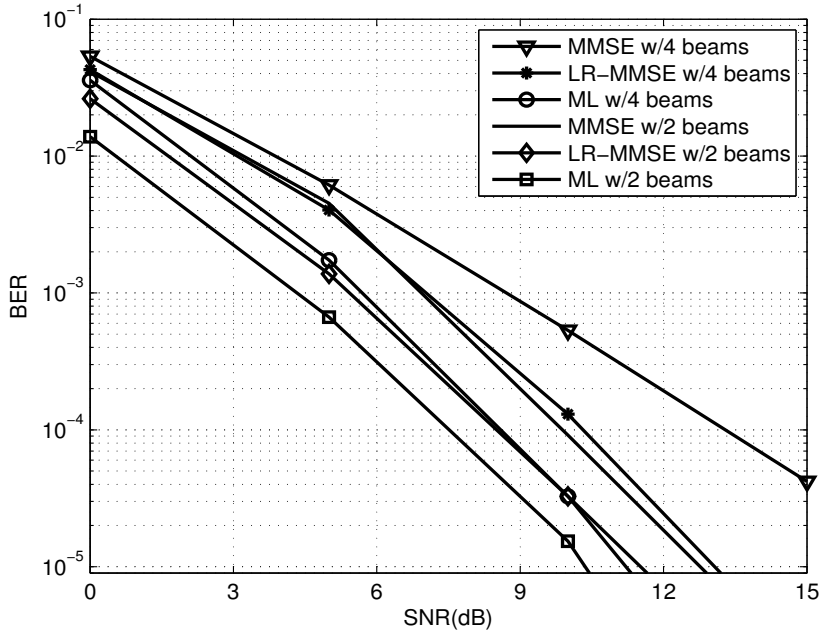

Figure 4.5: *BER performance versus SNR in comparison with ML, LR-MMSE and MMSE detection for ABPM with* $\eta = 3$ *and* 4 *bits/s/Hz.*

n_T. All three schemes are based on the optimal ML detection. The fourth transmission technique is V-BLAST-LR with $N_t = 3$, BPSK modulation and $\eta = 3$ bits/s/Hz.

ABPM's performance with ML detection and new antenna pattern design described in this chapter clearly outperforms other schemes as shown in Fig. 4.6, where gains of 3 dB when compared to SM 2x5 and GSSK, and more than 3.5 dB over SM 4x5 are observed at $P_{e,bit} = 10^{-5}$. It should be noted that the comparison between all schemes assumes identical transmission rate. To achieve the desired rate, SM is designed with different number of transmit antennas and modulation sizes as shown in Fig. 4.6. The complexity at the receiver side of these three schemes (SM, GSSK and ABPM-ML) is comparable because they all use the ML detector. As Fig. 4.6 shows, ABPM-LR (dashed line) presents gains over schemes based on SM at $P_{e,bit} = 10^{-5}$: around 2 dB over SM 2x5 and GSSK, 2.5 dB when compared to SM 4x5; even when the SM schemes are based on ML detection which has a higher complexity than the linear detection used in ABPM-LR.

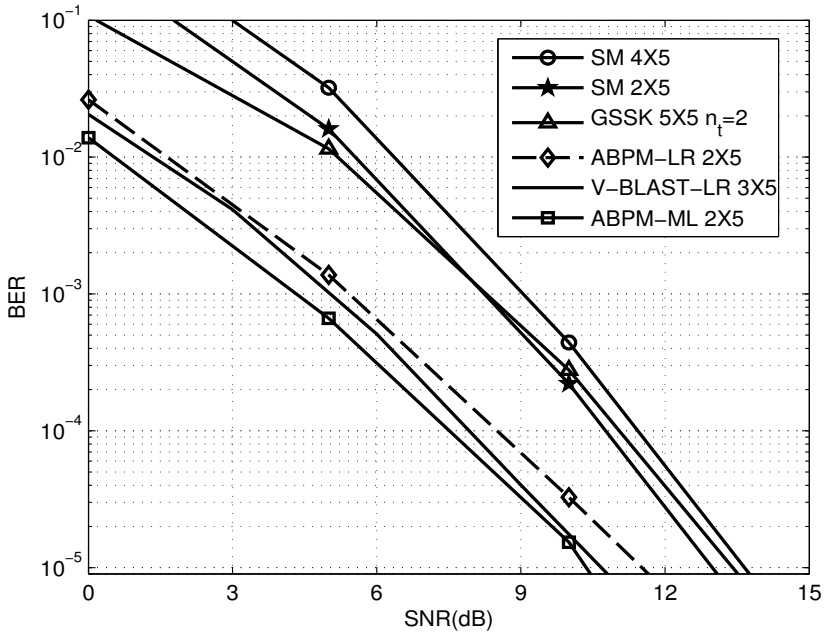

Figure 4.6: *BER comparison between ABPM with optimal and suboptimal detectors, spatial modulation and GSSK. For all systems* $N_r = 5$.

In comparing ABPM-LR to V-BLAST, it can be observed that the BER performance of the two is almost the same at low values of SNR. At $P_{e,bit} = 10^{-5}$, V-BLAST has less than 1 dB gain when compared to ABPM-LR. However, it should be noted that ABPM-LR uses less transmit antennas to achieve the same spectral efficiency as V-BLAST. The advantages of using fewer transmitters are decreased costs of RF chains, saving of physical space, reduced requirement in synchronisation and less interference between transmit antennas. The performance gain of ABPM-ML can be attributed to the improvement of spectral efficiency using antenna beam patterns which permit higher transmission diversity by transmitting the same information at each antenna.

Fig. 4.7 shows the comparison of ABPM and SM schemes with CSIT and CSIR. An exhaustive study of SM is presented in [4, 69], including an analysis of SM considering CSIT. Adaptive spatial modulation (ASM) [70] and optimal hybrid spatial modulation (OH-SM) [71] have explored the transceiver channel diversity through the use of CSIT to minimise the transmission rate. ASM utilises different modulation order for different channel conditions. OH-SM

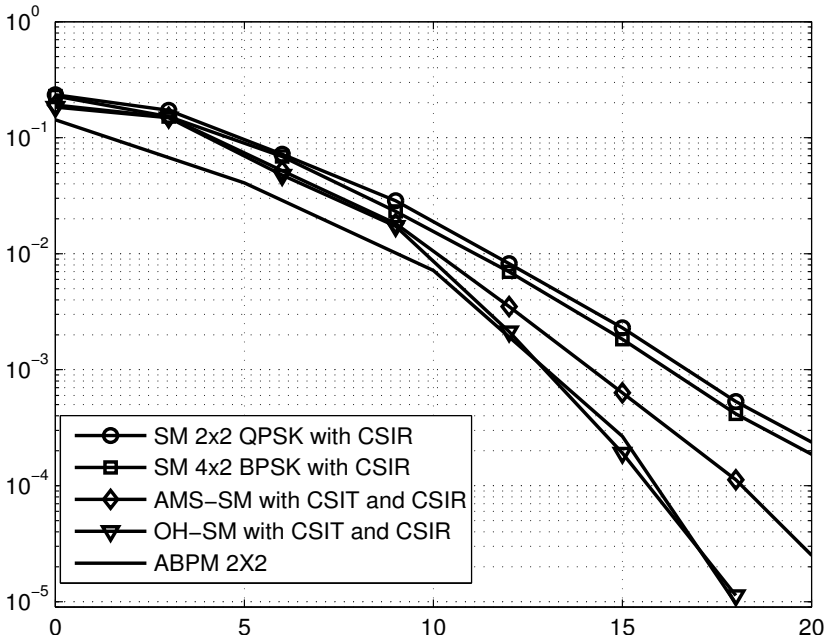

Figure 4.7: *BER versus SNR to compare ABPM and schemes based on SM considering CSIT and CSIR.*

is an extension of ASM, which incorporates the transmission mode switching (TMS) to use different transmission modes. All the schemes have a data rate of $\eta = 3$ bits/s/Hz. ABPM achieves a gain of 1.5 dB when compared to ASM and performance similar to that of OH-SM at $P_{e,bit} = 10^{-3}$. However, at low SNRs, ABPM outperforms OH-SM of 2 dB. In addition, adaptive modulation and TMS require high computational complexity and the number of required bits for feedback is large, particularly at high spatial dimension [71]. The traditional SM curves are shown in Fig. 4.7 only as a reference.

Figure 4.8 illustrates ABPM's performance with different number of transmit and receive antennas. Examples are presented to evaluate ABPM's performance using the same data rate (3 bits/s/Hz) with two different antenna beam patterns and QPSK modulation. It can be noticed that when $N_t \leq N_r$, ABPM has better performance with larger amounts of transmitters and receivers, since this scheme exploits the diversity at both sides. However, it is also noticeable that when $N_t > N_r$, (such as $N_t = 3$, $N_r = 2$) the performance is degraded compared to $N_t = 2$, $N_r = 2$ scheme. This is because each element

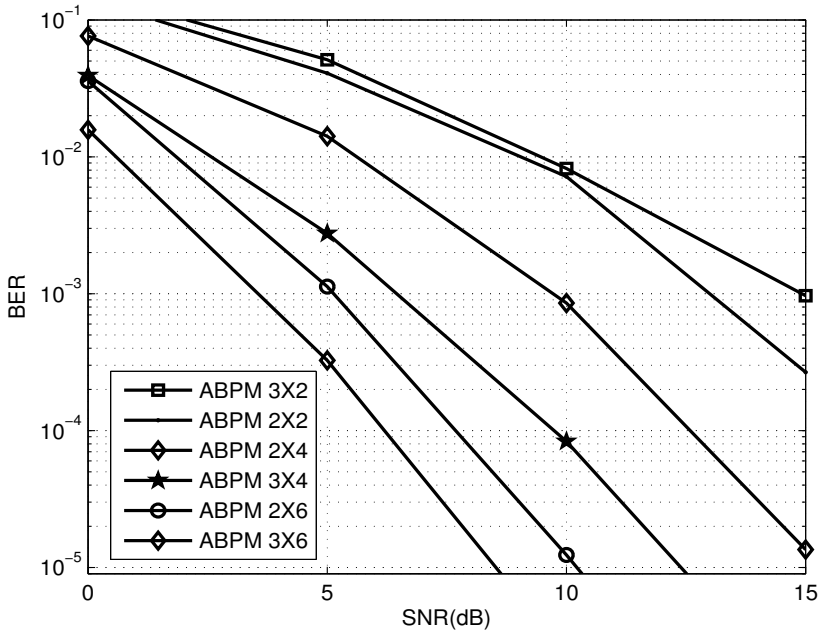

Figure 4.8: *Performance of ABPM with different MIMO scheme features (N_t and N_r), two different transmission beam patterns and QPSK symbols.*

of the vector **w** is transmitted by one antenna and then multiplied with one APM symbol. This transmission process is similar to spatial multiplexing. Then, it is expected that the constraint $N_t \leq N_r$ must be satisfied to recover the signal at the receiver.

Figure 4.9 illustrates the BER performance of ABPM with $N_t = 2$, $N_r = 5$ with two and four beam patterns carrying 4-QAM symbols in comparison with their upper bound. Each ABPM scheme has a spectral efficiency of 3 and 4 bits/s/Hz respectively. The 4-QAM with 2 beam patterns outperforms the system using 4-QAM with 4 beam patterns. The ML detector is used to demodulate the ABPM symbols. From this observation, it is clear that increasing the number of patterns degrades the BER performance due to the fact that the minimum distance between transmit vectors is reduced when more beam patterns are introduced. The upper bound is presented in order to validate the results obtained by simulations as explained in Section 4.4. It can be noticed that in the case of ABPM with 2 beams, the upper bound is tighter than ABPM with 4 beams. The reason for this is because (4.11) depends on

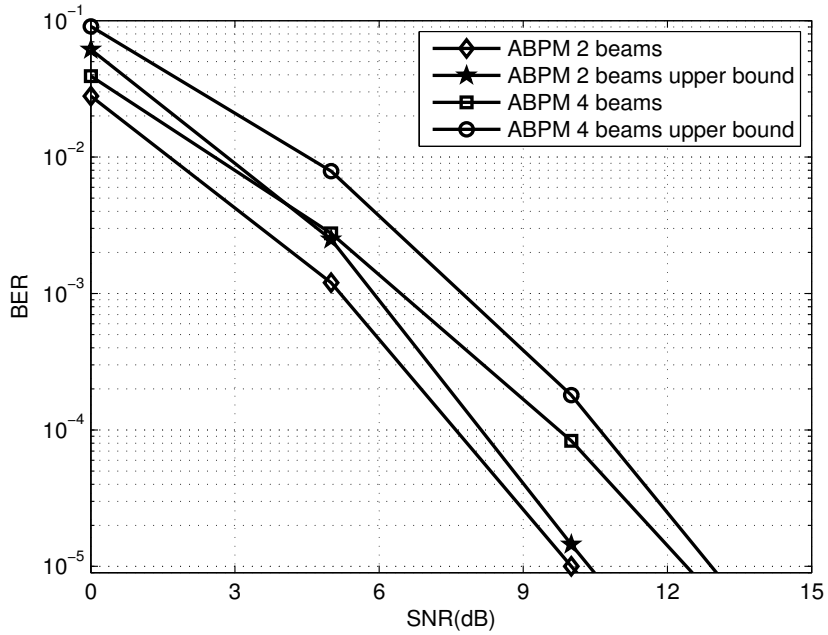

Figure 4.9: *BER versus SNR for* 4*-QAM modulation scheme with* 2 *and* 4 *beam patterns and their respective upper bounds.*

the number of beams and the Euclidean distance. Therefore, by increasing the number of beams, the value of parameter u in (4.11) increases, which will impact the accuracy of the bound.

It has been demonstrated that LR in combination with linear detectors (e.g. ZF, MMSE, etc) guarantees a performance similar to that of the optimal detector ML but with a lower computational complexity. Figure 4.10 compares the complexity between ML $\mathcal{O}((N_t N_r)^2 L)$, LR-MMSE and MMSE $\mathcal{O}(2N_r N_t^2 + b^2 + N_t N_r)$ detectors. It has been shown that ML has higher computational complexity in comparison to LR-MMSE. The number of arithmetic operations are increased when the numbers of N_t and/or N_r increase. The increased computational complexity of LR-MMSE over MMSE is caused by the calculation of the LLL algorithm $\mathcal{O}(N_t^4)$ to find the new basis and the inverse of $\mathbf{T}$ for ABPM. As previously mentioned, the utilisation of an LR-MMSE detector reduces the computational complexity achieving almost the same BER performance as with an ML detector.

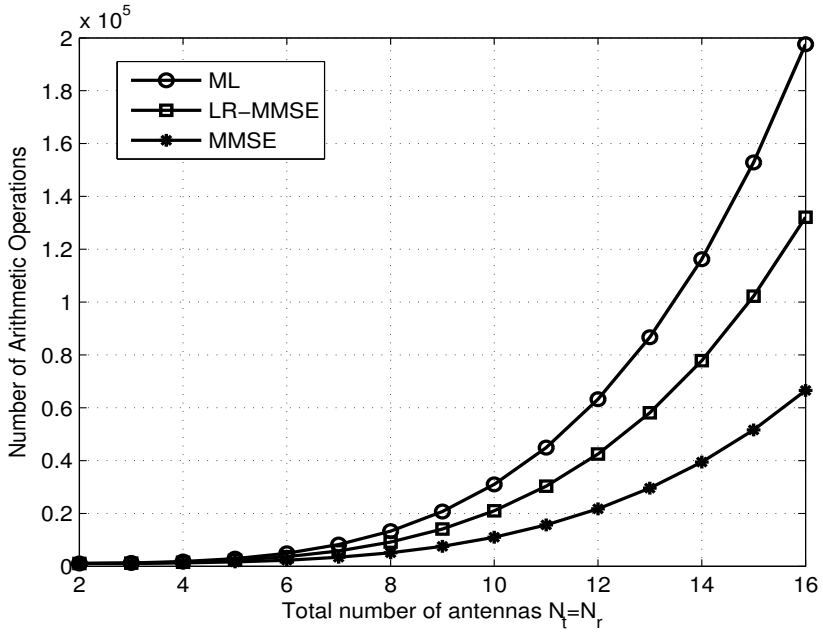

Figure 4.10: *Number of arithmetic operations of three different detectors.*

4.6 Summary

In this chapter, the ABPM scheme is presented. This is a transmission technique which proposes a criterion to select the antenna beam patterns based on the correlation between them and also introduces a new detection scheme based on LR which provides a performance close to that of the ML. In an ABPM system, the ML detector may not be viable for practical implementation when the constellation size or the number of antennas are large. For that reason LR techniques are employed, the performance of linear detectors approaches that of optimal detector ML while preserving low complexity.

In this chapter, an LR-aided linear equaliser for ABPM is proposed to reduce the detection complexity with the BER performance approaching that of the optimal detector ML. Simulation results show that even with this sub-optimal detection method, performance gain is achieved compared to different SM techniques using ML detection. The beam pattern design is based on the angle difference between main beam patterns to achieve low correlation. This ABPM with ML detection outperforms V-BLAST since ABPM exploits

diversity by sending the same information on all the transmitters. For the detection, an LR-aided algorithm combined with MMSE, is proposed as a suitable solution to achieve performance similar to that of the ML detector but with lower complexity. BER simulation results show that the ABPM outperforms the schemes based on SM using the optimal detector ML.

Therefore, a deeper study about the ABPM scheme regarding transmission and detection design has been presented. The antenna patterns are selected to minimise their correlation. A new LR-aided algorithm combined with MMSE is proposed as suboptimal detection to achieve performance which is similar to that of the optimal ML detector but with lower computational complexity. The BER results show that the ABPM-LR outperforms SM/ML and GSSK/ML by around 3 dB. An analytic upper bound has been derived to validate the simulation results. The performance of the antenna beam pattern modulation has indicated that it is a promising candidate for low complexity transmission techniques in future generations of communications systems such as in massive MIMO.

Chapter 5

Antenna Pattern Shift Keying Modulation

5.1 Introduction

GSSK modulation is a technique which exploits low-complexity spatial multiplexing for MIMO wireless systems. It is based on an SM system and improves the spectral efficiency compared with traditional MIMO transmissions. SM utilises the active antenna indices to carry information, as was discussed in Chapter 2. The scheme called generalised spatial modulation (GSMod) [72, 73] can be considered a generalisation of SM because GSMod sends identical symbols from any combination of the active antennas at each transmission time. GSSK and GSMod have the constraint of only using numbers of transmitters equal to powers of two to convey information among the possible active antenna combinations.

ABPM presented in Chapter 4 exploits the spatial channel using the antenna pattern to carry information, in order to achieve efficient information transmission. The beam pattern is determined by the antenna weights, using the AoD from the transmitter antenna array. The detectors of ABPM and the previously mentioned SM techniques, all use the ML detector. It is well-known that ML is the optimal detector but at the cost of high computation complexity when the number of antennas and/or the constellation size are very large.

The transmission techniques based on SM exploit receive diversity when channel state information at the receiver (CSIR) is available, while ABPM exploits the space domain to achieve more robust and efficient transmission. Motivated by these considerations, a new transmission technique is proposed based on the above features. This scheme called antenna pattern shift keying (APSK) modulation combines GPSSK [74] and ABPM [68]. The proposed scheme takes advantage of the benefits of both techniques to achieve higher spectral efficiency with a simple design. The APSK symbol contains three blocks respectively corresponding to the indices of the active transmitters, the antenna beam pattern and the conventional modulated symbols. After being transmitted, the symbol is estimated at the receiver side using the ML principle to de-map it into the three blocks. At the end of the chapter, the APSK scheme is evaluated by numerical simulation over an i.i.d. Rayleigh fading channel. The result proves the potential improvement in both reliability and efficiency that this technique offers.

APSK may be considered in large scale antenna array (massive MIMO) because it is critical to reduce the number of RF chains for better channel conditions (reducing the correlation between many elements) and to improve the energy efficiency by reducing the power consumption.

5.2 System Model

The general APSK modulation system model consists of a MIMO wireless link with N_t transmit and N_r receive antennas. Figure 5.1 illustrates the block diagram of a transmitter in the proposed scheme. A random sequence of independent bits $\mathbf{b} = [b_1 \quad b_2 \quad \cdots \quad b_k]$ enters a serial-to-parallel converter, where the output is divided into three blocks. The first block of m bits selects the indices of the active transmitters in the entire transmit antenna array. The second block, b_{m+1} to b_n, chooses an antenna pattern to transmit the conventional amplitude/phase modulation (APM) symbol, which is selected by the last $k-n$ bits, the third block, and mapped to the transmission vector $\mathbf{x} = [x_1, \quad x_2, \quad \cdots, \quad x_{N_t}]^T$.

The modulated signal is then transmitted over a $N_r \times N_t$ wireless channel $\mathbf{H}$. The received signal is given by $\mathbf{y} = \mathbf{Hx} + \mathbf{v}$, where $\mathbf{v} = [v_1 \quad v_2 \quad \cdots \quad v_{Nr}]^T$ represents the additive white Gaussian noise (AWGN) vector observed at the receive antennas with zero mean and covariance matrix $\mathbb{E}[\mathbf{v}\mathbf{v}^H] = \sigma_v^2 I_{Nr}$. The matrix channel $\mathbf{H}$ has i.i.d. entries with $\mathcal{CN}(0, 1)$. The channel is assumed to be flat-fading where the channel coefficients are invariant during each symbol and independently change from symbol to symbol. $\mathbf{H}$ is known at the transmitter side and at the receiver end. At the receiver, the three blocks are estimated by the ABPM detector to de-map them into the transmitted bits.

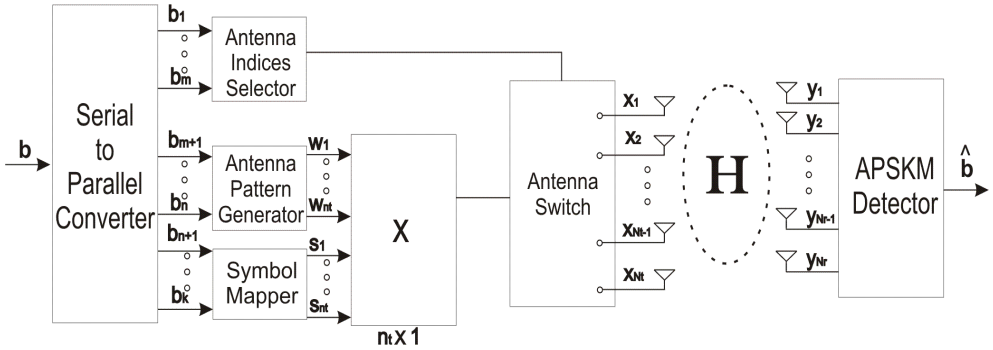

Figure 5.1: *APSKM system model.*

5.2.1 Transmission

For each symbol period, a stream of independent bits is sent to the serial-to-parallel converter and the output of the converter is divided into three blocks: the m bits in the first block indicate the antenna indices of n_t out of N_t transmission antennas. The number of possible combinations of n_t active antennas is $M' = \binom{N_t}{n_t}$. Then, 2^m must be smaller than or equal to M'. Hence the maximum number of bits that can be conveyed by n_t antenna indices is $\lfloor \log_2(M') \rfloor$. This model randomly selects 2^m antenna combinations from the overall M' possibilities and each m bit uniquely select one set of n_t active antennas. The second block determines the antenna pattern which is formed by n_t active transmit antennas. This second block corresponds to a certain

antenna beam pattern represented by a weight vector, which is denoted as $\mathbf{w} = [w_1, \quad w_2, \quad \cdots, \quad w_{n_t}]$. As previously mentioned, APSK is a combination of SPSK and ABPM schemes. The design criterion for the phase selection and the beam pattern can be found in Chapter 3 and Chapter 4 respectively.

Finally, the third block will determine the mapped PSK symbols and is denoted as s. Then, the weight vector $\mathbf{w}$ and the transmitted signal s are combined to generate the signal conveyed by all the active transmitters as shown in Figure 5.1. This signal is defined as $\mathbf{d} = [w_1 \cdot s, \quad w_2 \cdot s, \quad \cdots, \quad w_{n_t} \cdot s]^T$. The algorithm used to generate the antenna beam pattern weight vectors is explained in detail in Section 4.2.1.

The same symbol s is transmitted by all the active antennas, which is conveyed by the third block. Therefore, the transmission constellation vector, $[\frac{1}{\sqrt{n_t}} w_1 s \ , \frac{1}{\sqrt{n_t}} w_2 s, ..., \ \frac{1}{\sqrt{n_t}} w_{n_t} s]$ selected by the second and the third block can be mapped to the n_t active antennas which are selected by the first block. The factor $\frac{1}{\sqrt{n_t}}$ is used to normalise the power of the transmission vector to 1. All the other $N_t - n_t$ antennas remain idle (transmit 0) during the symbol period. In this way, the transmission vector $\mathbf{x} = [x_1, \quad x_2, \quad \cdots, \quad x_{N_t}]^T$ is determined. Mathematically, it is expressed as

$$x_n = \begin{cases} 0, & n \notin \mathbf{d} \\ \frac{1}{\sqrt{n_t}} w_l s, & n \in \mathbf{d} \ \ and \ \ n = d(l), \end{cases} \tag{5.1}$$

for $n = 1, ..., N_t$ and $l = 1, \cdots, n_t$.

Once established, the groups of k bits are mapped in a transmission vector $\mathbf{x}$, which contains the information of the active antenna beam pattern and the selected APM signal as Table 5.1 shown. The vector $\mathbf{x}$ contains information about the n_t active antennas, the antenna beam patterns and the APM symbols. To clarify the APSK modulation transmission scheme, a simple example with two different antenna beam patterns and BPSK modulation will be explained below. In this example, $N_t = 5$ and $n_t = 2$.

The first step is to calculate the number of bits that the APSK symbols can convey. The first block is calculated as $M' = \binom{5}{2} = 10$, the maximum number of bits can be contain in for this block in this example is $m \leq \lfloor \log_2(10) \rfloor = 3$. In this example, the scheme only has two different patterns, so the second

Table 5.1: *APSK modulation mapping rule with BPSK*

$\mathbf{b} = [b_1\ b_2\ b_3\ b_4\ b_5]$	j	$\mathbf{x} = [x_1 \quad x_2 \quad x_3 \quad x_4 \quad x_5]^T$
[0 0 0 0 0]	1	$\left[-\frac{w_{11}}{\sqrt{2}} \quad -\frac{w_{12}}{\sqrt{2}} \quad 0 \quad 0 \quad 0\right]^T$
[0 0 0 0 1]	2	$\left[+\frac{w_{11}}{\sqrt{2}} \quad +\frac{w_{12}}{\sqrt{2}} \quad 0 \quad 0 \quad 0\right]^T$
[0 0 0 1 0]	3	$\left[-\frac{w_{21}}{\sqrt{2}} \quad -\frac{w_{22}}{\sqrt{2}} \quad 0 \quad 0 \quad 0\right]^T$
[0 0 0 1 1]	4	$\left[+\frac{w_{21}}{\sqrt{2}} \quad +\frac{w_{22}}{\sqrt{2}} \quad 0 \quad 0 \quad 0\right]^T$
[0 0 1 0 0]	5	$\left[-\frac{w_{11}}{\sqrt{2}} \quad 0 \quad -\frac{w_{12}}{\sqrt{2}} \quad 0 \quad 0\right]^T$
[0 0 1 0 1]	6	$\left[+\frac{w_{11}}{\sqrt{2}} \quad 0 \quad +\frac{w_{12}}{\sqrt{2}} \quad 0 \quad 0\right]^T$
[0 0 1 1 0]	7	$\left[-\frac{w_{21}}{\sqrt{2}} \quad 0 \quad -\frac{w_{22}}{\sqrt{2}} \quad 0 \quad 0\right]^T$
[0 0 1 1 1]	8	$\left[+\frac{w_{21}}{\sqrt{2}} \quad 0 \quad +\frac{w_{22}}{\sqrt{2}} \quad 0 \quad 0\right]^T$
[0 1 0 0 0]	9	$\left[-\frac{w_{11}}{\sqrt{2}} \quad 0 \quad 0 \quad -\frac{w_{12}}{\sqrt{2}} \quad 0\right]^T$
[0 1 0 0 1]	10	$\left[+\frac{w_{11}}{\sqrt{2}} \quad 0 \quad 0 \quad +\frac{w_{12}}{\sqrt{2}} \quad 0\right]^T$
[0 1 0 1 0]	11	$\left[-\frac{w_{21}}{\sqrt{2}} \quad 0 \quad 0 \quad -\frac{w_{22}}{\sqrt{2}} \quad 0\right]^T$
[0 1 0 1 1]	12	$\left[+\frac{w_{21}}{\sqrt{2}} \quad 0 \quad 0 \quad +\frac{w_{22}}{\sqrt{2}} \quad 0\right]^T$
[0 1 1 0 0]	13	$\left[-\frac{w_{11}}{\sqrt{2}} \quad 0 \quad 0 \quad 0 \quad -\frac{w_{12}}{\sqrt{2}}\right]^T$
[0 1 1 0 1]	14	$\left[+\frac{w_{11}}{\sqrt{2}} \quad 0 \quad 0 \quad 0 \quad +\frac{w_{12}}{\sqrt{2}}\right]^T$
[0 1 1 1 0]	15	$\left[-\frac{w_{21}}{\sqrt{2}} \quad 0 \quad 0 \quad 0 \quad -\frac{w_{22}}{\sqrt{2}}\right]^T$
[0 1 1 1 1]	16	$\left[+\frac{w_{21}}{\sqrt{2}} \quad 0 \quad 0 \quad 0 \quad +\frac{w_{22}}{\sqrt{2}}\right]^T$
[1 0 0 0 0]	17	$\left[0 \quad -\frac{w_{11}}{\sqrt{2}} \quad -\frac{w_{12}}{\sqrt{2}} \quad 0 \quad 0\right]^T$
[1 0 0 0 1]	18	$\left[0 \quad +\frac{w_{11}}{\sqrt{2}} \quad +\frac{w_{12}}{\sqrt{2}} \quad 0 \quad 0\right]^T$
[1 0 0 1 0]	19	$\left[0 \quad -\frac{w_{21}}{\sqrt{2}} \quad -\frac{w_{22}}{\sqrt{2}} \quad 0 \quad 0\right]^T$
[1 0 0 1 1]	20	$\left[0 \quad +\frac{w_{21}}{\sqrt{2}} \quad +\frac{w_{22}}{\sqrt{2}} \quad 0 \quad 0\right]^T$
[1 0 1 0 0]	21	$\left[0 \quad -\frac{w_{11}}{\sqrt{2}} \quad 0 \quad -\frac{w_{12}}{\sqrt{2}} \quad 0\right]^T$
[1 0 1 0 1]	22	$\left[0 \quad +\frac{w_{11}}{\sqrt{2}} \quad 0 \quad +\frac{w_{12}}{\sqrt{2}} \quad 0\right]^T$
[1 0 1 1 0]	23	$\left[0 \quad -\frac{w_{21}}{\sqrt{2}} \quad 0 \quad -\frac{w_{22}}{\sqrt{2}} \quad 0\right]^T$

$[1\ 0\ 1\ 1\ 1]$	24	$\left[0 \quad +\frac{w_{21}}{\sqrt{2}} \quad 0 \quad +\frac{w_{22}}{\sqrt{2}} \quad 0\right]^T$
$[1\ 1\ 0\ 0\ 0]$	25	$\left[0 \quad -\frac{w_{11}}{\sqrt{2}} \quad 0 \quad 0 \quad -\frac{w_{12}}{\sqrt{2}}\right]^T$
$[1\ 1\ 0\ 0\ 1]$	26	$\left[0 \quad +\frac{w_{11}}{\sqrt{2}} \quad 0 \quad 0 \quad +\frac{w_{12}}{\sqrt{2}}\right]^T$
$[1\ 1\ 0\ 1\ 0]$	27	$\left[0 \quad -\frac{w_{21}}{\sqrt{2}} \quad 0 \quad 0 \quad -\frac{w_{22}}{\sqrt{2}}\right]^T$
$[1\ 1\ 0\ 1\ 1]$	28	$\left[0 \quad +\frac{w_{21}}{\sqrt{2}} \quad 0 \quad 0 \quad +\frac{w_{22}}{\sqrt{2}}\right]^T$
$[1\ 1\ 1\ 0\ 0]$	29	$\left[0 \quad 0 \quad -\frac{w_{11}}{\sqrt{2}} \quad -\frac{w_{12}}{\sqrt{2}} \quad 0\right]^T$
$[1\ 1\ 1\ 0\ 1]$	30	$\left[0 \quad 0 \quad +\frac{w_{11}}{\sqrt{2}} \quad +\frac{w_{12}}{\sqrt{2}} \quad 0\right]^T$
$[1\ 1\ 1\ 1\ 0]$	31	$\left[0 \quad 0 \quad -\frac{w_{21}}{\sqrt{2}} \quad -\frac{w_{22}}{\sqrt{2}} \quad 0\right]^T$
$[1\ 1\ 1\ 1\ 1]$	32	$\left[0 \quad 0 \quad +\frac{w_{21}}{\sqrt{2}} \quad +\frac{w_{22}}{\sqrt{2}} \quad 0\right]^T$

block only carries one bit. Finally the third block is represented by the APM symbol, and in this example the modulation is BPSK, so this block contains only one bit.

Taking all the above into account, the transmission vector will convey five bits. The first three bits ($b_1\ b_2\ b_3$) indicate which antennas are active or in other words, the indices of active antennas. Thus, b_4 indicates the antenna beam pattern used to carry the symbol information corresponding to b_5. Then, the total number of constellation points in this example is 32. Table 5.1 shows the list of the transmission vectors for two different beams and BPSK modulation. In this example, when $b_4 = 0$, the first beam is generated by the weight vector $\mathbf{w}_1 = [0.5000 + 0.0000i \quad 0.0000 - 0.5000i]$. When $b_4 = 1$, the second beam is generated by the weight vector $\mathbf{w}_2 = [0.5000 + 0.5000i \quad -0.5000i - 0.5000i]$. Thereby, b_5 is mapped to BPSK symbols based on Table 5.1, i.e. when $b_5 = 0 \quad s = -1$ and when $b_5 = 1 \quad s = +1$. These patterns have been selected because of their low correlation. The design and selection of antenna patterns have been explained in Section 4.2.1.

Figure 5.2 illustrates the transmission process for APSK explained above, where an APSK symbol has 5 bits and is transmitted using $n_t = 2$ out of $N_t = 5$. In this example, two possible weight vectors are selected in combination with BPSK modulation symbols.

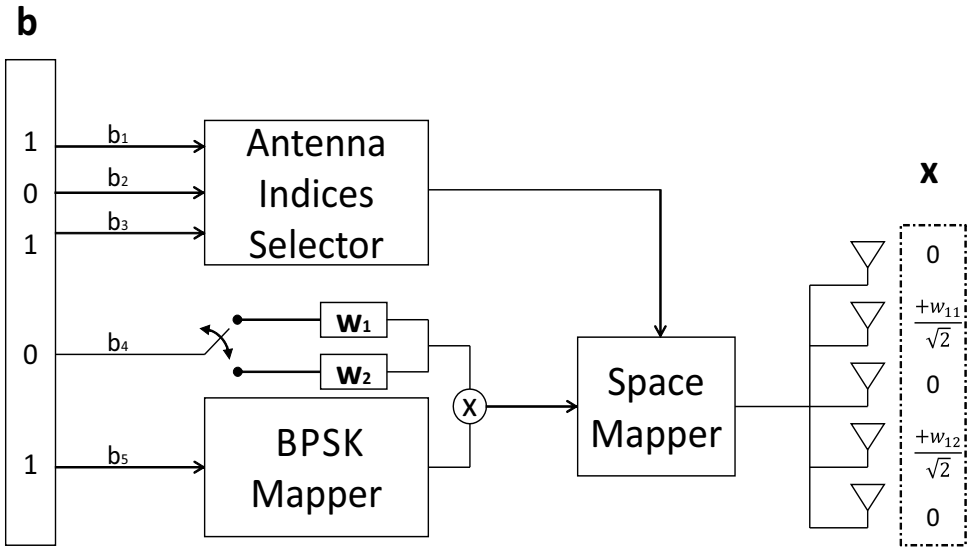

Figure 5.2: *Transmission for APSK modulation.*

5.2.2 Detection

The information data contains the indices of the n_t active transmitters which convey an antenna beam pattern and an APM symbol. Therefore, the estimation of the three blocks is an important task in the scheme. As previously described, the output of the channel is

$$\mathbf{y} = \mathbf{H}\mathbf{x} \ + \ \mathbf{v}. \tag{5.2}$$

The objective of the detector is to estimate the APSK symbol, which contains three blocks: the indices of the active antennas, the antenna patterns and the APM symbols. Assuming all the constellation vectors are equally likely to be transmitted, the optimum detection is given by the ML method

$$\widehat{j} = \arg\min_{j} \|\mathbf{y} - \mathbf{H}\mathbf{x}_j\|^2. \tag{5.3}$$

The ML detection of $\widehat{j}$ can be performed by an exhaustive search over all possible transmission vectors $\mathbf{x}_j$ for the minimum Euclidean distance $\|\mathbf{y} - \mathbf{H}\mathbf{x}_j\|^2$. As soon as $\widehat{j}$ is detected, the APSK symbol can be de-mapped. For

the case illustrated in Table 5.1, there are 32 possible vectors for $\mathbf{x}_j$. This number increases with larger amounts of beam patterns, modulation orders or transmitters. For example, there are 64 $\mathbf{x}_j$ vectors when APSK modulation is used with the same antenna array ($N_t = 5$, $n_t = 2$) but with 4 beam patterns and 2 APM symbols or with 2 beam patterns and 4 APM symbols. However, even with 64 vectors, the complexity load at the receiver is not significantly increased compared to the systems based on SM schemes.

Considering the advantages previously mentioned, a potential application of APSK in future wireless systems may be in large scale antenna systems, where the reduction of the RF chains numbers is vital.

5.3 Simulation Results

In this section, simulation results of APSK are presented. The performance is evaluated using Monte Carlo simulations for 10^6 channel realisations and the plots illustrate the BER performance versus the signal-to-noise ratio. The simulated channel is of a flat Rayleigh fading with i.i.d. fading over all wireless links.

The APSK data rate per symbol is $\eta = 5$ bits/s/Hz transmission with $N_r = 5$ antennas. Figure 5.3 shows the average BER performance for APSK, GSSK and V-BLAST schemes. For comparison purposes all the systems are based on the ML detector. In order to achieve the same η, APSK is set with the parameters described in Section 5.2.1. GSSK has $N_t = 5$ and $n_t = 3$. V-BLAST transmits BPSK symbols to $N_t = 5$ transmit antennas, this scheme utilises all the transmitters at any time. The number of RF chains of APSK, GSSK and V-BLAST is 2, 3 and 5 respectively. Then, the power consumption used by APSK is lower in comparison to GSSK and V-BLAST.

Figure 5.3 shows that the APSK modulation scheme outperforms both the GSSK and V-BLAST schemes. It can be noticed that APSK has a gain of 3 dB at $P_{e,bit} = 10^{-4}$ over GSSK. The gain is smaller when APSK is compared to V-BLAST. Nevertheless, in this simulation APSK is designed with $n_t = 2$ active transmitters whereas in V-BLAST all transmitters are always

active ($N_t = 5$). Therefore, APSK has less RF chains which has an impact on hardware design, channel estimation, synchronisation, ICI and cost. The performance gain obtained by APSK is attributed to the low correlation of the two selected beam patterns and the space diversity of the APM information, achieved through sending the same data from each transmitter.

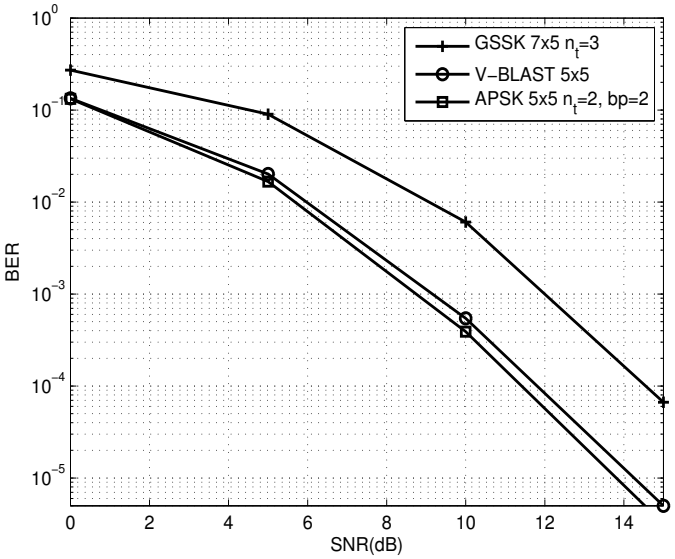

Figure 5.3: *BER performance of APSK versus GSSK and V-BLAST for $\eta = 5$ bits/s/Hz transmission ($N_r = 5$).*

5.4 Summary

In this chapter the APSK modulation is introduced. The APSK modulation is a novel hybrid transmission scheme for multiple antenna wireless systems. It conveys information jointly using a general phase modulation, the indices of active transmitter antennas and antenna beam patterns to improve the spectral efficiency and reliability while keeping the detection affordable. The idea behind this transmission technique is to map the bit vector corresponding to one transmission vector in three information-carrying blocks: the first block determines the active antenna indices, the second maps to the antenna beam

patterns and the third block maps to the conventional APM symbols. The detector estimates these three blocks and uses them to de-map the signal.

APSK modulation combines two novel transmission schemes: SPSK modulation and ABPM. SPSK was proposed in [74] and exploits the antenna indices to carry information. ABPM was presented in [68] and uses the beam patterns to carry information.

Throughout the chapter, APSK modulation principles are laid out as the building ground for new hybrid modulation schemes. APSK outperforms GSSK and V-BLAST when all three have the same data rate since APSK uses low correlated beam patterns and exploits space diversity to transmit APM symbol information. BER simulation results were illustrated where the APSK scheme outperforms GSSK modulation (up to 3 dB) and the V-BLAST scheme with the same ML detection and the same spectral efficiency. These advantages make APSK modulation a promising candidate for low complexity transmission techniques in future generations of communications systems such as massive MIMO.

APSK might be implemented in large scale antenna systems by activating a few transmitters only, yet it can improve the efficiency of both spectrum usage and power consumption. Improving these parameters is very important and represents a major challenge for massive MIMO schemes APSK could be a good solution to these challenges.

Chapter 6

Lattice Reduction Pre-Coding Aided Spatial Modulation

6.1 Introduction

USING multiple antennas at the transmitter and receiver side in wireless communications has led to unprecedented improvements over single antenna systems. For this reason, MIMO techniques such as V-BLAST [16] and STBC [13] have been adopted in many standards such as 3GPP-LTE and 802.11 as was mentioned in Chapter 2.

In Chapter 2, the concept of SM proposed in [8] has been established as a beneficial transmission scheme, subsuming the numerous MIMO systems family. MIMO transmission SM is more suitable for massive MIMO because it reduces the requirement of estimation of huge number of channel paths. It is a single-RF large-scale MIMO wireless system but exploits multiple antennas in a novel fashion compared to high complexity classic MIMO systems. SM takes advantage of the whole antenna array at the transmitter, while using a limited number of RF chains [27]. This effectively simplifies the channel estimation and makes it an ideal choice for massive MIMO. The distinctive feature of SM is that its symbols are divided in two blocks, where the first block contains the active transmitter index and the second block carries the information of the conventional APM. These unique characteristics facilitate high data rate

MIMO implementations with reduced signal processing and system complexity, as well as improved energy efficiency [30].

Currently, the schemes based on SM assume that the transmit antenna indices carry information and that the receiver has CSI. In some MIMO systems, the CSIT mode is preferable because it reduces the complexity of the receiver [75]. Additional advantages of using CSIT have also been observed such as: SNR gain can be observed at the receiver in space-time diversity schemes, in addition to the transmit diversity gain. Another advantage is, higher system capacity than with CSIR for MIMO systems with more transmitters than receivers [76].

Given CSIT, the family of pre-coding aided spatial modulation (PSM) schemes are proposed by Yang in [77] to convey extra information by choosing the receivers' indices wisely. In PSM, the indices provide additional information in the spatial domain. PSM successfully decreases the cost and complexity of the receiver side. Thus, it may be considered suitable for downlink transmission. The scheme called Generalised Pre-coding Aided Spatial Modulation (GPSM) described in [29, 77] is a variation of SM [8, 24, 27, 28, 58, 78]. GPSM uses the indices of the antennas at the receiver to convey information in addition to a conventional APM. The GPSM transmission contains two components, the first one is the preprocessing scheme which selects a desired receive antenna and the second one chooses the conventional APM symbol. GPSM requires a perfect CSIT and uses ML detection.

As massive MIMO usually works for TDD mode, GPSM can be a good candidate for this systems. However, the use of hundreds of antennas is not affordable with ML detection. This chapter proposes a sub-optimal detection method to address this disadvantage. However, as expected this sub-optimal detection method causes performance degradation. To solve this problem, a novel LR based pre-coder is proposed, which greatly improves the BER performance and makes the use of a low-complexity detector possible. As a result, the BER performance of [29] and the proposed scheme is comparable in spite of the latter using a linear detector. In this chapter, the proposed pre-coding technique is used to improve the performance of GPSM. However,

it is also possible to utilise the technique to improve the BER performance of other systems.

The chapter is structured as follows. Section 6.2 introduces the conventional GPSM system model, the pre-coding transmission matrix and the original detection. Section 6.3, the LR pre-coder matrix and the linear detector are introduced. Section 6.4 presents simulation results and the chapter summary can be found in Section 6.5.

6.2 Generalised Pre-coding Aided Spatial Modulation

The GPSM method presented in [29] will be explained first. GPSM can be defined as a system which relies on activating a set of receivers with the aid of a pre-coder at the transmitter side. The particular set of active receivers selected (i.e. indices of active receive antennas) convey additional information, to that carried by the conventional APM symbols mapped to it.

6.2.1 GPSM Transmission

The general system model consists of an MIMO wireless link with N_t transmit and N_r receive antennas. GPSM mitigates the ICI at the transmitter side using a pre-coding matrix $\mathbf{P} \in \mathbb{C}^{N_r \times Nt}$ before the source signal is transmitted, exploiting the CSIT [77]. The GPSM symbol is divided into two blocks, the first block indicates the indices of the active receivers (n_r) out of N_r and the second block is mapped to the APM symbol sent by all the transmitters. Thus, the GPSM symbol $\mathbf{s}_m^c \in \mathbb{C}^{N_r \times 1}$ is defined as $\mathbf{s}_m^c = \mathbf{\Omega}_c \mathbf{b}_m$, where $c = 1, ..., \mathcal{B}$, $\mathcal{B}$ is the number of all the possible selections of n_r out of N_r, $\mathbf{b}_m$ is a vector $n_r \times 1$ which contains the particular APM symbol selected by the second block of the GPSM symbol and $\mathbf{\Omega}_c$ represents a diagonal matrix corresponding to the c selected receivers, representing the information given by the first block of the GPSM symbol.

In [77], the transmitter pre-processing scheme applied to the N_r antennas is based on the ZF algorithm. The transmitter pre-coding matrix $\mathbf{P}$ allocates all

the energy received to the selected receivers, trying to generate the maximal possible output through preventing the power leaking to the other receivers. $\mathbf{P}$ is expressed as:

$$\mathbf{P} = \beta \mathbf{H}^{*}(\mathbf{H}^{T}\mathbf{H}^{*})^{-1}, \tag{6.1}$$

where $\beta = \sqrt{N_t}$ is a normalising factor. After the pre-coding process, the resultant transmit signal $\mathbf{x} \in \mathbb{C}^{N_t \times 1}$ is expressed as:

$$\mathbf{x} = \mathbf{P}^{T}\mathbf{s}_{m}^{c}. \tag{6.2}$$

GPSM Transmission Design

An example of the GPSM transmission scheme is given in Figure 6.1 which illustrates the system utilising $N_t = 5$, $N_r = 4$ and $n_r = 2$ active receivers. In this example, GPSM transmits QPSK modulation symbols.

The length of the two GPSM blocks has to be calculated to set the number of bits per transmit symbol. The first block contains information related to the possible n_r active receiver combinations and it is calculated as follows

$$m = \left\lfloor \log_2 \binom{N_r}{n_r} \right\rfloor = \lfloor \log_2 \binom{4}{2} \rfloor = 2,$$

where m is the number of bits contained in the first block. It is also important to define c, which indicates the number of possible combinations of n_r active receivers. Then, c is expressed as:

$$c = 2^{m} = 4.$$

In Table 6.1, the four possible combinations of c are shown. It is observed that each pair of bits are mapped to their corresponding n_r combination. Then, n_{r_1} and n_{r_2} are thr active antennas out of the four receivers N_r (N_{r_1}, N_{r_2}, N_{r_3} and N_{r_4}).

In the example provided in Figure 6.1, the GPSM symbol is [1 0 0 1]. The first block [1 0] assumes that the n_r active receivers are N_{r_1} and N_{r_4} and the second block [0 1] is mapped into a QPSK symbol equal to $-1+i$. The matrix $\mathbf{\Omega}_{c_3} \in \mathbb{Z}^{N_r \times n_r}$ is shown in Figure 6.1. The vector $\mathbf{b}_m = [-1+i \quad -1+i]^{T}$. Then, the vector $\mathbf{s}_m^c$ is obtained to finally, with the pre-coder $\mathbf{P}$, generate the transmit signal $\mathbf{x} \in \mathbb{C}^{N_t \times 1}$.

Table 6.1: *Mapping table for the first block in a GPSM system with $N_r = 4$ and $n_r = 2$*

$[b_1$	$b_2]$	c	n_{r_1}	n_{r_2}
0	0	c_1	N_{r_1}	N_{r_2}
0	1	c_2	N_{r_1}	N_{r_3}
1	0	c_3	N_{r_1}	N_{r_4}
1	1	c_4	N_{r_2}	N_{r_3}

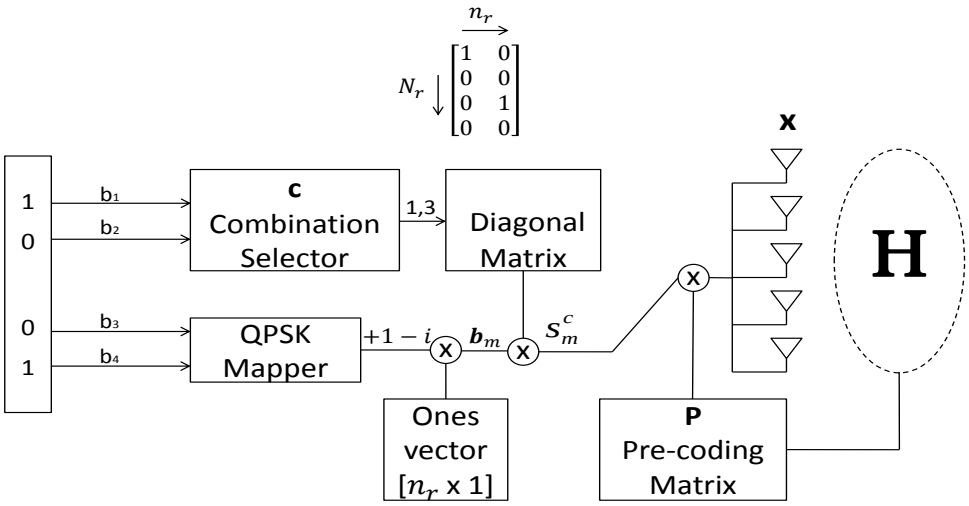

Figure 6.1: *Transmission design for GPSM.*

6.2.2 GPSM Detection

The signal observed at N_r receive antennas, is written as

$$\mathbf{y} = \mathbf{Hx} + \mathbf{v}, \tag{6.3}$$

where $\mathbf{v} = [v_1 \quad v_2 \quad \cdots \quad v_{N_r}]^T$ represents the AWGN vector observed at the receive antennas with zero mean and covariance matrix $E[\mathbf{v}\mathbf{v}^H] = \sigma_v^2 \boldsymbol{I_{Nr}}$. $\mathbf{H} \in \mathbb{C}^{N_r \times N_t}$ represents the matrix channel involved, where each entry is assumed to be flat Rayleigh fading and all entries are uncorrelated.

In [29] an ML based detector is employed. The detection process can be divided into two stages. The first stage detects the indices of the active receivers and is expressed as:

$$\hat{k} = \arg\max_{w \in [1,c]} \sum_{p=1}^{n_r} |\mathbf{y}_w(p)|^2, \tag{6.4}$$

where $\mathbf{y}_w$ is the matrix that contains the rows extracted from $\mathbf{y}$ with subscript set w indicating the selected n_r rows out of N_r. p indicates the index of the corresponding row. The second stage estimates the APM symbol and is expressed as:

$$\hat{n} = \arg\min_{n \in [1,M]} |\mathbf{y}_{\hat{k}}/\beta - b_n|^2. \tag{6.5}$$

This two-step decoding method has the complexity of $\mathcal{O}(N_r^2 L + n_r^2 c)$ which is lower than a conventional ML detector for MIMO.

6.3 Proposed GPSM System Model

The GPSM system model has attractive features which are useful for future wireless system applications such as massive MIMO. However, as massive MIMO increases the number of transmitters and receivers, an estimator based on ML, even with separate detection, is not feasible due to its high computational complexity. Taking this into consideration, a linear detection algorithm which has lower complexity than the ML estimator is proposed. As linear detectors generally do not perform as well as ML, a novel pre-coding matrix based on the LR algorithm is employed to compensate the performance degradation.

In Section 2.4, the lattice reduction algorithm was presented. As was mentioned, a lattice can be represented by different bases. The lattice reduction goal is to find the basis with the best orthogonal conditions for a given lattice. Recently, LR in combination with linear equalisers has been used to improve the performance for detection in MIMO systems. The performance improvement is achieved when the lattice basis is orthogonal or close to that. The ML detector is based on exhaustive search so it is not limited by the aforementioned condition. However, when the ML detector is not used, this condition is not satisfied which consequently degrades the performance.

Typically, LR aided detectors utilise the LLL algorithm [55] because in spite of not guaranteeing that the optimal basis will be found, it guarantees finding a basis with better orthogonal conditions than without it[48].

Using LR with linear detectors has proven a good solution for achieving performance which is comparable to that of ML but with lower computational complexity [11, 48, 50, 51, 52, 55, 64, 65].

6.3.1 Transmission

As previously mentioned, LR detectors have been utilised to achieve performance similar to that of ML through the channel treatment. Then, the improved orthogonal conditions of a channel with the LR scheme can make the detection more accurate. The LR algorithm has also been used as part of the decoder to improve the performance of linear equalisers in MIMO systems. The LR algorithm replaces $\mathbf{H}$ for $\tilde{\mathbf{H}}$ with improved orthogonality between columns. The output of the LLL algorithm is a matrix $\mathbf{T}$, which has two properties: it is formed only by integers and its determinant is ± 1.

Based on this principle, the LR scheme is used to enhance the GPSM performance by maximising the energy to the n_r active receivers. The $\tilde{\mathbf{H}} = \mathbf{H}^T\mathbf{T}$ matrix channel is close to orthogonal.

In this chapter, the pre-coding matrix is calculated based on the matrix obtained from the LR procedure and is expressed as:

$$\tilde{\mathbf{P}} = \beta\tilde{\mathbf{H}}^*(\tilde{\mathbf{H}}^T\tilde{\mathbf{H}}^*)^{-1}. \tag{6.6}$$

Thus, the GPSM transmit signal $\mathbf{x} \in \mathbb{C}^{N_t \times 1}$ is rewritten as:

$$\mathbf{x} = \tilde{\mathbf{P}}\mathbf{s}_m^c. \tag{6.7}$$

6.3.2 Detection

The received signal observed is written as:

$$\mathbf{y} = \mathbf{H}\mathbf{x} + \ \mathbf{v}. \tag{6.8}$$

The proposed detection method can be divided into two steps. First, the rows of the $\tilde{\mathbf{z}}$ are sorted in descending order based on their power magnitude as follows:

$$\begin{aligned} \tilde{\mathbf{z}} &= \text{sort}\{\mathbf{y}\}. \\ &= \begin{bmatrix} \tilde{z}_{\hat{\lambda}_1} \\ \tilde{z}_{\hat{\lambda}_2} \\ \vdots \\ \tilde{z}_{\hat{\lambda}_{nr-1}} \\ \tilde{z}_{\hat{\lambda}_{n_r}} \\ \tilde{z}_{\hat{\lambda}_{n_r+1}} \\ \vdots \\ \tilde{z}_{\hat{\lambda}_{Nr}}, \end{bmatrix} \end{aligned} \tag{6.9}$$

and then the indices of the first n_r elements in (6.9) are the estimation of the indices of the n_r active receive antennas. The estimation of the n_r active receivers is done based on the mapping list associated with the $\mathcal{B}$ possible combinations. The mapping list is expressed as:

$$\begin{bmatrix} c_1 \\ c_2 \\ \vdots \\ c_{\mathcal{B}} \end{bmatrix} \Rightarrow \begin{bmatrix} 0 & 0 & \cdots & 0 \\ 0 & 0 & \cdots & 1 \\ \vdots & & \ddots & \vdots \\ 1 & 1 & \cdots & 1 \end{bmatrix}$$

If the estimation is correct, the indices of the n_r elements should be identical to one of the selection patterns. This can be detected by comparing with all possible selection of n_r out of N_r. This method is sub-optimal because if the combination is not found in the selection patterns, the $\tilde{z}_{\hat{\lambda}_{n_r}}$ element is replaced

by the $\tilde{z}_{\hat{\lambda}_{n_r+1}}$ element, $\tilde{z}_{\hat{\lambda}_{n_r+2}}$ and so on. This process is repeated until the first block is de-mapped.

The resulting vector with the n_r elements is defined as $\mathbf{y}(\hat{k})$. Then, the APM symbol $\hat{m}$ can be estimated as:

$$\hat{m} = \mathcal{Q}\Big(\sum_{p=1}^{n_r} \mathbf{y}_{\hat{k}}(p)\Big), \tag{6.10}$$

where $\mathcal{Q}()$ is the symbol quantiser to the APM constellation set and $\mathbf{y}(\hat{k})$ includes the n_r maximum values from the vector $\hat{\mathbf{z}}$.

The computational complexity of the proposed decoding method is $\mathcal{O}(N_r^2 + n_r c)$. This complexity is assuming that the pattern c is found until the last possible combination. Thus, it requires N_r operations but this scenario is not likely for all the iterations.

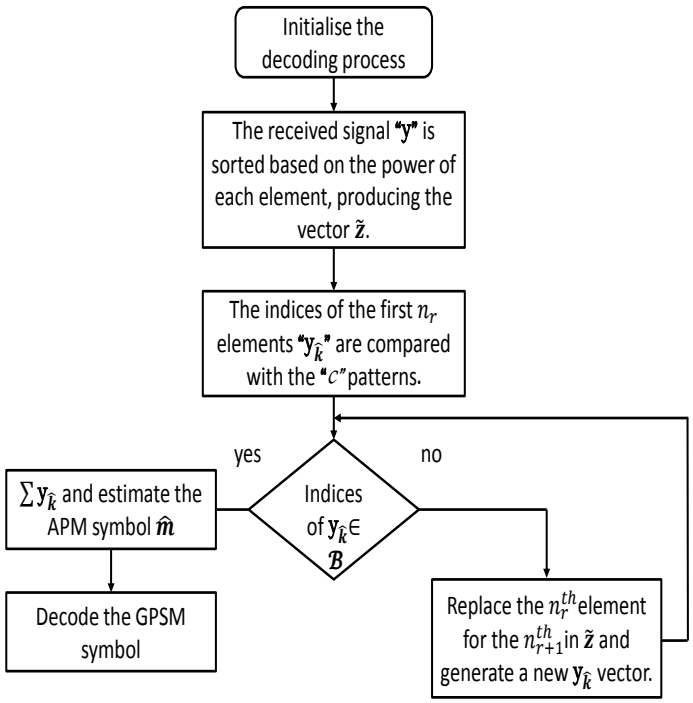

Figure 6.2: *Diagram block algorithm for the proposed GPSM decoding method.*

Fig. 6.2 illustrates the block diagram of the decoding algorithm proposed for GPSM. This diagram shows how (6.9) and (6.10) work to estimate the receiver indices and the APM symbol, respectively. It is worth noticing that (6.9) is repeated until a pattern c can be estimated. The n_r^{th} element is replaced because it is most likely that the elements with lowest power may be the idle receivers. However, the simulation results show that it is most likely that the indices of the first n_r elements represent the right active receivers, particularly at moderate or high SNRs. Therefore, the possibility of repeating the comparison is very low, and hence this procedure has very low complexity.

The ML detection method of the original GPSM works in the following manner (GPSM/ML); the power of all elements are calculated, the highest elements are selected and compared with the power of all the possible patterns. In addition, the proposed detection method utilises linear method to detect the APM symbol. On the other hand, with the original GPSM, APM is detected by comparing with all the possible APM symbols, which may increase the complexity significantly for high APM constellation schemes.

Fig. 6.3 shows the comparisons between the original GPSM/ML and the proposed LR-GPSM using linear decoding scheme (LR-GPSM/LD) in terms of computational complexity. Both systems (GPSM/ML and LR-GPSM/LD) are analysed using different percentages of active receivers n_r. The proposed decoding scheme requires less operations because it only utilises a matrix multiplication, a sort function and the quantisation operator. On the other hand, the GPSM/ML decoding method uses the ML algorithm at each step to decode the symbol. For that reason, the LR-GPSM/LD decoding scheme does not utilise as many comparisons as the conventional GPSM/ML and the decoding process is faster than GPSM/ML. Another aspect to highlight is that the complexity is higher when the number of possible patterns c increases because the decoder has to compare all the possible combinations. This has a bigger impact on the ML scheme than a linear scheme.

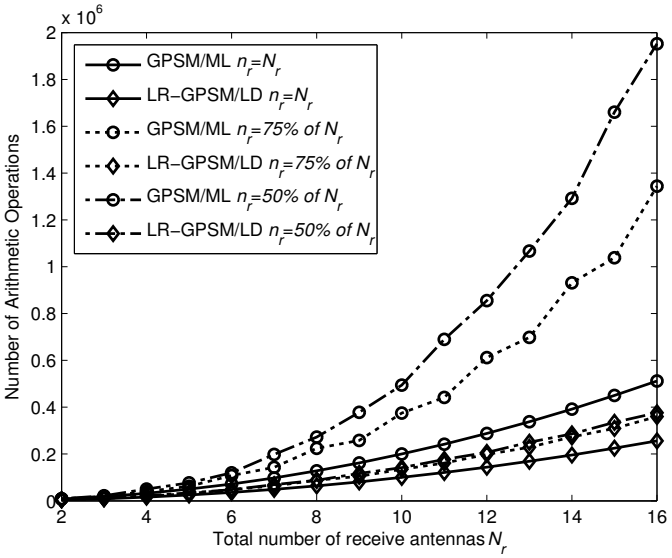

Figure 6.3: *Decoding processing computational time of GPSM/ML vs LR-GPSM/LD.*

6.4 Simulation results

In this section, the proposed LR-GPSM results compared to the original GPSM scheme [29] are presented. Monte Carlo simulations are performed at least 10^6 channel realisations. For simulation parameters are: a flat Rayleigh fading channel, $\eta = 4$ bits/s/Hz transmission with $N_t = 8$, $N_r = 4$ and $n_r = 3$.

Fig. 6.4 shows the BER performance of the GPSM/ML [29] in comparison with the proposed LR-GPSM using ML detection (LR-GPSM/ML) and LR-GPSM/LD.

As seen in the figure, LR-GPSM/ML produces a gain of more than 1 dB over the original GPSM in terms of BER, showing the effectiveness of LR-based pre-coding. The LR-GPSM/LD has a performance comparable to the original GPSM but with much lower complexity. It is noticed that at low SNR the original GPSM performs sightly better than GPSM-LR/LD. This is because the impact of noise at low SNRs is bigger and will lead to wrong estimation of the indices and worse performance.

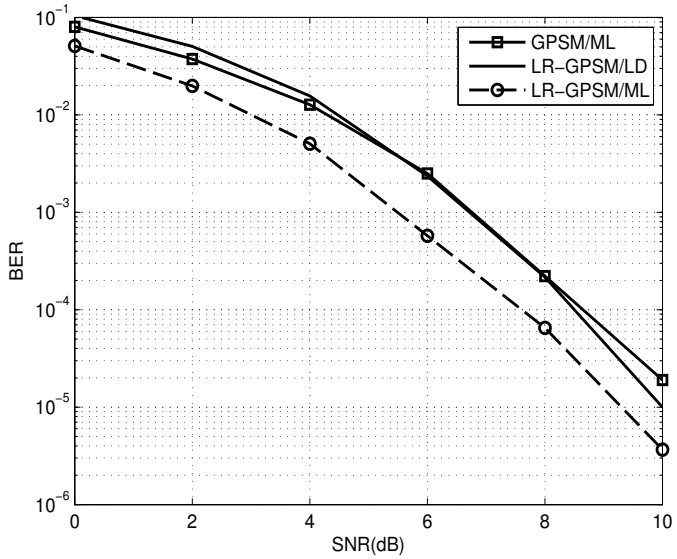

Figure 6.4: *BER performance of GPSM versus SNR, for* $N_t = 8$, $N_r = 4$ *and* $n_r = 3$.

6.5 Summary

In this chapter, a novel pre-coding scheme and a sub-optimal detector applied to GPSM are proposed, which also can be used in other systems. It is demonstrated that performance gain and complexity reduction are achieved in comparison with the work presented in [29]. The simulation results demonstrate that GPSM-LR/LD has performance which is similar to that of the conventional GPSM but with significant complexity reduction in the decoding process. The LR based pre-coding GPSM with low complexity detection scheme can be considered an ideal candidate for emerging technologies such as massive MIMO.

Chapter 7

Conclusions and Future Work

7.1 Conclusion

In this chapter a brief revision of the main contributions of this thesis and some proposed directions for future work are explained. At the outset, the objective of this thesis is to explore alternatives for novel transmission schemes and low complexity decoders, which may improve the overall system performance for future wireless communication systems. The proposed techniques are designed to improve the traditional system as follows:

- Three transmission methods based on SM are proposed to improve the spectral efficiency. These methods convey extra information through the use of the antenna indices, beam patterns and a combination of these. In addition, these methods reduce the power consumption and complexity as not all the transmitters are used.

- The ML detector is not feasible when there is a large number of antennas or with higher-order forms of modulation. A sub-optimal detection scheme based on LR is proposed to reduce the decoding complexity. This sub-optimal scheme achieves performance similar to that of the ML detector.

A summary of the technical work already explained in the previous chapters now follows. Some suggestions for potential future research in wireless communication systems are then discussed.

7.2 Thesis Summary

- The first chapter explained the motivation of this work and the necessary prerequisites to solve some of the difficulties in wireless communications. It begins with some historic facts in the development of communication systems. The evolution of wireless systems and some concepts are explained briefly as background information and to ensure understanding of the later chapters.

- In the second chapter, traditional MIMO is described, explaining the fundamental concepts of the diversity and multiplexing tradeoff for MIMO systems. All the advantages and disadvantages for its most important transmission schemes are explained in detail. Pre-coding and decoding definitions are explained and the importance of these schemes in the communication systems is discussed. Then, an alternative to reduce the decoding complexity is introduced, which uses LR in combination with traditional low-complexity decoders. The aim of LR is to transform the original channel matrix into a new one but with better orthogonality conditions.

- In the third chapter, a new transmission technique scheme is proposed in order to bridge the gap between spectral and energy efficiency. The proposed scheme is based on SM and is called SPSK modulation. In SPSK, only a few antennas are active at any time. In addition to the antenna indices, the phases transmitted on active antennas also carry information to further improve spectral efficiency. The phases selection criterion is analysed and optimised by choosing the phases with the larger diameter (distance between the phase points). This selection impacts the performance in terms of BER. Thus, the SPSK modulation scheme shows performance gain when compared to systems based on SM and spatial multiplexing. An upper bound is also derived to validate the results achieved by SPSK and it can be proposed as a good alternative for a future MIMO transmission scheme.

- In the fourth chapter, ABPM is introduced as a novel transmission technique for MIMO channels. ABPM improves the spectral efficiency by selecting different antenna beam patterns to carry additional information. An optimum method is proposed to select the beam pattern based on low correlation to achieve BER performance gain. Another novel feature proposed for this scheme is the decoding algorithm based on LR. This technique improves the BER performance by improving the orthogonality conditions to the channel matrix. Then, a linear equaliser is used to estimate the transmitted signal. Simulations show that ABPM outperforms systems based on SM even with the LR decoder. Analytical performance is derived to support the ABPM with ML decoder's results.

- The fifth chapter investigates a novel transmission scheme (APSK), which combines the ABPM principle and SPSK modulation. It increases the spectral efficiency by sending extra information by the antenna indices and the beam patterns. This scheme only utilises a few transmitters at any time, so APSK scheme can be considered an energy efficient system. APSK results show improvements when compared to technique based on SM and spatial multiplexing, which makes this scheme a great candidate for future generation wireless systems such as massive MIMO.

- In the sixth chapter, a pre-coding scheme based on LR is proposed as the pre-coder in GPSM. CSIT is assumed to be available to use LR as a pre-coding matrix, which facilitates the detection at the receiver side. The use of pre-coding scheme in GPSM improves the spectral efficiency and system reliability. This technique uses all the transmitter antennas but only a few receiver antennas at any time. As LR is used as pre-coder, it facilitates the use of a linear equaliser at the receiver side. The simulation results show that if these two proposed techniques are applied to GPSM, the BER performance is improved with reduced computational complexity.

7.3 Suggestions for Further Work

Many interesting questions arise from the work previously presented. The most important problem would seem to be to design a system with high spectral efficiency, simple transmission design, low decoding complexity and as few RF chains as possible. There are some schemes, which propose a tradeoff between these features. Achieving all these characteristics appears quite challenging and particularly for future wireless system communications such as massive MIMO. Therefore, this section outlines some of the potential areas for future work based on the work presented within this thesis.

- **Extending the proposed schemes to massive MIMO.**
  Massive MIMO seems to be the future for wireless communications. However, the research on this topic still raises a lot of questions which have to be resolved, such as the transmission mode for the downlink (TDD or FDD). Then, with the addition of large amounts of antennas but only utilising a few of them, a criterion should be established to set the optimum number of active transmitters. In addition to this idea, a criterion has to be established for when not all the receivers are active.

- **Evaluation under realistic channels.**
  Many novel transmission techniques have been analysed, which have good features and characteristics in comparison with the well-known spatial multiplexing (V-BLAST) and SM. However, the performance of these proposed schemes and all the gains may be radically different in realistic channels. The European WINNER project [79], which is part of the Framework 6 effort, is currently researching the outline of a system design of such a "beyond-3G" system. The WINNER project started recently and there is an immediate demand for models suitable for initial usage. This channel modelling is used for initial evaluation of "beyond-3G" technologies in outdoor scenarios within the WINNER project. It is highlighted in [80, 81] that the WINNER channel modelling takes the following key cluster parameters into consideration: delay, power, AoD, AoA, Ricean K-factor, mobile station, mobile station speed, number of rays

per cluster, ray powers, cluster and composite cluster azimuth-spread at mobile station and at base station. All the schemes analysed are going to be affected by the WINNER channel modelling.

- **Exploit the CSIT in a more efficient way.**
  ABPM and APSK are schemes which use the CSIT. However, they did not take into consideration the channel conditions in the design of the patterns at the moment. Therefore, the establishment of a criterion where the CSIT can be made in a more efficient use to achieve better channel diversity and overall performance can be investigated.

- **Adaptive modulation scheme.**
  The channel conditions change with time. For that reason, link-adaptation schemes are required to achieve better system performance. For different channel conditions, a low-complexity modulation order selection criterion is developed to decide the optimal transmission mode that yields the best BER performance while remaining with the average transmission bit rate target. Throughout this thesis, many systems have been proposed with diverse features that show some improvements over well-known MIMO techniques. Each of these novel methods have demonstrated better performance at either low or high SNR. The channel information is made available through the feedback information. This means that not only the transmission information rate can be varied but also the number of active transmitters and/or receivers can change between transmission techniques.

- **Unification of the proposed schemes.**
  Different schemes have been analysed in this thesis, which propose many good characteristics for future wireless communication systems. Many improvements have been shown, where some of them are for systems that use all the transmitters and others for systems which only have a few active transmitters. Schemes for pre-coding and decoding have been introduced which aim to improve the overall system performance and/or reduce the complexity. Therefore, an interesting research topic would be

to analyse the possibility of designing a framework which utilises only a few transmitters and a few receivers but exploits the advantages of the whole antenna array at both sides as in the proposed schemes in this thesis.

In summary, much remains to be done in this area because the demand for high data rates continuously increases. In addition to these demands, the future wireless systems are focused on being energy efficient. Taking into consideration that massive MIMO seems to be the future in wireless communications, the reduction of RF chains and decoding complexity in combination with other techniques such as SM, CSIT, LR, etc. may fulfil the user demands.

Appendix A

Pairwise Error Probability Derivation

In this appendix the derivation of the PEP for MIMO block fading channel is explained. For code systems, the PEP uses the basic structure for the union bound calculation of the error probability and it is utilised as the main criteria for code design. Considering a signal constellation which contains a set of M signal vectors $\{\tilde{\mathbf{s}}_m\}_{m=1}^{M}$. As all the signal vectors are equally likely the $P_m = 1/M$ [82]. Observing the received signal $\tilde{\mathbf{r}}$, the ML detector selects the signal vector $\tilde{\mathbf{s}}_m$ that reduces the squared Euclidean distance $\|\tilde{\mathbf{r}} - \tilde{\mathbf{s}}_m\|^2$. It is important to notice that all $\tilde{\mathbf{r}} \in R_m$, where R_m indicates the decision regions and is defined as:

$$R_m = \{\tilde{\mathbf{r}} : \|\tilde{\mathbf{r}} - \tilde{\mathbf{s}}_m\|^2 \leq \|\tilde{\mathbf{r}} - \tilde{\mathbf{s}}_{\tilde{m}}\|^2, \forall \tilde{m} \neq m\}. \tag{A.1}$$

The decision regions are hyperplanes that are defined by the locus of the signal points which are equidistant from two neighbouring signal vectors.

Then, the conditional error probability linked with $\tilde{\mathbf{s}}_m$ is expressed as:

$$\begin{aligned} P(c, \tilde{\mathbf{s}}_m) = &\ P(\tilde{\mathbf{r}} \notin R_m) \\ = &\ 1 - P(\tilde{\mathbf{r}} \in R_m) \\ = &\ 1 - P(e|\tilde{\mathbf{s}}_m), \end{aligned} \tag{A.2}$$

where $P(e|\tilde{\mathbf{s}}_m)$ indicates the conditional probability of correct estimation. Then, using the joint conditional probability density function (PDF), (A.2) can be expressed as:

$$P(c, \tilde{\mathbf{s}}_m) = \ 1 - \int_{R_m} p(\tilde{\mathbf{r}}|\tilde{\mathbf{s}}_m) \mathrm{d}\tilde{\mathbf{r}}. \tag{A.3}$$

Therefore, the average error probability is

$$P(c) = \frac{1}{M}\sum_{m=1}^{M} P(c, \tilde{\mathbf{s}}_m). \tag{A.4}$$

The PEP determines the probability of decision error at the receiver, considering that only two signal points exist. Then, the PEP can be defined for each pair of signal vectors in the constellation. Considering two signal vectors $\tilde{\mathbf{s}}_j$ and $\tilde{\mathbf{s}}_k$, separated by the squared Euclidean distance $\tilde{d}^2_{jk}$, the PEP is

$$P(c, \tilde{\mathbf{s}}_j) = Q\left(\sqrt{\frac{\alpha^2 \tilde{d}^2_{jk}}{4N_o}}\right), \tag{A.5}$$

where α is the magnitude of the fading gain and N_o is the noise density. Finally, $P(c, \tilde{\mathbf{s}}_j) = P(c, \tilde{\mathbf{s}}_k)$ and the PEP between the signal vectors is

$$P(\tilde{\mathbf{s}}_j, \tilde{\mathbf{s}}_k) = P(c, \tilde{\mathbf{s}}_j) = P(c, \tilde{\mathbf{s}}_k) = Q\left(\sqrt{\frac{\alpha^2 \tilde{d}^2_{jk}}{4N_o}}\right). \tag{A.6}$$

Applying these definitions to the techniques proposed in this thesis, the PEP between two arbitrary code-words $\mathbf{c}$ and $\mathbf{e}$ over N time slots in the Rayleigh L-block fading channel [60] is expressed as:

$$\begin{aligned} P(\mathbf{c} \to \mathbf{e}) &= 1 - \int_{R_m} p(\mathbf{c}|x)\mathrm{d}x \\ &= aE_w\left[Q\left(\sqrt{\sum_{j=1}^{N_t}\sum_{v=1}^{N_r} \mid w_j^v \mid^2}\right)\right], \end{aligned} \tag{A.7}$$

where R_m is the decision regions, $p(\mathbf{c}|x)$ is the joint conditional probability density function (PDF), $a = \frac{E_s}{4N_t N_o}$, E_s is the symbol energy, N_o is Gaussian noise variance and $\mid w_j^v \mid$ is Rayleigh distributed.

Denote $\mathbf{w} = \mathbf{w}_1^1$ and $\mathbf{z}_j^v = \frac{\mathbf{w}_1^v}{\mathbf{w}}$, $(j,v) \neq (1,1)$. Their joint PDF, $f(w, z_j^v \cdots z_{N_t}^{N_r})$ can be obtained from their cumulative density function
$F(w, z_j^v \cdots z_{N_t}^{N_r})$ and expressed as:

$$\begin{aligned} f(w, z_j^v \cdots z_{N_t}^{N_r}) =& w^{2N_r N_t - 1}. \\ & \prod_{\substack{j=1 \\ (j,v)\neq(1,1)}}^{N_t}\prod_{v=1}^{N_r} z_j^v e^{-\frac{w^2}{2}\left(1+\sum_{j=1}^{N_t}\sum_{v=1}^{N_r}{}_{(j,v)\neq(1,1)}(z_j^v)^2\right)}. \end{aligned} \tag{A.8}$$

One of the properties of the complementary Gaussian cumulative distribution function (Q-function) is the integral property [83], which is expressed

$$\int_0^\infty x^{2n-1} \mathrm{e}^{-\frac{x^2}{2}} Q\left(\frac{x}{N_o}\right) \mathrm{d}x = \frac{(n-1)!}{2}(1-(N_o^2+1)^{-\frac{1}{2}})^n \times \sum_{k=0}^{n-1} 2^{-k} \binom{n-1+k}{k} (1+(N_o^2+1)^{-\frac{1}{2}})^k. \tag{A.9}$$

Utilising (A.8) and (A.9), the PEP can be expressed as:

$$P(\mathbf{c} \to \mathbf{e}) = \left(\frac{1-\frac{1}{u}}{2}\right)^\Lambda \sum_{k=0}^{\Lambda-1} 2^{-k} \binom{\Lambda-1+k}{k} \left(1+\frac{1}{u}\right)^k, \tag{A.10}$$

where $u = \sqrt{1+\frac{1}{a}}$, $\Lambda = N_t N_r$.

References

[1] Z. Hasan, H. Boostanimehr, and V. K. Bhargava, "Green cellular networks: A survey, some research issues and challenges," *Communications Surveys & Tutorials, IEEE*, vol. 13, no. 4, pp. 524–540, 2011. xiii, 5

[2] D. Gesbert, M. Kountouris, R. W. Heath, C.-B. Chae, and T. Salzer, "Shifting the mimo paradigm," *IEEE Signal Process. Mag,*, vol. 24, no. 5, pp. 36–46, 2007. 2, 5, 12, 17

[3] S. Cui, A. J. Goldsmith, and A. Bahai, "Energy-constrained modulation optimization," *IEEE Trans. Wireless Commun.*, vol. 4, no. 5, pp. 2349–2360, 2005. 3, 21

[4] M. Di Renzo, H. Haas, A. Ghrayeb, S. Sugiura, and L. Hanzo, "Spatial modulation for generalized mimo: challenges, opportunities, and implementation," *IEEE Proc.*, vol. 102, no. 1, pp. 56–103, 2014. 3, 18, 19, 20, 22, 25, 65

[5] L. M. Correia, D. Zeller, O. Blume, D. Ferling, Y. Jading, I. Gódor, G. Auer, and L. Van Der Perre, "Challenges and enabling technologies for energy aware mobile radio networks," *IEEE Commun. Mag.*, vol. 48, no. 11, pp. 66–72, 2010. 4

[6] G. Da Costa, J.-P. Gelas, Y. Georgiou, L. Lefevre, A.-C. Orgerie, J. Pierson, O. Richard, and K. Sharma, "The green-net framework: Energy

efficiency in large scale distributed systems," in *IEEE Int. Symp. Parallel & Distributed Processing (IPDPS) 2009.* IEEE, 2009, pp. 1–8. 4

[7] S. Schwarz, R. W. Heath Jr, and M. Rupp, "Single-user mimo versus multi-user mimo in distributed antenna systems with limited feedback," *EURASIP J. Adv. Signal Process.*, vol. 2013, no. 1, pp. 1–20, 2013. 5, 16

[8] R. Y. Mesleh, H. Haas, S. Sinanovic, C. W. Ahn, and S. Yun, "Spatial modulation," *IEEE Trans. Veh. Technol.*, vol. 57, no. 4, pp. 2228–2241, 2008. 5, 18, 19, 81, 82

[9] A. Younis, S. Sinanovic, M. Di Renzo, R. Mesleh, and H. Haas, "Generalised sphere decoding for spatial modulation," *IEEE Trans. Commun.*, vol. 61, no. 7, pp. 2805–2815, 2013. 5, 19

[10] E. Agrell, T. Eriksson, A. Vardy, and K. Zeger, "Closest point search in lattices," *IEEE Trans. Inf. Theory*, vol. 48, no. 8, pp. 2201–2214, 2002. 6, 26, 59

[11] Q. Zhou and X. Ma, "Element-Based Lattice Reduction Algorithms for Large MIMO Detection," *IEEE J. Sel. Areas Commun.*, vol. 31, no. 2, pp. 274–286, 2013. 6, 27, 87

[12] G. Foschini, "Layered space-time architecture for wireless communication in a fading environment when using multi-element antennas," *Bell Labs Tech. J.*, vol. 1, no. 2, pp. 41–59, 1996. 11

[13] S. Alamouti, "A simple transmit diversity technique for wireless communications," *IEEE J. Sel. Areas Commun.*, vol. 16, no. 8, pp. 1451–1458, 1998. 12, 14, 15, 81

[14] V. Tarokh, N. Seshadri, and A. Calderbank, "Space-time codes for high data rate wireless communication: Performance criterion and code construction," *IEEE Tran. Inf. Theory*, vol. 44, no. 2, pp. 1185–1191, 1998. 12, 14, 17

[15] B. Cantrell, J. Rao, G. Tavik, M. Dorsey, and V. Krichevsky, "Wideband array antenna concept," in *Radar Conference, 2005 IEEE International*. IEEE, 2005, pp. 680–684. 13

[16] P. W. Wolniansky, G. J. Foschini, G. Golden, and R. Valenzuela, "V-blast: An architecture for realizing very high data rates over the rich-scattering wireless channel," in *Proc. 1998 URSI Int. Symp. Signals Syst. Electron.* IEEE, 1998, pp. 295–300. 15, 81

[17] L. Zheng and D. Tse, "Diversity and multiplexing: A fundamental tradeoff in multiple-antenna channels," *IEEE Tran. Inf. Theory*, vol. 49, no. 5, pp. 1073–1096, 2003. 17, 18

[18] V. Tarokh, A. Naguib, N. Seshadri, and A. Calderbank, "Combined array processing and space-time coding," *IEEE Trans. Inf. Theory*, vol. 45, no. 4, pp. 1121–1128, 1999. 17, 18

[19] M. Chiani, M. Z. Win, and A. Zanella, "On the capacity of spatially correlated MIMO Rayleigh-fading channels," *IEEE Trans. Inf. Theory*, vol. 49, no. 10, pp. 2363–2371, 2003. 17

[20] M. O. Damen, A. Abdi, and M. Kaveh, "On the effect of correlated fading on several space-time coding and detection schemes," in *Veh. Technol. Conf. (VTC) 2001-Fall*, vol. 1. IEEE, 2001, pp. 13–16. 17

[21] H. Jafarkhani, *Space-time coding: theory and practice*. Cambridge university press, 2005. 17, 47

[22] R. Vaughan and J. Andersen, *Channels, propagation and antennas for mobile communications*. IET, 2003, pp. 46–47. 18

[23] A. M. Tonello, "Space-time bit-interleaved coded modulation with an iterative decoding strategy," in *52nd Veh. Technol. Conf. (VTC-Fall) 2000*, vol. 1. IEEE, 2000, pp. 473–478. 18

[24] R. Mesleh, H. Haas, C. Ahn, and S. Yun, "Spatial modulation: A new low complexity spectral efficiency enhancing technique," in *1st Int. Conf. Commun. and Networking China (ChinaCom) 2006*, 2006, pp. 1–5. 18, 19, 31, 82

[25] M. Di Renzo and H. Haas, "Performance analysis of spatial modulation," in *5th Int. Conf. Commun. and Networking in China (CHINACOM) 2010*. IEEE, 2010, pp. 1–7. 18, 19

[26] G. J. Foschini and M. J. Gans, "On limits of wireless communications in a fading environment when using multiple antennas," *Wireless Pers. Commun.*, vol. 6, no. 3, pp. 311–335, 1998. 19

[27] J. Jeganathan, A. Ghrayeb, and L. Szczecinski, "Spatial modulation: optimal detection and performance analysis," *IEEE Commun. Lett.*, vol. 12, no. 8, pp. 545–547, 2008. 19, 63, 81, 82

[28] A. ElKalagy and E. AlSusa, "A novel two-antenna spatial modulation technique with simultaneous transmission," in *17th Int. Conf. Softw., Telecommun. Comput. Networks (SoftCOM) 2009*, sept. 2009, pp. 230 –234. 19, 82

[29] R. Zhang, L. Yang, and L. Hanzo, "Generalised pre-coding aided spatial modulation," *IEEE Trans. Wireless Commun.*, vol. 12, no. 11, pp. 5434–5443, 2013. 19, 82, 83, 86, 91, 92

[30] A. Stavridis, S. Sinanovic, M. Di Renzo, H. Haas, and P. Grant, "An energy saving base station employing spatial modulation," in *IEEE 17th Int. Workshop Comput. Aided Modelling and Design of Commun. Links and Networks (CAMAD) 2012*. IEEE, 2012, pp. 231–235. 20, 82

[31] J. Mietzner, R. Schober, L. Lampe, W. H. Gerstacker, and P. A. Hoeher, "Multiple-antenna techniques for wireless communications-a comprehensive literature survey," *IEEE Commun. Surv. Tut.*, vol. 11, no. 2, pp. 87–105, 2009. 20

[32] F. Héliot, M. A. Imran, and R. Tafazolli, "On the energy efficiency-spectral efficiency trade-off over the mimo rayleigh fading channel," *IEEE Trans. Commun.*, vol. 60, no. 5, pp. 1345–1356, 2012. 20

[33] J. Xu and L. Qiu, "Energy efficiency optimization for mimo broadcast channels," 2012. 20

[34] H. Kim, C.-B. Chae, G. De Veciana, and R. W. Heath, "A cross-layer approach to energy efficiency for adaptive mimo systems exploiting spare capacity," *IEEE Trans. Wireless Commun.*, vol. 8, no. 8, pp. 4264–4275, 2009. 20

[35] A. Nosratinia, T. E. Hunter, and A. Hedayat, "Cooperative communication in wireless networks," *IEEE Commun. Mag.*, vol. 42, no. 10, pp. 74–80, 2004. 21

[36] R. Mesleh, S. S. Ikki, E.-H. M. Aggoune, and A. Mansour, "Performance analysis of space shift keying (ssk) modulation with multiple cooperative relays," *EURASIP J. Adv. Signal Process.*, vol. 2012, no. 1, pp. 1–10, 2012. 21

[37] X. Xie, Z. Zhao, M. Peng, and W. Wang, "Spatial modulation in two-way network coded channels: Performance and mapping optimization," in *IEEE Int. Symp. Pers. Indoor Mobile Radio Commun. (PIMRC) 2012*. IEEE, 2012, pp. 72–76. 21

[38] N. Serafimovski, S. Sinanovic, M. Di Renzo, and H. Haas, "Dual-hop spatial modulation (dh-sm)," in *IEEE Veh. Technol. Conf. (VTC Spring) 2011*. IEEE, 2011, pp. 1–5. 21

[39] Z. Zhang, H. JI, Y. LI, and H.-l. ZHANG, "Novel incremental relaying protocol based on spatial modulation," *J. China Univ. Posts and Telecommun.*, vol. 19, no. 4, pp. 73–79, 2012. 21

[40] F. R. Gfeller and U. Bapst, "Wireless in-house data communication via diffuse infrared radiation," *Proc. IEEE*, vol. 67, no. 11, pp. 1474–1486, 1979. 22

[41] R. Mesleh, H. Elgala, and H. Haas, "Optical spatial modulation," *IEEE/OSA J. Opt. Commun. Netw.*, vol. 3, no. 3, pp. 234–244, 2011. 22

[42] J. Hoydis, S. Ten Brink, and M. Debbah, "Massive mimo: How many antennas do we need?" in *49th Annu. Allerton Conf. Commun., Control and Comput.* IEEE, 2011, pp. 545–550. 23, 24, 53

[43] E. G. Larsson, F. Tufvesson, O. Edfors, and T. L. Marzetta, "Massive mimo for next generation wireless systems," *IEEE Commun. Mag.*, 2014. 24

[44] F. Rusek, D. Persson, B. K. Lau, E. G. Larsson, T. L. Marzetta, O. Edfors, and F. Tufvesson, "Scaling up mimo: Opportunities and challenges with very large arrays," *IEEE Signal Process. Mag.*, vol. 30, no. 1, pp. 40–60, 2013. 24

[45] J. Nam, J.-Y. Ahn, A. Adhikary, and G. Caire, "Joint spatial division and multiplexing: Realizing massive MIMO gains with limited channel state information," in *46th Annu. Conf. Inf. Sci. and Syst. (CISS) 2012*. IEEE, 2012, pp. 1–6. 24

[46] Y. Jiang, M. Varanasi, and J. Li, "Performance analysis of ZF and MMSE equalizers for MIMO systems: an in-depth study of the high SNR regime," vol. 57, no. 4. IEEE, 2011, pp. 2008–2026. 25, 26, 52

[47] J. Cassels, *An introduction to the geometry of numbers*. Springer Verlag, 1997. 25

[48] F. T. Luk, S. Qiao, and W. Zhang, "A lattice basis reduction algorithm," *Institute for Comput. Mathematics Technol. Report 10*, vol. 4, 2010. 26, 87

[49] O. Damen, A. Chkeif, and J.-C. Belfiore, "Lattice code decoder for space-time codes," *IEEE Commun. Lett.*, vol. 4, no. 5, pp. 161–163, 2000. 26

[50] D. Wubben, R. Bohnke, V. Kuhn, and K. Kammeyer, "Near-maximum-likelihood detection of MIMO systems using MMSE-based lattice reduction," in *IEEE Int. Conf. Commun.*, vol. 2. IEEE, 2004, pp. 798–802. 26, 52, 59, 87

[51] H. Yao and G. Wornell, "Lattice-reduction-aided detectors for MIMO communication systems," in *IEEE Global Telecommun. Conf. (GLOBECOM) 2002*, vol. 1. IEEE, 2002, pp. 424–428. 26, 52, 59, 87

[52] X. Ma and W. Zhang, "Performance analysis for MIMO systems with lattice-reduction aided linear equalization," vol. 56, no. 2. IEEE, 2008, pp. 309–318. 26, 27, 52, 63, 87

[53] C. Windpassinger and R. F. Fischer, "Low-complexity near-maximum-likelihood detection and precoding for MIMO systems using lattice reduction," in *Proc. Inf. Theory Workshop*. IEEE, 2003, pp. 345–348. 26, 59

[54] D. Wubben, R. Bohnke, V. Kuhn, and K.-D. Kammeyer, "MMSE extension of V-BLAST based on sorted QR decomposition," in *58th Veh. Technol. Conf. (VTC) 2003-Fall*, vol. 1. IEEE, 2003, pp. 508–512. 26, 27, 59

[55] P. Q. Nguyen and B. Valle, *The LLL algorithm: survey and applications*. Springer Publishing Company, Incorporated, 2009. 26, 87

[56] A. Lenstra, H. Lenstra, and L. Lovász, "Factoring polynomials with rational coefficients," *Mathematische Annalen*, vol. 261, no. 4, pp. 515–534, 1982. 26, 59

[57] M. Taherzadeh, A. Mobasher, and A. Khandani, "Lattice-basis reduction achieves the precoding diversity in MIMO broadcast systems," in *39th Conf. Inf. Sci. and Syst. (CISS) 2005*, 2005. 27

[58] J. Jeganathan, A. Ghrayeb, and L. Szczecinski, "Generalized space shift keying modulation for MIMO channels," in *19th IEEE Int. Symp. Pers.,*

Ind. and Mobile Radio Commun. (PIMRC) 2008, 2008, pp. 1–5. 31, 35, 37, 45, 48, 63, 82

[59] J. Proakis and M. Salehi, *Digital communications*. McGraw-hill New York, 2001, pp. 261–262. 44, 61

[60] Z. Lin, E. Erkip, and A. Stefanov, "The exact pairwise error probability for MIMO block fading channel," in *Proc. Int. Symp. Inf. Theory Appl.* Citeseer, 2004, pp. 728–732. 45, 62, 100

[61] O. N. Alrabadi, C. B. Papadias, A. Kalis, and R. Prasad, "A universal encoding scheme for mimo transmission using a single active element for psk modulation schemes," *IEEE Trans. Wireless Commun.*, vol. 8, no. 10, pp. 5133–5142, 2009. 51

[62] A. Kalis and C. Papadias, "An espar antenna for beamspace-mimo systems using psk modulation schemes," in *IEEE Int. Conf. Commun. (ICC) 2007*. IEEE, 2007, pp. 5348–5353. 51

[63] L. Szczecinski and D. Massicotte, "Low complexity adaptation of mimo mmse receivers, implementation aspects," in *Global Telecommunications Conference, 2005. GLOBECOM'05. IEEE*, vol. 4. IEEE, 2005, pp. 6–pp. 52

[64] J. Niu and I. Lu, "A new lattice-reduction-based receiver for MIMO systems," in *41st Annu. Conf. Inf. Sci. and Syst. (CISS) 2007*. IEEE, 2007, pp. 499–504. 52, 87

[65] Y. Gan, C. Ling, and W. Mow, "Complex lattice reduction algorithm for low-complexity full-diversity MIMO detection," vol. 57, no. 7. IEEE, 2009, pp. 2701–2710. 52, 87

[66] J. Andrews, A. Ghosh, and R. Muhamed, *Fundamentals of WiMAX: understanding broadband wireless networking*. Prentice Hall PTR, 2007. 54

[67] M. Leng and Y.-C. Wu, "Low-complexity maximum-likelihood estimator for clock synchronization of wireless sensor nodes under exponential delays," *IEEE Trans. Signal Process.*, vol. 59, no. 10, pp. 4860–4870, 2011. 58

[68] R. Ramirez-Gutierrez, L. Zhang, J. Elmirghani, and A. Almutairi, "Antenna Beam Pattern Modulation for MIMO Channels," in *8th Int. Wireless Commun. and Mobile Comput. Conf. (IWCMC) 2012*. IEEE, 2012, pp. 591–595. 61, 72, 80

[69] M. Di Renzo, H. Haas, A. Ghrayeb *et al.*, "Spatial modulation for mimo wireless systems," in *IEEE Wireless Commun. Network Conf. WCNC 2013*, 2013. 65

[70] P. Yang, Y. Xiao, Y. Yu, and S. Li, "Adaptive spatial modulation for wireless mimo transmission systems," *IEEE Commun. Lett.*, vol. 15, no. 6, pp. 602–604, 2011. 65

[71] P. Yang, Y. Xiao, L. Li, Q. Tang, Y. Yu, and S. Li, "Link adaptation for spatial modulation with limited feedback," *IEEE Trans. Veh. Technol.*, vol. 61, no. 8, pp. 3808–3813, 2012. 65, 66

[72] A. Younis, N. Serafimovski, R. Mesleh, and H. Haas, "Generalised spatial modulation," in *44th Conf. Signals, Syst. and Comput. (ASILOMAR) 2010*. IEEE, pp. 1498–1502. 71

[73] J. Fu, C. Hou, W. Xiang, L. Yan, and Y. Hou, "Generalised spatial modulation with multiple active transmit antennas," in *IEEE GLOBECOM Workshops (GC Wkshps) 2010*. IEEE, 2010, pp. 839–844. 71

[74] R. Ramirez-Gutierrez, L. Zhang, J. Elmirghani, and R. Fa, "Generalized Phase Spatial Shift Keying Modulation for MIMO Channels," in *73rd Veh. Technol. Conf. (VTC Spring) 2011*, may 2011, pp. 1 –5. 72, 80

[75] L.-L. Yang, *Multicarrier communications*. John Wiley & Sons, 2009. 82

[76] E. Telatar, "Capacity of multi-antenna gaussian channels," *European Trans. Telecommun.*, vol. 10, no. 6, pp. 585–595, 1999. 82

[77] L.-L. Yang, "Transmitter preprocessing aided spatial modulation for multiple-input multiple-output systems," in *IEEE 73rd Veh. Technol. Conf. (VTC Spring) 2011.* IEEE, 2011, pp. 1–5. 82, 83

[78] J. Jeganathan, A. Ghrayeb, L. Szczecinski, and A. Ceron, "Space shift keying modulation for MIMO channels," vol. 8, no. 7. IEEE, 2009, pp. 3692–3703. 82

[79] W. Mohr, "The winner (wireless world initiative new radio) project–development of a radio interface for systems beyond 3g," *Int. J. Wireless Inf. Netw.*, vol. 14, no. 2, pp. 67–78, 2007. 96

[80] D. S. Baum, J. Hansen, and J. Salo, "An interim channel model for beyond-3g systems: extending the 3gpp spatial channel model (scm)," in *61st Veh. Technol. Conf. (VTC-Spring) 2005*, vol. 5. IEEE, 2005, pp. 3132–3136. 96

[81] T. Jämsä, J. Meinilä, P. Kyösti, D. Baum, H. E. Sallabi, T. Rautiainen, C. Schneider, M. Milojević, and P. Zetterberg, "Overview of winner channel modelling activities," in *15th WWRF meeting, Paris-France*, 2005. 96

[82] G. L. Stüber, *Principles of mobile communication.* Springer, 2011. 99

[83] S. Verdu, *Multiuser detection.* Cambridge university press, 1998. 101

Note that the last number(s) at the end of each reference indicate the page number(s) where this reference has been cited.